Landsat Analysis of Coastal Turbidity Dynamics Along Northeastern North America

October 1989

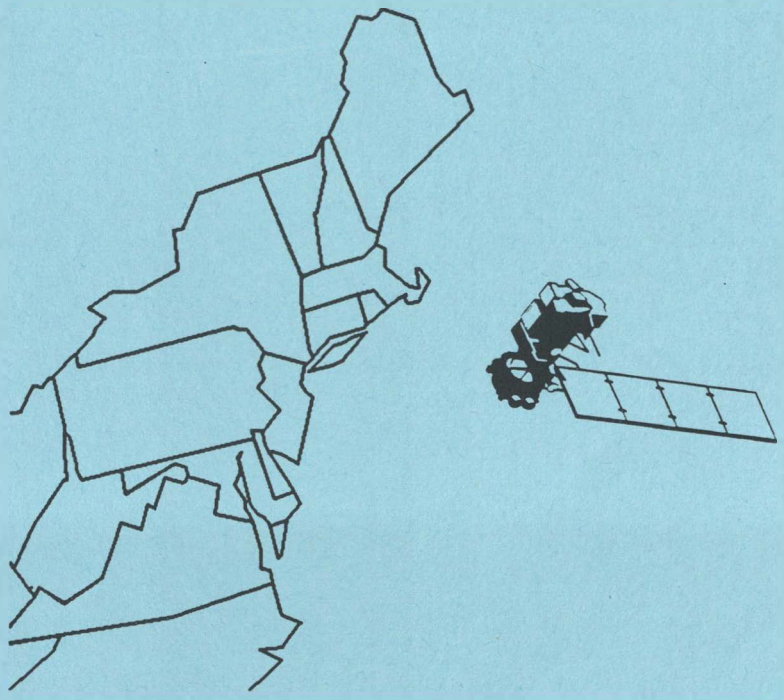

U.S. DEPARTMENT OF COMMERCE
National Oceanic and Atmospheric Administration
NOAA Estuarine Programs Office

Landsat Analysis of Coastal Turbidity Dynamics Along Northeastern North America

John C. Munday, Jr.
Michael S. Fedosh

Final Report
Contract NA-80-FA-C-00051
October 1989

U.S. DEPARTMENT OF COMMERCE
Robert A. Mosbacher, Sr., Secretary

National Oceanic and Atmospheric Administration
John A. Knauss, Under Secretary

NOAA Estuarine Programs Office
Samuel E. McCoy, Director (Acting)

ACKNOWLEDGMENTS

For support of this research, part of the Ocean Pulse/Northeast Monitoring Program, we acknowledge and thank the Northeast Fisheries Center, National Marine Fisheries Service, National Oceanic and Atmospheric Administration (Contract NA-80-FA-C-00051), U.S. Department of Commerce. Dr. James Thomas, Project Monitor, has faithfully supported this and many other investigations of continental shelf waters, with the goal of encouraging the wiser use of our national marine resources. We thank Mrs. Cynthia Gaskins and Mrs. Barbara Bilyk for secretarial assistance, Mrs. Karen Fedosh for preparation of the illustrations, and Mr. Charles Alston for photographic services.

ABSTRACT

Estuarine plumes on the continental shelf of northeastern North America emanating from bays and river mouths were studied in 335 Landsat MSS and 68 HCMM thermal infrared images. Plume boundaries were interpreted from surface turbidity and temperature discontinuities as revealed from image analysis. Techniques involved color additive enhancement, video density slicing, and visual analysis. The shelf region of study extended from southern Virginia to Boston, Massachusetts. For the Chesapeake, Delaware, and New York Bay entrances, plume thermal boundaries were detected in nearly all HCMM images, and turbidity boundaries were detected often in Landsat images. Plume waters at these bay entrances, as inferred from turbid and thermal boundaries on sets of sequenced images, generally move southward along coastlines, due to net non-tidal coastal current, tidal current subject to the Coriolis force, fresh-water discharge, and predominant local wind. Wind has a large influence on locations of boundaries: Under strong southwest to west winds, plumes move eastward from bay mouths, spreading laterally, and sometimes entering or passing through waste disposal areas. Northern winds drive plumes southward along coastlines. Plume boundaries are more dispersed during ebb tide. Seasonal effects are mixed. In the region of Long Island to Boston, tidal ranges and currents are greater, there are fewer bays and rivers discharging turbid plumes onto the shelf, the plumes are less turbid, and there are more instances of turbidity derived locally via tidal resuspension. Consequently, turbidity-tracing of water movement is less useful. Available evidence in the images suggests oscillatory movements in Long Island Sound, and south of Cape Cod. Tidally-induced resuspension reveals the bathymetry in the shallows of Boston and Plymouth Bays, off Nantucket, and at the eastern tip of Long Island.

CONTENTS

FIGURES

TABLES

ADMINISTRATIVE INFORMATION

1. Principal Investigator's name: Dr. John C. Munday Jr.

2. Organization receiving funding:

   Virginia Institute of Marine Science, College of William and Mary, Gloucester Point, Virginia.

3. Total funding, contract phases, funding, and reports:

   Total Funding: $25,156.42

   Contract Starting and Closing Date and Funding:

   a. NA80FAC00051 August 1, 1980-April 30, 1981. $5,038.00

   (Report: Munday, J.C., Jr. and M.S. Fedosh. 1981. Landsat analysis of the dynamics of the Chesapeake Bay plume on the continental shelf. Final Report NMFS NA80FAC00051. Virginia Inst. Marine Sci., Gloucester Point, Va., 32 p.)

   b. NA80FAC00051 July 1, 1981-September 30, 1982. $10,057.77

   c. NA80FAC00051 August 2, 1982-June 30, 1983. $10,060.65

4. Title of work unit or investigation:

   Landsat Analysis of Coastal Turbidity Dynamics Along Northeastern North America.

5. Major NEMP cruises participated in: None.

6. Other publications produced under this funding:

   1) Munday, J.C., Jr. and M.S. Fedosh. 1980. Southern Chesapeake Bay circulation and suspended sediment transport analyzed using Landsat imagery. Proc. ACSM-ASP Fall Techn. Mtg., Niagara Falls, N.Y., Amer. Soc. Photogr., Falls Church, VA, RS-3-F: 1-5.

2) Munday, J.C., Jr. and M.S. Fedosh. 1981. Chesapeake Bay plume dynamics from Landsat. In Chesapeake Bay Plume Study-Superflux 1980 (eds. J.W. Campbell and J.P. Thomas), NASA Conf. Publ. 2188, p. 79-92.

3) Fedosh, M.S. and J.C. Munday Jr. 1982. Satellite analysis of estuarine plume behavior. Oceans 82, Washington, D.C., IEEE, New York, p. 563-571.

7. NEMP work unit monitor:

Dr. James P. Thomas, Chief, Biological Oceanography Investigation.

8. Duration that work unit covered: August 1, 1980 to June 30, 1983.

OBJECTIVES

The objectives of this research were to use Landsat images to:

1. Find the directional patterns of the movement of turbid plumes emanating from bays and estuaries of the mid-Atlantic coast from Massachusetts to North Carolina.

2. Determine the effects of meteorological, seasonal, and oceanographic influences on the direction and distance of plume movement.

3. Find the seaward extent of turbid plume boundaries.

4. Determine the frequencies with which turbid plumes reach waste disposal sites located on the continental shelf.

LANDSAT ANALYSIS OF COASTAL TURBIDITY DYNAMICS ALONG NORTHEASTERN NORTH AMERICA

John C. Munday Jr. and Michael S. Fedosh

Remote Sensing Center
Virginia Institute of Marine Science
School of Marine Science
College of William and Mary
Gloucester Point, Virginia 23062
804/642-2111

Final Report

Contract NA-80-FA-C-00051

for

United States Department of Commerce
National Oceanic and Atmospheric Administration
National Marine Fisheries Service
Northeast Fisheries Center
Sandy Hook Laboratory
Highlands, New Jersey 07732

July 1, 1983

INTRODUCTION

A significant question for management of coastal marine fisheries is the distribution of nutrients and pollutants outwelled from coastal bays and estuaries. Investigations of the seaward flux of materials, both spatially and temporally, should be fruitful toward understanding fishery productivity and its fluctuations. From such understanding the fishery management questions can be addressed.

The National Marine Fisheries Service has undertaken and supported studies of estuarine flux for some time, and in the late 1970s initiated a cooperative program with NASA and university research groups to utilize remote sensing in these flux studies. The first large program was called LAMPEX (Large Area Marine Productivity Experiment), followed by Superflux, which investigated the effects of the Chesapeake Bay plume on continental shelf waters (see Campbell and Thomas, 1981).

The present research program was begun under Superflux as a Landsat study of the Chesapeake Bay turbidity plume (Munday and Fedosh, 1981a,b). This Landsat study was subsequently expanded to include the entire region from North Carolina to Massachusetts (Fedosh and Munday, 1982). The Landsat coverage of this region is shown in Figure 1.

SETTING

The waters of the continental shelf from Virginia to Massachussetts are significantly impacted by human activity. The waters are used for fishing, transportation, recreation, and direct disposal of waste materials. Three-quarters of the nation's offshore dumping occurs here (Gross, 1976). This Middle Atlantic Bight also receives estuarine discharges from fluvial systems whose shores are among the world's most urbanized areas. Municipal and industrial wastes entering these fluvial systems eventually reach Atlantic shelf waters, there impairing water quality and settling onto benthic substrates.

The estuaries of this region also produce nutrients for the marine food web which are outwelled into the nearshore Atlantic waters to be utilized by the marine community. Any change in the concentration and dispersal of these nutrients can impact marine fisheries. Fish populations feeding in plumes of estuarine water can be impacted when these plumes pass through offshore waste disposal sites.

Thus, estuarine flushing of pollutants from human activity is in direct competition with estuarine supply of nutrients for the marine food web, and provision of nursery habitats. Depending on the levels and locations of waste releases, the outwelling of estuarine water onto the Middle Atlantic continental shelf waters can be either beneficial or detrimental to the marine community. Because of the dynamics of estuarine flux and shelf circulation, as a function of seasonal discharge, winds, and coastal currents, it is obvious that the timing of waste releases, and not only the locations, may be significant.

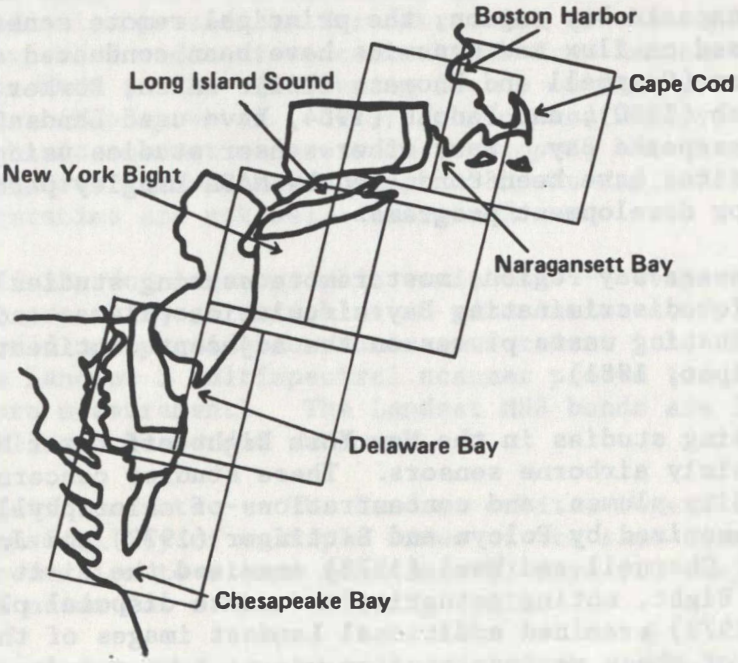

Figure 1. Landsat Scene Coverage from North Carolina to Massachusetts.

It is therefore important to investigate the seaward flux of estuarine waters, and the spatial and temporal distribution of pollutants and nutrients. Results can help in the location of fish populations which are congregating in feeding zones, aid in the siting of waste disposal areas away from plumes, and help in tracking the movement and dispersal of contaminants and nutrients.

Ship-based studies have been carried out for some time on estuarine plumes in nearshore waters, but vessel costs and the large areas to be covered limit these studies and the number of plumes which can be investigated. It is advantageous to use remote sensing to reduce the effort and provide repetitive synoptic views over large areas (see Campbell and Thomas, 1981).

REMOTE SENSING OF COASTAL WATERS ALONG NORTHEASTERN NORTH AMERICA

In the Chesapeake Bay region, the principal remote sensing studies which have focused on flux and dynamics have been conducted as part of the Superflux program (Campbell and Thomas, 1981). Also, Bowker et al. (1975), Munday and Fedosh (1980), and Fedosh (1984) have used Landsat imagery in study of the Chesapeake Bay. Many other sensor studies using Bay and shelf waters as test sites have been conducted by NASA Langley personnel in support of sensor development programs.

In the Delaware Bay region, most remote sensing studies involved the use of Landsat for discriminating Bay circulation (Klemas and Polis, 1977), and for discriminating waste plumes on the adjacent continental shelf (Klemas and Philpot, 1981).

Remote sensing studies in the New York Bight off Lower New York Bay have involved mainly airborne sensors. These studies concerned waste disposal, turbidity plumes, and concentrations of chlorophyll and suspended sediment, as summarized by Polcyn and Sattinger (1979) and Johnson and Harriss (1980). Charnell and Maul (1973) examined the first Landsat image of the New York Bight, noting estuarine and waste disposal plumes. Polcyn and Sattinger (1979) examined additional Landsat images of this region. The general purpose of these various studies was to test sensing systems, and determine their capability for acquiring useful oceanographic data.

Northward, from Long Island to Boston harbor, there have been no extensive Landsat studies focused on flux and dynamics.

Over the whole region, from Virginia to Massachussetts, there have been remote sensing studies involving the Seasat Synthetic Aperture Radar. These studies are published in Beal et al. (1981).

LANDSAT STUDY OF COASTAL PLUMES

When the first Landsat satellite was launched in 1972, there were numerous publications describing analyses of turbid plumes on continental shelf regions (see, e.g., NASA Goddard, 1973). The new perspective from space gave oceanographers for the first time a truly wholistic picture of the

surface waters in these regions (see Figure 2), which contrasted dramatically with earlier efforts to see the whole by assembling a mosaic of ship data or aerial photographs. The oceanographic community, however, was not able to extract a large amount of useful information from the images. This disappointment had its roots in several technical considerations:

1) Atmospheric variability --- Cloud cover and hazy atmospheres reduced the efficiency of data collection by Landsat. Of twenty orbital passes per year, one-third to two-thirds were rendered useless. Unlike the case with studies of land cover, marine water bodies are highly dynamic, requiring data collection throughout tidal cycles as well as during extreme events and over seasonal variations. Landsat data available from a small number of years are insufficient to provide oceanographers with a comprehensive picture of the dynamics of marine waters.

2) Algorithms --- In the early 1970s, algorithms were not available to permit analysis of the image data for variables of interest. The initial effort was on data reduction procedures for extraction of chlorophyll concentrations and suspended sediment concentrations from Landsat data. Much progress has been made in the intervening decade on the best algorithms for these two variables (Munday et al., 1979; Johnson and Munday, 1983). Algorithms for atmospheric correction are well-developed, but there is a variety of them in use (see Johnson and Munday, 1983; Munday, 1983), and their comparative accuracies are not well-determined.

3) Lack of specificity for oceanographic variables --- Temperature, salinity, and current are critical variables in circulation study, but Landsats 1, 2, and 3 did not provide for their measurement (the thermal sensing system on the Landsat 3 multispectral scanner proved too noisy for sea surface temperature measurement). The Landsat MSS bands are less than optimum for chlorophyll and suspended sediment.

4) Inadequate repetition rate --- The Landsat orbital repeat cycle of 18 days eliminated the possibility of multiple views of the same oceanographic conditions. Even a reduction to 9 (and sometimes 6) days via dual Landsats could not satisfy the needs for a short viewing cycle.

These limitations led to the development and launch of the Coastal Zone Color Scanner on board Nimbus 7 (Hovis et al., 1980). The CZCS was designed specifically as an oceanographic color and temperature sensor. Unfortunately, its spatial resolution is coarse (800 m) and data reduction procedures have taken many years to be established. For coastal environments, the procedures are still considered inadequate, because they were designed for clear water while coastal water is relatively turbid. Although it is true that with appropriate surface information, the limitations in atmospheric correction procedures and procedures for calibration to aquatic variables may be overcome, the large area covered in each CZCS image necessitates extensive surface data collection, as oceanographic variation upsets calibrations extrapolated across entire images.

The finer spatial resolution afforded by the Landsat series is its principal advantage over the CZCS. Also, understanding of the capabilities and limitations of the Landsat MSS has accumulated to the point that useful

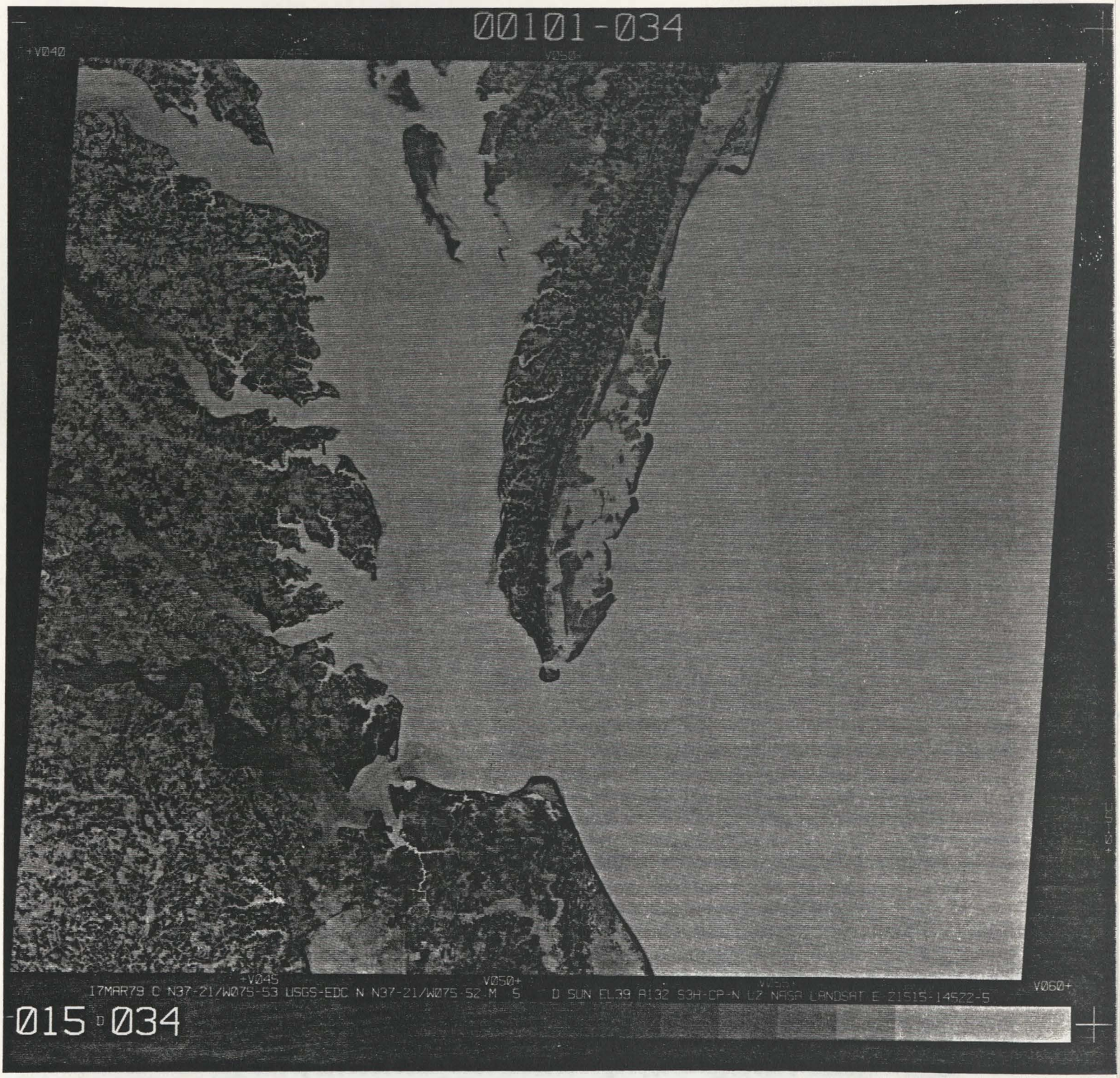

Figure 2. Landsat Image of Chesapeake Bay.

information may be obtained about the marine environment if large numbers of scenes are analyzed. After a decade, the usable scenes of a single region usually number between 70 and 120, permitting appropriate sorting for the variety of oceanographic conditions of importance, including tidal phase, wind vector, fresh water runoff, and seasonal variations in coastal currents.

On such a basis, this study of coastal plumes using Landsat data was initiated for the region along the mid-Atlantic coast of North America, from southern Virginia to Boston, Massachusetts. Low funding necessitated reliance entirely on the use of photographic images, as opposed to computer compatible tapes (CCTs). The study has been carried out mainly with Landsat images; however, some Heat Capacity Mapping Mission (HCMM) images were also obtained and analyzed.

METHODS

General Approach

The Landsat multispectral scanner records scene radiances in image format (see Figure 2), and the data can be reduced to suspended sediment concentrations and/or turbidity in the upper few metres of the water column. Some images from the Heat Capacity Mapping Mission (HCMM) thermal infrared radiometer were used here (see Figure 3). HCMM data can be reduced to surface temperatures (Wiesnet et al., 1980). In this study, none of the satellite data were reduced to quantitative measurements of turbidity or temperature; instead, photographic images of Landsat and HCMM scenes were analyzed visually and by machine-enhancement for plumes and boundaries formed by turbidity and temperature.

Although satellite images are only snapshots, that is, pictures at a single point in time, of continuous dynamic processes, they can be interpreted for the movement of water masses, especially when a large number of images is available. The information on turbidity and water temperature is useful because these variables act as Lagrangian tracers of water motion.

Turbid plumes outwelled from Massachusetts Bay, Long Island Sound, and Lower New York Bay, and Delaware Bay and Chesapeake Bay along the Middle Atlantic Bight, have been studied using Landsat and HCMM images. Waste disposal sites off each estuary were noted in reference to plume front locations. Images were sorted according to tidal phase, wind vector, and season to determine the influence of these factors on plume movement. Shelf and nearshore circulation patterns described in the literature were also used in analyzing plume behavior seen in the images.

Data Acquisition

For the Chesapeake Bay entrance, 94 dates of Landsat images were used (path 15, row 34). The Delaware Bay entrance was examined in 128 Landsat images (path-rows 14-33 and 15-33) and 39 HCMM images. The New York Bay entrance was examined in 58 Landsat images (path-row 14-32) and 28 HCMM images. The Long Island area was examined in 66 Landsat images (path-row 13-32), and Massachusetts Bay in 51 images (path-rows 12-31 and 13-31). The

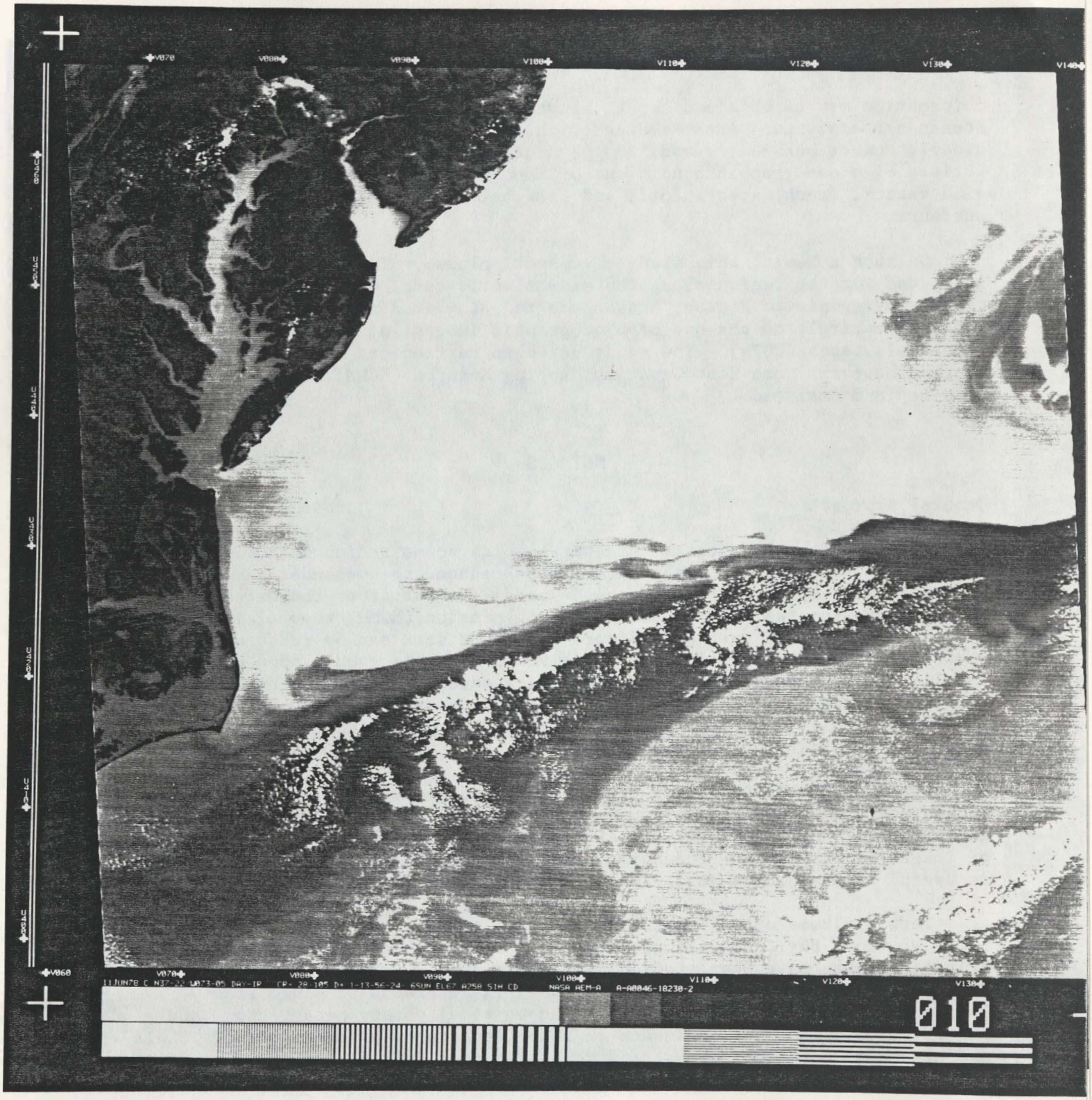

Figure 3. Heat Capacity Mapping Mission (HCMM) Image of the Middle Atlantic Bight.

The Narragansett Bay was examined in 100 Landsat images (path-rows 12-31 and 13-31). Figure 1 shows the scene coverage of the study area.

The Landsat images, from 1972 to 1982, were obtained from the USGS EROS Data Center, Sioux Falls, South Dakota, and the HCMM images, from 1978 to 1979, were obtained from the National Space Science Data Center, NASA Goddard Space Flight Center, Greenbelt, Maryland. The formats are 18.5 cm and 24.1 cm positive transparencies, for Landsat (scale 1:1M) and HCMM (1:3.85M) images respectively. The Landsat and HCMM images are tabulated in Appendices 1 and 2. The overpass dates are distributed throughout all months of the year at no more than 15 day intervals, for each region of study (see Figure 4). The HCMM passes are concentrated in the summer and fall months.

Wind data for Norfolk, Virginia, for Cape May and Sandy Hook, New Jersey, for Montauk Point, New York, and for Boston, Massachusetts, appropriate to the Chesapeake, Delaware, and New York Bay entrances, eastern Long Island, and Boston Harbor, respectively, were obtained from the National Climatic Center in Asheville, North Carolina. The Cape May and Sandy Hook wind data were reduced to vector averages for the 24-hour period preceding each Landsat overpass, while the Norfolk wind data were reduced to vector averages for the preceding 12-hour period. Acquired wind data for Montauk Point and Boston, Massachusetts consist of hourly records for the 24 hours preceding the overpass, but the lack of significant plumes for the associated waters did not justify the effort of vector-averaging. The wind data are tabulated in Appendix 1. No wind data were obtained for the HCMM images. The composite wind regimes for all passes in the Chesapeake, Delaware, and New York Bay regions are shown in Figure 5, alongside a long-term record for comparison in the case of Chesapeake Bay.

For use in image analysis, the wind data were divided into quadrants deemed appropriate for each region. The quadrants selected were 1-90 degrees, 91-180, 181-270, and 271-360, labeled as (1, 2, 3, and 4), and representing northeast, southeast, southwest, and northwest winds.

Actual tidal data for Sewells Point in Virginia, for the Breakwater on Cape Henlopen, Delaware, for Sandy Hook, New Jersey, for Narragansett, Rhode Island, and for Boston, Massachusetts, were obtained from the National Ocean Survey in Rockville, Maryland. When no actual data were available, predicted times of high tide were used as obtained from NOAA tide tables, an event which occurred for less than 10% of the images.

The satellite images for each region were classified by comparing the overpass time to the nearest time of high tide at the reference tidal station. Each image was assigned a time in hours and minutes according to whether the overpass occurred before (-) or after (+) the reference high tide. The images for each region of study were evenly distributed over a representative diurnal tidal cycle. The tide data are tabulated in Appendices 1 and 2. Distributions over the tidal cycle are shown in Figure 6. A summary of the data is provided in Table 1.

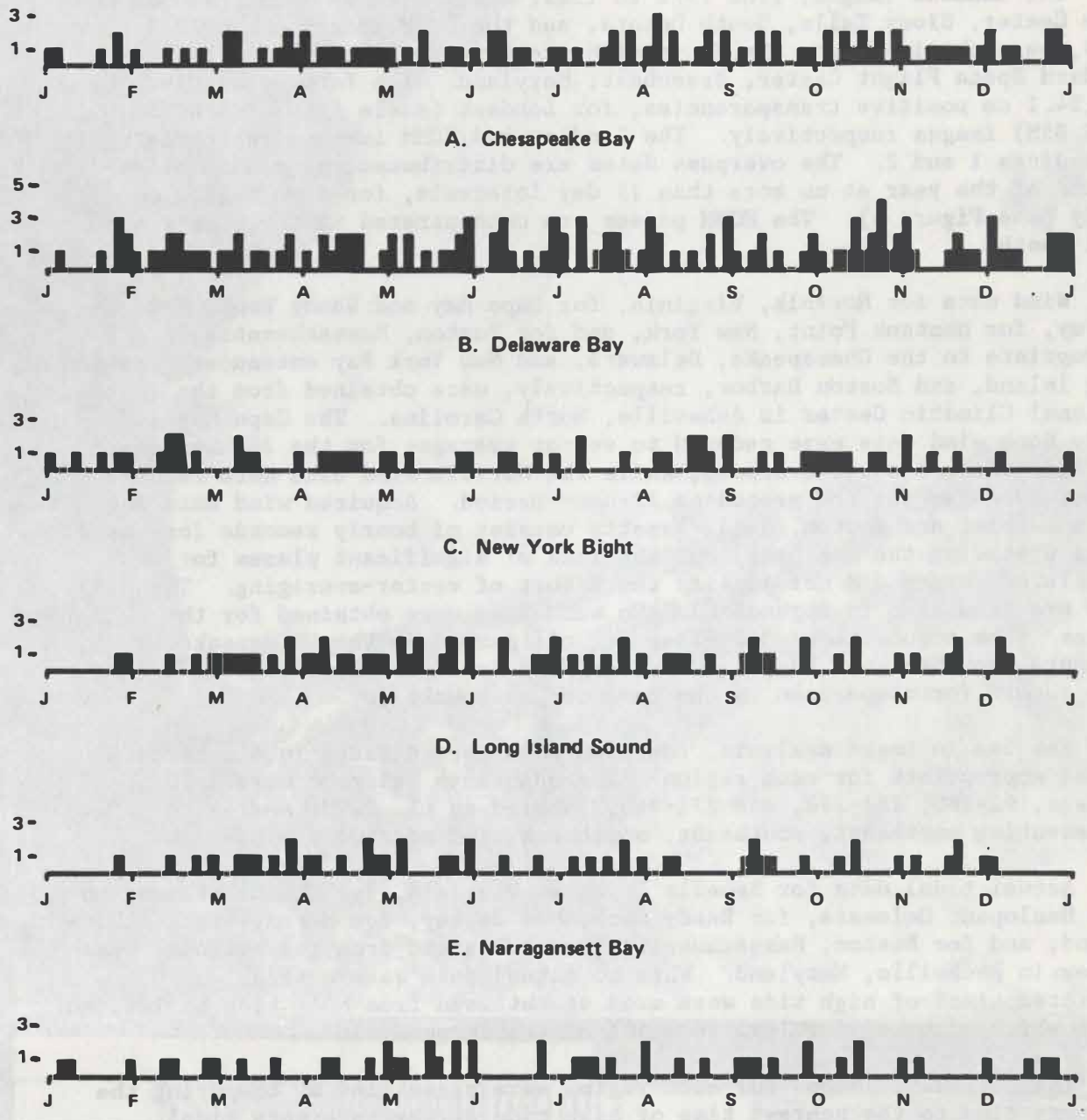

Figure 4. Calendar Distributions of Landsat Passes Analyzed in this Study, 1972-1982.

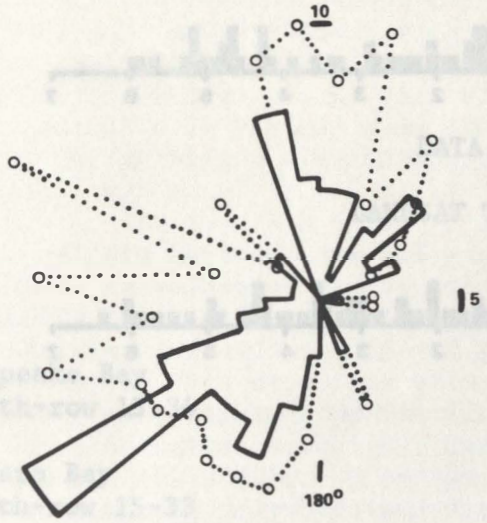

A. Chesapeake Bay

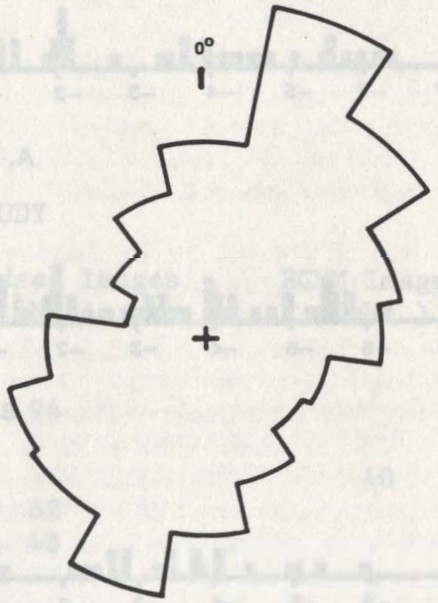

B. Chesapeake Bay Wind Frequency only for 1946-1970

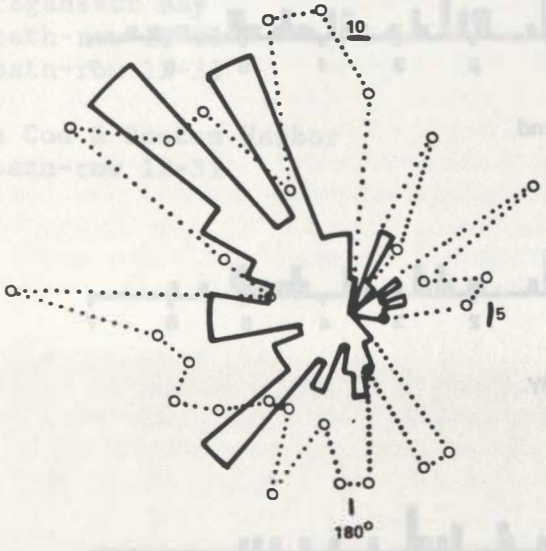

C. Delaware Bay

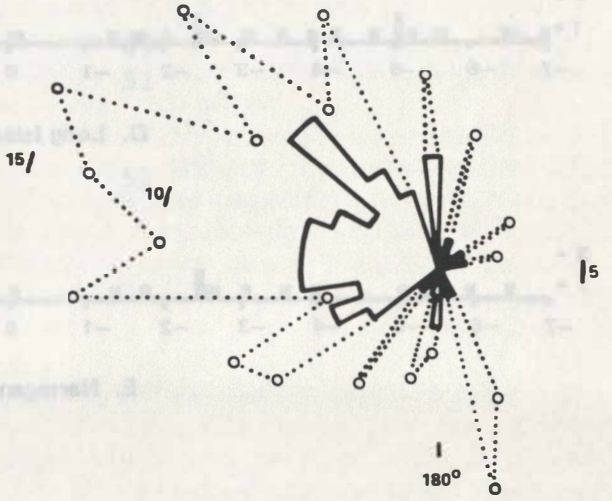

D. New York Bight

Figure 5. Wind Regimes During Landsat Passes.
Solid line = wind frequency; dotted line = average wind speed in knots.

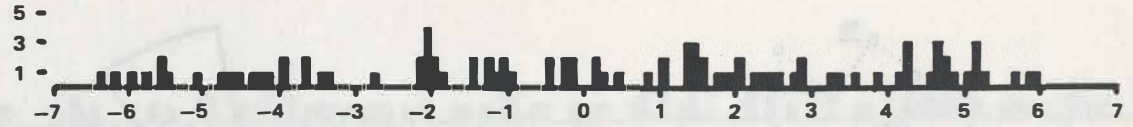

A. Chesapeake Bay

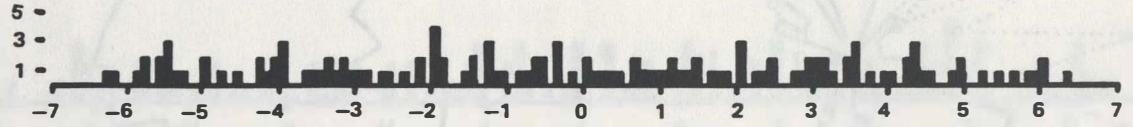

B. Delaware Bay

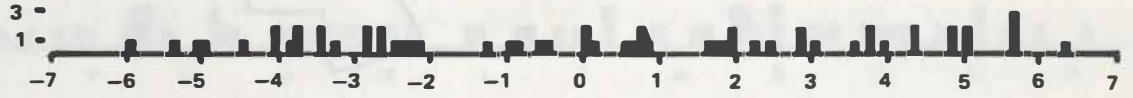

C. New York Bight

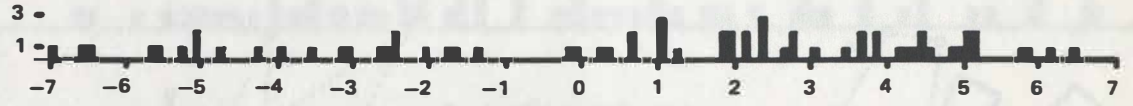

D. Long Island Sound

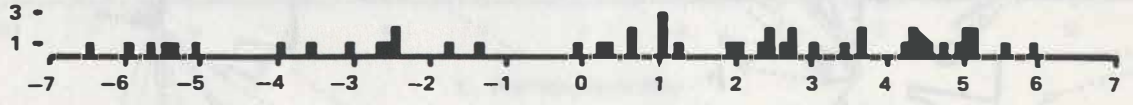

E. Narragansett Bay

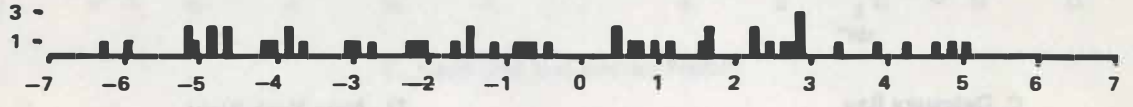

F. Cape Cod and Boston Harbor

Figure 6. Distribution of Landsat Passes over the Tidal Cycle.

TABLE 1

DATA SUMMARY FOR

LANDSAT TURBIDITY STUDY

	Landsat Images (No.)	HCMM Images (No.)
Chesapeake Bay		
path-row 15-34	94	
Delaware Bay		40
path-row 15-33	82	
path-row 14-33	48	
New York Bay		28
path-row 14-32	58	
Long Island Sound		
path-row 13-32	66	
Narragansett Bay		
path-row 13-31	49	
path-row 12-31	51	
Cape Cod & Boston Harbor		
path-row 12-31	51	

Image Analysis

The methods of image analysis included visual interpretation coupled with machine-assisted enhancement (Munday and Fedosh, 1981b). The Landsat and HCMM images were visually analyzed on a light table with turbid plumes and thermal boundaries traced onto overlays. In many cases, especially the HCMM images, the visual analysis was accomplished with the aid of a Bausch and Lomb ZT4H Zoom Transfer Scope, which permitted variable magnification for easy viewing and tracing.

The small set of 70 mm images for Chesapeake Bay was enhanced with an International Imaging Systems (I2S) color additive viewer, courtesy of NASA Langley, and these color enhancements were photographed on color slide (35 mm) film for projection during later analysis. The 18.5 cm Landsat images were enhanced with 32-channel video optical density analyzers with color-coded television display. The video systems were I2S and Spatial Data Systems (SDS) analyzers at VIMS and USGS (Reston, Virginia) respectively. Most of the video enhancements were also photographed on color slide (35 mm) film for projection during later analysis. A black mask covering land areas was used during enhancement to focus attention on water patterns. That the mask had negligible effect on the density analysis was evidenced by the constancy of patterns when the image was rotated through 90 degrees (the danger is that electronic band width limitations during scanning across sharp brightness gradients will cause smearing in the color-coded output).

Also, for many enhancements, a contour map of optical density was prepared from the television monitor display by placing an acetate sheet over the image on the I2S light table and manually drawing contours while viewing the display monitor; this procedure produced contour maps at the original image scale.

The above procedures produced two types of maps. The one consists of visually-discriminated turbidity boundaries extending sometimes over long distances, possibly through background turbidity gradients not noticeable visually. Missed background gradients would be weak, because the eye during the mapping process ignores weak gradients, but enhances sharp gradients and emphasizes the continuity of turbidity-marked hydrodynamic features over long distances.

The second type of map is of photographic density contours which quantitatively represent the absolute turbidity levels. With appropriate calibration, this type of map could become a map of absolute concentrations of suspended particulate material.

Combinations of visual tracings and video contour maps were used to find turbid boundaries. The video maps are needed because the eye sees only relatively sharp density gradients in the images. The I2S is more sensitive than the eye to weak density changes, revealing turbidity boundaries which would not be detected by visual analysis alone, thus improving the detection of weak gradients, and permitting extension of plume fronts beyond the visual range.

However, video enhancements cannot be used solely, because there are many parallel density isopleths on a video enhancement, and the wrong contour may be chosen as a plume boundary. Often, the plume boundary itself is a turbidity gradient, hence image density isopleths will dissect the boundary and obscure it. The result may be a displaced plume boundary, or a failure in detection.

It is emphasized that visual maps and video density maps enhance different aspects of an image, and should not be expected to be similar. Examples of the maps are shown in Figure 7.

The distance and direction of turbidity boundaries were measured from origins at the bay mouths. Measurements were based on a 1 mm grid overlay (ordinary graph paper) facilitating use of the image scale of 1 mm to 1 km. The centers of the bay mouths were taken as the mid-points between the capes for both Chesapeake and Delaware Bays, and 40 degrees 30 minutes North Latitude, 74 degrees West Longitude for New York Bay. Patterns on the original 18.5 cm images and on the several data reduction products were simultaneously compared during extraction of measurements.

The distribution of turbidity boundaries was also analyzed by a counting procedure based on especially-prepared grid overlays. The special grid overlays were maps having segments formed by 10 degree azimuthal sectors and 10 km radial zones as shown in Figure 8. These overlays were used for making records of segments "visited" by plume boundaries. When a turbid boundary was noticed at some radial distance and direction from the origin, sector/zone segments radially outward to this position were recorded (as having been "visited"), if they contained pronounced turbidity. In some cases, where boundary segments were isolated from any large pattern, and relatively non-turbid water was noticed bayward of such segments, only the sector/zone containing the boundary segment was recorded.

The counting results for each sector-zone segment on the overlay were sorted according to the following numeric frequency code: 1-5 counts = 1, 6-10 counts = 2, 11-20 counts = 3, 21-30 counts = 4, 31-40 counts = 5, and 41-50 counts = 6. Choropleth maps were then prepared using the frequency code.

Analyses of the Long Island, Cape Cod, and Massachusetts Bay areas were limited to visual study of non-enhanced images. Turbid and thermal plumes were generally absent in these regions.

Definition of "Plumes"

The counting of areas as "visited" by turbidity was based on the presence of turbidity zones and discontinuities which appeared to be significant with respect to dynamics under study. This counting policy was deliberately made somewhat vague, because of the lack of historical data on plume dynamics. It gave the interpreters much freedom of choice. In subsequent studies of each of the regions, a more restrictive policy could be used based on the results reported here.

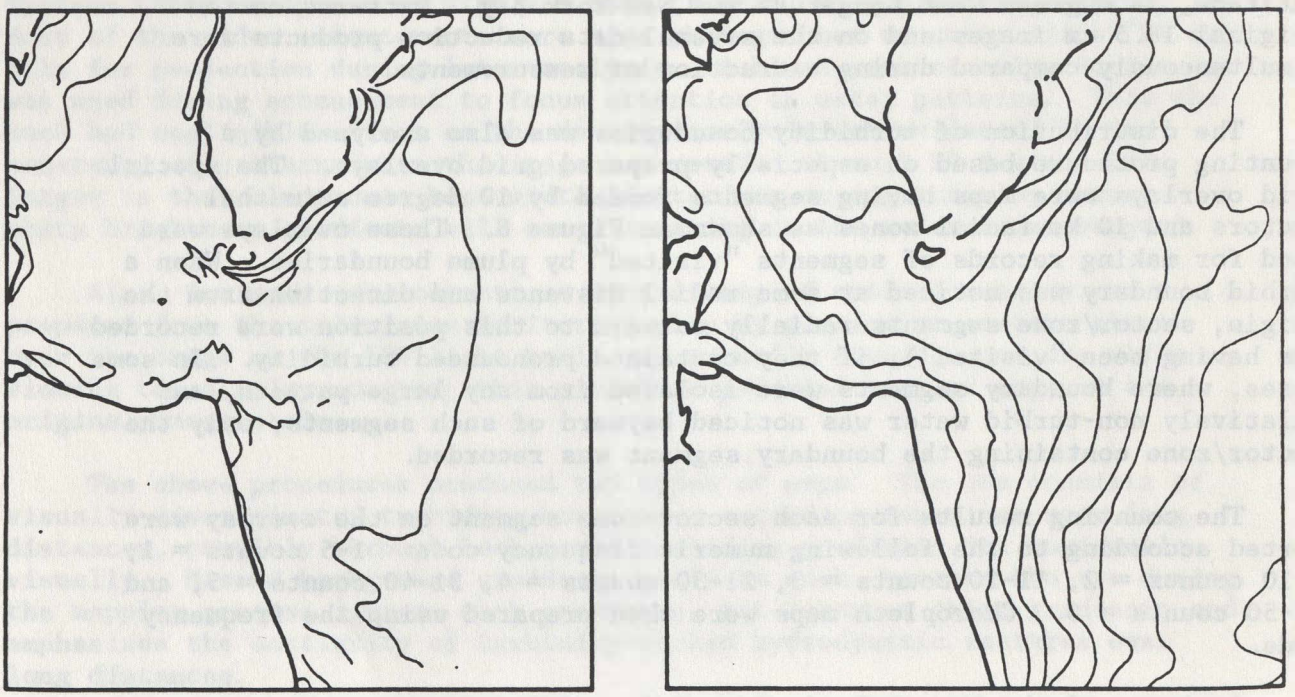

A. Visually discriminated turbidity boundaries.

B. Photographic density contours from density analyzer enhancement.

Figure 7. Samples of Turbidity Boundary Maps Obtained from Chesapeake Bay Landsat Images of 8 July 1978.

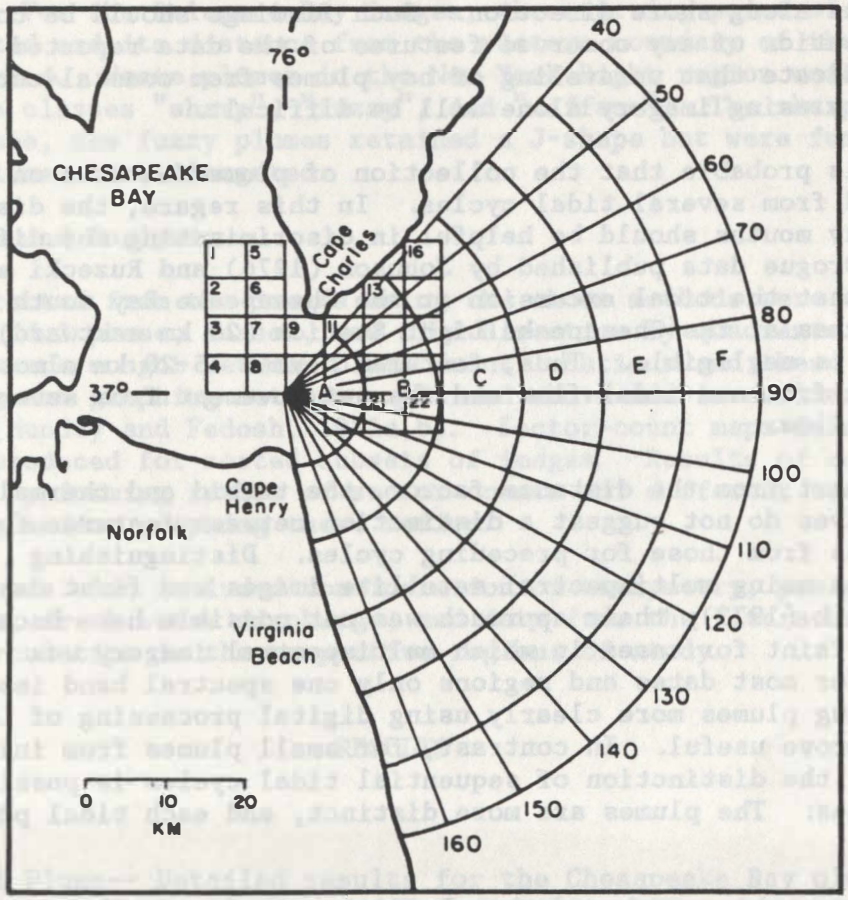

Figure 8. Sector Map for Image Data Extraction of Chesapeake Bay Images.

There are several consequences of the above policy. First, some of the turbidity zones and discontinuities are directly the result of bay plumes, while others may be associated, not with plumes, but with along-shore currents. According to Bumpus (1973), there is generally a net non-tidal southerly current along Virginia's Eastern Shore and the Virginia-North Carolina border toward Cape Hatteras. This current could involve shear and turbidity gradients (some images of the Chesapeake Bay region gave the impression of turbidity discontinuities parallel to shore at the 30 m isobath).

Second, studies by Harrison et al. (1967), Johnson (1976), and Ruzecki et al. (1976) show that flow adjacent to Cape Henry at the mouth of the Chesapeake Bay is sporadic rather than continuous, and that flow is wind-influenced in the along-shore direction. Such findings should be considered in the interpretation of any observed features of the data reported here, because they indicate that unraveling of bay plumes from coastal-current induced turbidity using imagery alone will be difficult.

Third, it is probable that the collection of plume features on any one image is derived from several tidal cycles. In this regard, the distance of features from bay mouths should be helpful in discriminating the different tidal cycles. Drogue data published by Johnson (1976) and Ruzecki et al. (1976) suggest that the tidal excursion at the Chesapeake Bay mouth is only about 8 km, whereas at the Chesapeake Light Station (23 km eastward) the tidal excursion is negligible. Thus, features beyond 15-20 km almost certainly result from non-tidal flow and the net movement from several cycles of tidal flow.

However, apart from the distance factor, the turbid and thermal features themselves do not suggest a distinction between features for the cycle in progress from those for preceding cycles. Distinguishing sequential plumes using multispectral satellite images was first described by Mairs and Clark (1973); their approach was not possible here because plumes were too faint for cases in which multispectral imagery was available, and for most dates and regions only one spectral band image was on hand. Defining plumes more clearly using digital processing of Landsat CCT data might prove useful. In contrast, for small plumes from inlets along the coast, the distinction of sequential tidal cycles is possible on single band images: The plumes are more distinct, and each tidal pulse is small in size.

Fourth, it must be remembered that Landsat records upwelling radiance from only the surface layers. The depth of the observed turbidity varies inversely with its opacity, with the depth of observation for prevailing turbidities being perhaps 5 m (Whitlock, 1976). Thus, plume features at greater depth are not recorded.

Fifth, surface turbidities are influenced by scour and resuspension when the depths are less than 15 m (Fedosh, 1984). Images of the Nantucket region showed the bathymetry clearly, despite the fact that the depth was too great for direct bottom reflection. In regions of resuspension, turbidity patterns are produced by a mixture of plumes and resuspended material, and turbidity discontinuity dynamics may not be used to infer water motion.

Generally, it should be remembered that Landsat is not always recording plume water boundaries as defined by vertical profiles of temperature, salinity, nutrients, and biological variables.

Waste Disposal Sites

For each bay mouth, an overlay was prepared with the Environmental Protection Agency (EPA) waste disposal site boundaries for sewage sludge, dredge spoil, and acid. These overlays were used to determine plume front distances from the disposal sites.

Acid waste plumes were visible in Landsat images of the Delaware Bay and the New York Bight, with sludge plumes also visible in the New York Bight images. For the Delaware Bay images, the starting point of each acid plume was marked and its distance from the western boundary of the disposal area was recorded. Waste plumes in the New York Bight region were sorted into the three classes "sharp", "fuzzy", and "diffuse". The sharp plumes showed a J-shape, the fuzzy plumes retained a J-shape but were fuzzy, and the diffuse plumes were elongated.

Data Reduction and Analysis

Data extracted from the images using the above methods were sorted according to tidal phase, season, and wind direction by quadrants. Simple relationships were sought between plume front locations and these variables using counting and graphing methods explained above and in earlier publications (Munday and Fedosh, 1981a,b). Sector-count maps described earlier were produced for sorted subsets of images. Results of counting were enhanced by forming ratios of sector counts for different conditions, and tabulating and/or graphing these ratios.

Analysis has also included consideration of bathymetry, passage of weather fronts, fresh water discharge, and data from the literature concerning circulation in the respective regions of study.

RESULTS

CHESAPEAKE BAY

The Turbid Plume-- Detailed results for the Chesapeake Bay plume have been presented previously (Munday and Fedosh, 1981a,b), and are included here for completeness. The map in Figure 9 shows the distribution of counts for all images, regardless of wind, tidal, and seasonal classes. It is seen that zones A through E (0-50 km outward) for sectors near 150 degrees are the most frequently visited. Similar results were obtained by other investigators during the Superflux program (Campbell and Thomas, 1981), indicating that plume behavior during the program was typical of general plume behavior, despite low discharge conditions during the program.

Tides-- During ebb tide, plumes are usually seen close to the Virginia coast south of Cape Henry. Figure 10B shows a composite of ebb tide turbidity boundaries, which in the mouth of the Bay itself are aligned toward 120 degrees. Distant from the mouth, the boundaries are oriented in

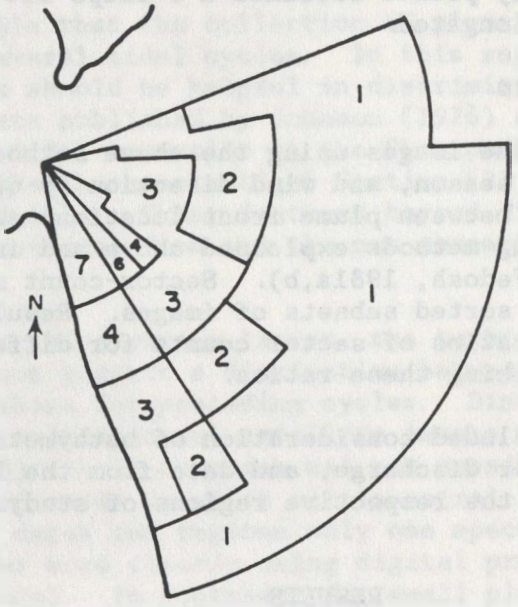

Figure 9. Areas Visited by Turbidity Boundaries, Chesapeake Bay, All Landsat Images.
The numerals are frequency codes representing sector/zone counts as follows: 1:1–5 counts; 2:6–10; 3:11–20; 4:21–30; 5:31–40; 6:41–50; 7:>50.

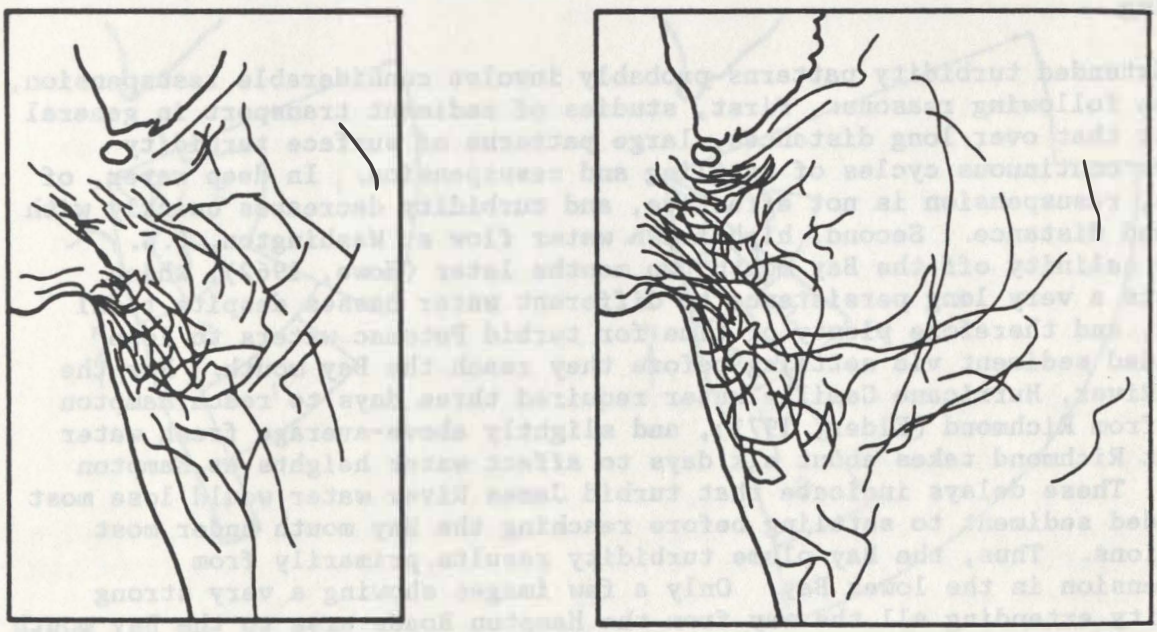

A. Flood Tide

B. Ebb Tide

Figure 10. Composite of Turbidity Boundaries Extracted from All Landsat Images of Chesapeake Bay.

many directions and are widely dispersed, but are more common in the region southward from the Bay mouth. The eastward boundaries are situated up to 40 km beyond the Bay mouth, and dispersed widely, while the southward boundaries equally distant from the mouth are found within 15 km of shore. Figure 11B, the sector-count map for ebb tide, shows the high concentration of boundaries along the shore south of the mouth. The concentration of plumes along the southern shoreline was explained by Ludwick and Melchor (1972) as due to the Coriolis effect and the net non-tidal southerly flow along the adjacent shelf. Turbidity patterns suggest that flood tide is stronger on the north side of the mouth, while ebb is stronger on the south.

The turbidity in the plumes often appears to extend from sites in the western Chesapeake Bay below the Rappahannock River (Munday and Fedosh, 1980; Fedosh, 1984), and from the James River, identified by Ludwick (1973) as a bay plume sediment source. Some images in times of high discharge show river plumes entering the Bay from the Potomac River. It does not appear that much of this fluvial suspended sediment reaches the Bay mouth before settling.

Extended turbidity patterns probably involve considerable resuspension, for the following reasons: First, studies of sediment transport in general suggest that over long distances, large patterns of surface turbidity involve continuous cycles of settling and resuspension. In deep water, of course, resuspension is not effective, and turbidity decreases quickly with time and distance. Second, high fresh water flow at Washington, D.C. lowers salinity off the Bay mouth two months later (Howe, 1962), which suggests a very long persistence to different water masses despite tidal action, and therefore plenty of time for turbid Potomac waters to lose suspended sediment via settling before they reach the Bay mouth. For the James River, Hurricane Camille water required three days to reach Hampton Roads from Richmond (Elder, 1971), and slightly above-average fresh water flow at Richmond takes about six days to affect water heights at Hampton Roads. These delays indicate that turbid James River water would lose most suspended sediment to settling before reaching the Bay mouth under most conditions. Thus, the Bay plume turbidity results primarily from resuspension in the lower Bay. Only a few images showing a very strong turbidity extending all the way from the Hampton Roads area to the Bay mouth would indicate otherwise.

For ebb tide, the plume for northerly winds is tongue-shaped, but the shape is difficult to characterize further. Little was observed which would suggest rotary motion off Cape Henry as observed by Harrison et al. (1967).

For flood tide, turbidity boundaries are found closer to the bay mouth than ebb tide boundaries. Plumes close to the mouth and shore are smaller and lobate, while plumes away from the mouth have larger, more linear boundaries. Figure 10A is a composite of the boundaries during flood tide images, and Figure 11A is the corresponding sector-zone count map.

A striking feature of many flood-tide images is a strong turbidity pattern on the shallow northern side of the Bay mouth adjacent to Fisherman's Island. The pattern suggests higher current speeds on the northern side during flood tide, due to the Coriolis force. Analysis shows that the turbidity is relatively greater during flood tide and northeastern

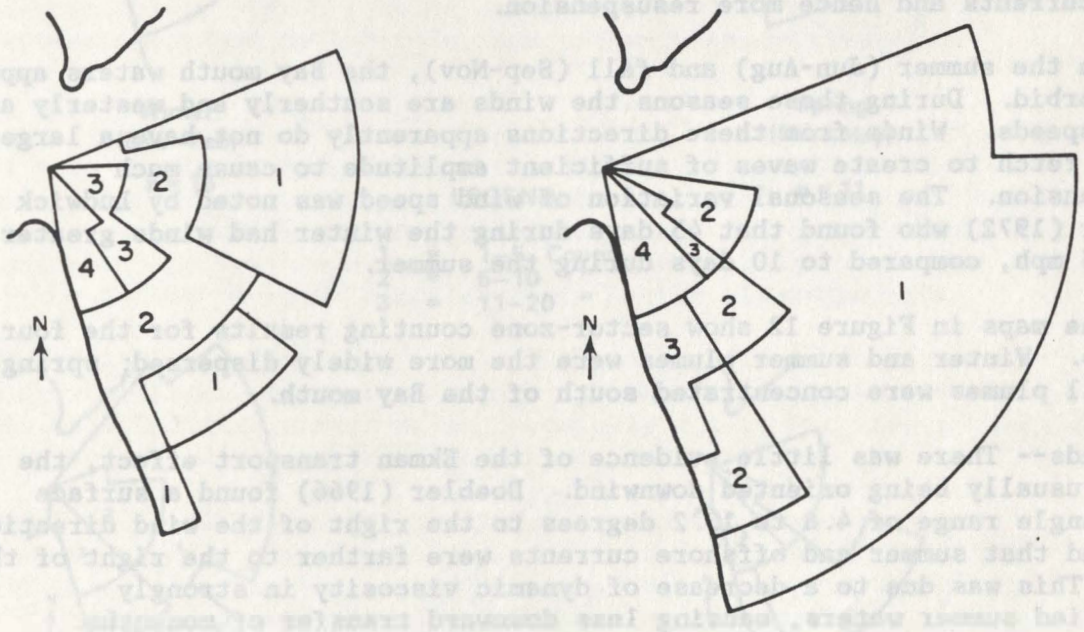

A. Flood Tide

B. Ebb Tide

LEGEND

1	=	1–5 Counts
2	=	6–10 "
3	=	11–20 "
4	=	21–30 "

Figure 11. Areas Visited by Turbidity Boundaries, Chesapeake Bay, According to Tidal Phase.

winds. No such patterns are observed for flood tide in the southern portion of the Bay mouth; in addition to the northward Coriolis deflection of flooding waters, the water in the southern portion is much deeper, reducing surface turbidities which originate in tidal scour.

Seasons-- Seasonal results are analyzed because of obvious interest, but it should be noted that it is the physical factors varying with the seasons, not the seasons per se, which influence plume behavior.

The Bay mouth waters are turbid (except over deeper channels) during winter (Dec-Feb) and spring (Mar-May). During these seasons the winds are mainly from the north, with higher than average wind speeds. The Bay axis, parallel to these winds, provides a long fetch allowing development of large waves which can mix the water column and stir up bottom sediment. The deeper water is not disturbed, hence less turbidity is found over the shipping channels (Fedosh, 1984). Doebler (1966) also found higher tides at the Bay mouth with northerly winds, which would be accompanied by greater tidal currents and hence more resuspension.

In the summer (Jun-Aug) and fall (Sep-Nov), the Bay mouth waters appear less turbid. During these seasons the winds are southerly and westerly at lower speeds. Winds from these directions apparently do not have a large enough fetch to create waves of sufficient amplitude to cause much resuspension. The seasonal variation of wind speed was noted by Ludwick and Melchor (1972) who found that 45 days during the winter had winds greater than 15 mph, compared to 10 days during the summer.

The maps in Figure 12 show sector-zone counting results for the four seasons. Winter and summer plumes were the more widely dispersed; spring and fall plumes were concentrated south of the Bay mouth.

Winds-- There was little evidence of the Ekman transport effect, the plumes usually being oriented downwind. Doebler (1966) found a surface drift angle range of 4.8 to 13.2 degrees to the right of the wind direction. He found that summer and offshore currents were farther to the right of the wind. This was due to a decrease of dynamic viscosity in strongly stratified summer waters, causing less downward transfer of momentum. Moderate winds had drift currents to the right of strong winds presumably because, in shallow waters, strong winds mix the water vertically and permit currents to "feel" the bottom.

Sorting the pass dates by wind quadrants, Qi, yields Q1=20 images, Q2=3, Q3=41, and Q4=17. Maps for wind quadrants 1, 3, and 4 are shown in Figure 13 (a map is omitted for quadrant 2 because of its low number of images). Quadrant 4 produced the tightest pattern along the Virginia-North Carolina coastline. Quadrant 3 (southwest winds) produced the most dispersed pattern (notice especially the visits to zones D-F (30-60 km outward) for sectors at 90 degrees).

To enhance the differences between results from different wind quadrants, ratios were formed of sector-zone counts using the data from quadrants 3 and 1, and then from 4 and 1. Each sector-zone's total count from a quadrant data set was adjusted upward by 1 count for each pass where no plume was discriminated, in order to avoid bias from neglect of images

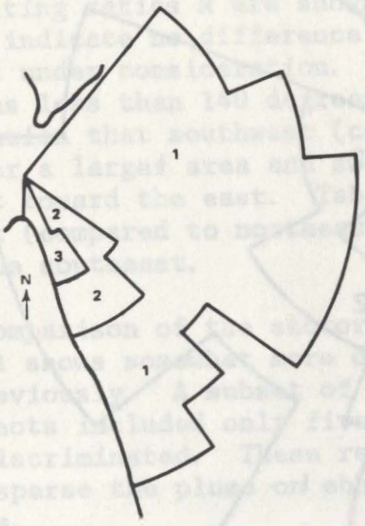

Winter
(Dec–Feb)
n = 15

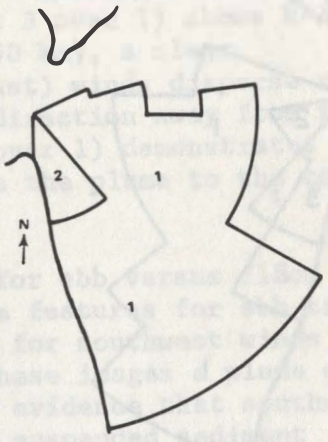

Spring
(Mar–May)
n = 11

LEGEND

1 = 1–5 Counts
2 = 6–10 "
3 = 11–20 "

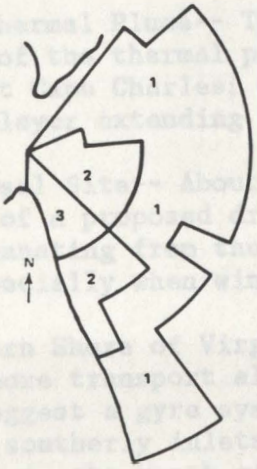

Summer
(Jun–Aug)
n = 17

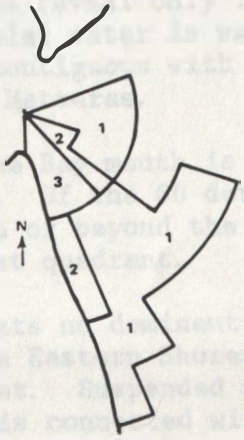

Fall
(Sept–Nov)
n = 18

Figure 12. Areas Visited by Turbidity Boundaries, Chesapeake Bay, According to Season.

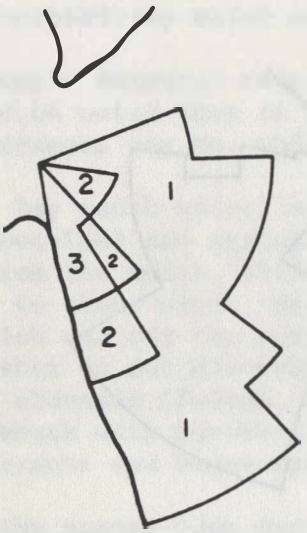

A. Quadrant 1

1°-90°

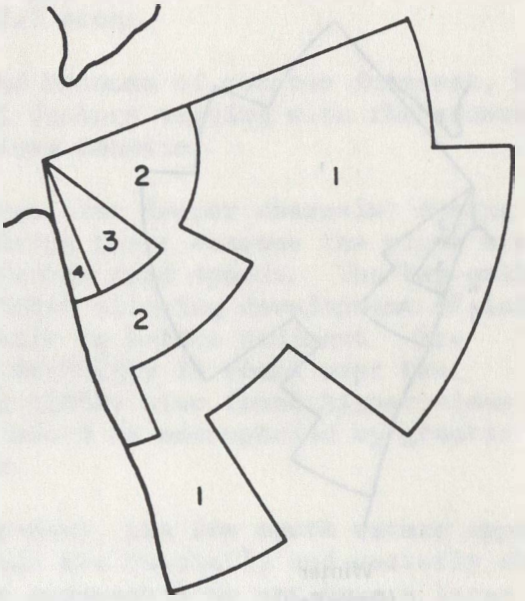

B. Quadrant 3

81°-270°

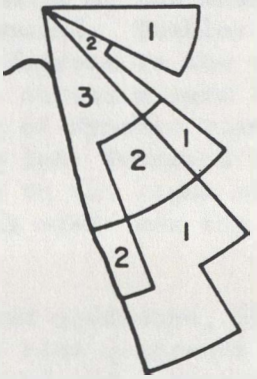

C. Quadrant 4

271°-360°

Figure 13. Areas Visited by Turbidity Boundaries, Chesapeake Bay, According to Wind Quadrant.

with uniform distributions of turbidity. The adjustment frequencies for each quadrant were small, being 1, 1, 6, and 0 respectively. The ratios of counts were formed, and then normalized for differences among the Qi values. The resulting ratios R are shown in Tables 2 and 3. Numerical values of R near 1.0 indicate no difference in effects of wind direction for the two quadrants under consideration. Table 2 (quadrant 3 over 1) shows R>1 for directions less than 140 degrees (zones B-E, 10-50 km), a clear demonstration that southwest (compared to northeast) winds disperse the plume over a larger area and swing its dominant direction away from the southeast toward the east. Table 3 (quadrant 4 over 1) demonstrates that northwest (compared to northeast) winds constrain the plume to the coastline toward the southeast.

A comparison of the sector-zone count maps for ebb versus flood tide in Figure 11 shows somewhat more dispersion of plume features for ebb tide, as noted previously. A subset of the ebb tide data for southwest winds higher than 8 knots included only five images, and in these images a plume could not be discriminated. These results are further evidence that southwest winds disperse the plume on ebb tide, and weaken suspended sediment gradients.

These effects of winds have been shown using vector-averaged Norfolk wind data from the 12 hours preceding the Landsat overpass. Because the shelf water relaxation time from wind effects is probably greater than 12 hours, longer wind records should probably be used. Also, Chesapeake Light Tower winds would perhaps be more appropriate than Norfolk winds for examining the effect of shelf water currents on the plume dynamics.

The Thermal Plume-- The small scale HCMM images reveal only large features of the thermal plume (see Figure 3). Cooler water is usually evident at Cape Charles; warmer water is usually contiguous with a coastal boundary layer extending southward nearly to Cape Hatteras.

Disposal Site-- About 30 km from the Chesapeake Bay mouth is the location of a proposed dredge spoil disposal site. Of the 60 detected plumes emanating from the bay, 16 (27%) are within or beyond the disposal area, especially when winds blow from the southwest quadrant.

Eastern Shore of Virginia-- The imagery suggests no dominant direction of longshore transport along the ocean-side of the Eastern Shore. Some images suggest a gyre system off Chincoteague Inlet. Suspended sediment from the southerly inlets, in flood tide images, is connected with extensive turbidity on the north side of the Bay mouth. The patterns suggest that early flood waters moving into the northern side of the Bay mouth carry residual suspended sediment from waters originating northward along the Eastern Shore, and additional material resuspended in the shallow areas adjacent to Fisherman's Island. If true, turbidity on the western side of the mouth (compared to the eastern side) should be relatively more frequent during flood, as flooding waters traverse the shallows of the mouth itself.

To test this hypothesis quantitatively using Landsat images, a counting procedure was employed based on the square grid shown in Figure 8. A cell was counted when turbidity in the cell was higher than background as judged visually. Counts were made for ebb and flood tide passes, and subset into

TABLE 2

NORMALIZED RATIOS OF TURBID BOUNDARY FREQUENCIES AT

CHESAPEAKE BAY ENTRANCE FOR WIND QUADRANT 3 OVER 1

Zone	Sector	6*	7	8	9	10	11	12	13	14	15	16
	Bay											
A	Entrance	1.46	1.46	1.46	1.27	0.91	0.98	1.12	0.92	0.77	0.83	0.84
B		∞	2.93	1.95	2.44	1.83	1.83	1.95	1.66	1.25	0.84	0.88
C		3.41	4.39	4.88	2.68	1.79	1.34	2.11	1.71	0.98	0.80	0.98
D		3.90	3.90	4.39	4.39	3.90	4.39	4.39	2.44	1.46	0.98	0.98
E	Away From Entrance	2.93	3.41	3.41	3.41	3.41	3.41	3.41	2.93	1.46	1.30	1.22
			Northeast		East							South

* 10° interval from 60° to 69°; similarly for all sectors.

TABLE 3

NORMALIZED RATIOS OF TURBID BOUNDARY FREQUENCIES AT

CHESAPEAKE BAY ENTRANCE FOR WIND QUADRANT 4 OVER 1

Zone	Sector	6	7	8	9	10	11	12	13	14	15	16
A	Bay Entrance	0	0	0	0.24	0.17	0.34	1.01	1.18	1.01	1.09	1.02
B			0	0	0.39	0.29	0.29	0	1.88	1.57	1.02	1.02
C					0	0	0	0	0.29	1.18	1.32	1.62
D									0	0.39	0.94	1.18
E	Away From Entrance									0	0.39	0.29
		Northeast			East							South

the four wind quadrants. Ratios of flood to ebb counts were formed and normalized for flood and ebb pass frequencies; the normalized ratios truncated to integers are shown in Figure 14A. Western cells are, as expected, relatively more frequented by turbidity than eastern cells during flood tide.

Truncated normalized ratios for the wind quadrants are shown in Figure 14B for Q1 over Q3, and in Figure 14C for Q1 over Q4 (Figure 14C numbers were multiplied by 2 before plotting). The figures demonstrate that northeastern winds are more effective than western winds in increasing eastern turbidities.

Patterns of turbidity in shallow water are strongly and immediately influenced by changes in wind direction and speed, because of resuspension and the coupling of surface currents to wind (see Doebler, 1966). On the ocean-side of the Eastern Shore, turbid water is found often in areas less than 10 m deep, the amount of turbidity varying with wind speed. Off Ocean City, Maryland, inlet plumes are oriented in the wind direction.

DELAWARE BAY

The Bay-- The mouth of the Delaware Bay is similar to the mouth of the Chesapeake Bay in shape and depth. However, in the Delaware Bay there is no fluvial source close to the mouth (see Oostdam, 1971), as in the Chesapeake Bay with the nearby James River and other bay tributaries. Also, the Delaware Bay proper has a different shape and compass orientation, with more sensitivity to the prevailing northwest winds. Finally, the Delaware has a large shallow embayment in its northeast segment, characterised by a bottom clay outcrop of the Cape May formation (Kelly, 1983), which produces considerable suspended sediment. The corresponding region of the Chesapeake Bay consists of a deep channel aligned with the bay axis. These differences in the Delaware Bay produce different circulation and turbidity patterns, as evidenced in Landsat images previously studied by Klemas and Polis (1977).

The Turbid Plume-- Outside the bay mouth, the plumes differ from Chesapeake Bay plumes, turbidity often being found in two prominent bands, one off each cape, separated by relatively clear water (Figure 15).

The Cape May turbid zone, on the north side of the mouth, is usually very large, extending almost 70% of the distance across the bay mouth. This zone varies considerably in size, sometimes extending to the northeast embayment, often extending southeasterly onto the shelf, and sometimes extending northeasterly to the second or third tidal inlet along the New Jersey ocean coast. In late ebb and early flood, this turbidity is found more seaward.

The Cape Henlopen turbid zone on the south is an order of magnitude smaller in area, and more linear, oriented southeast from the cape. This turbid plume veers south, affected by the Coriolis force (Ketchum, 1953) and net non-tidal southerly flow along the coast. The southerly direction of flow at the shoreline is indicated by the shape of small plumes from tidal inlets clearly visible on the images. Plume fronts are noticed further south during flood tide.

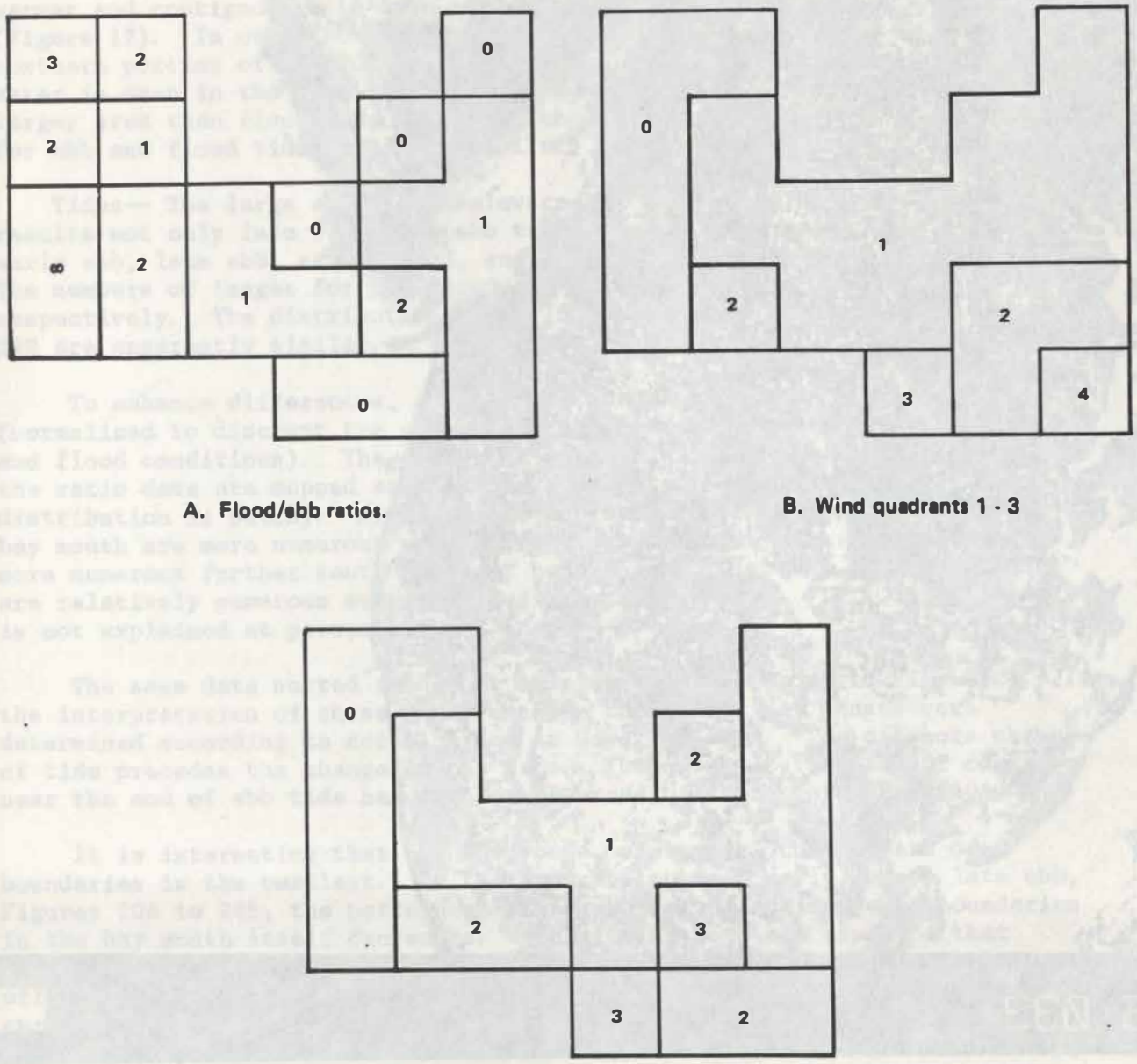

A. Flood/ebb ratios.

B. Wind quadrants 1 - 3

C. Wind quadrants 1 - 4.
(ratios x 2)

Figure 14. Relative Turbidity Near Cape Charles.
Frequency ratio for each grid cell normalized and truncated.

Figure 15. Landsat Image of Delaware Bay.

A composite diagram for all Delaware Bay plumes detected in Landsat imagery is shown in Figure 16. There is a nearly equal distribution of boundaries off Cape May and Cape Henlopen. Turbid boundaries extend further seaward and are more dispersed than thermal boundaries.

The Thermal Plume-- Thermal details in some HCMM images show three bands across the mouth, which correspond to the turbid zones; the central band is warmer and contiguous with warm waters along the entire axis of the bay (Figure 17). In other HCMM images, cooler ocean water is seen in the northern portion of the mouth on flood tide, while on ebb tide, warmer bay water is seen in the south around Cape Henlopen. Ebb tide plumes cover a larger area than flood tide plumes. The distributions of thermal boundaries for ebb and flood tide cases are similar, as shown in Figure 18.

Tides-- The large amount of Delaware Bay imagery permitted a sorting of results not only into flood and ebb tidal phases (Figure 19), but also into early ebb, late ebb, early flood, and late flood tidal phases (Figure 20). The numbers of images for the flood and ebb cases are 54 and 57 respectively. The distributions for flood and ebb shown in Figures 19A and 19B are apparently similar.

To enhance differences, a ratio was formed of ebb to flood counts (normalized to discount the effect of the differing number of images for ebb and flood conditions). The resulting distribution is shown in Table 4, and the ratio data are mapped as a binary display in Figure 19C. The distribution is patchy. Although the ebb-related boundaries close to the bay mouth are more numerous on the southern side, they are not uniformly more numerous further south as might be expected. Instead, ebb boundaries are relatively numerous at moderate distances eastward. This irregularity is not explained at present.

The same data sorted into four tidal phases are shown in Figure 20. In the interpretation of these maps remember that the tidal phases were determined according to actual tides at Cape Henlopen. The offshore change of tide precedes the change at the Cape. Therefore, relaxation of current near the end of ebb tide has already occurred offshore for Figure 20A.

It is interesting that for this case, early ebb, the pattern of boundaries is the smallest. In the progression from early ebb to late ebb, Figures 20A to 20B, the pattern enlarges, while the incidence of boundaries in the bay mouth itself decreases. Speculating, one can envision that during this time, boundaries may be developing at the greater distances offshore, where currents have turned to flood. At the mouth, where ebb currents are diminishing, turbidity boundaries may be weakening due to settling of particulates. More information is needed on tide-current relationships seaward of the bay mouth, and in particular, whether rotary current fields are present, plus the relative strengths of tidal currents versus net non-tidal currents.

The early flood pattern in Figure 20C is very similar to that for late ebb in Figure 20B. But in later flood, Figure 20D, the pattern has shrunk considerably, and the incidence of boundaries within 15 km of the mouth has substantially increased. Again, one may speculate that the higher current speeds of late flood near the mouth have produced or strengthened turbid boundaries.

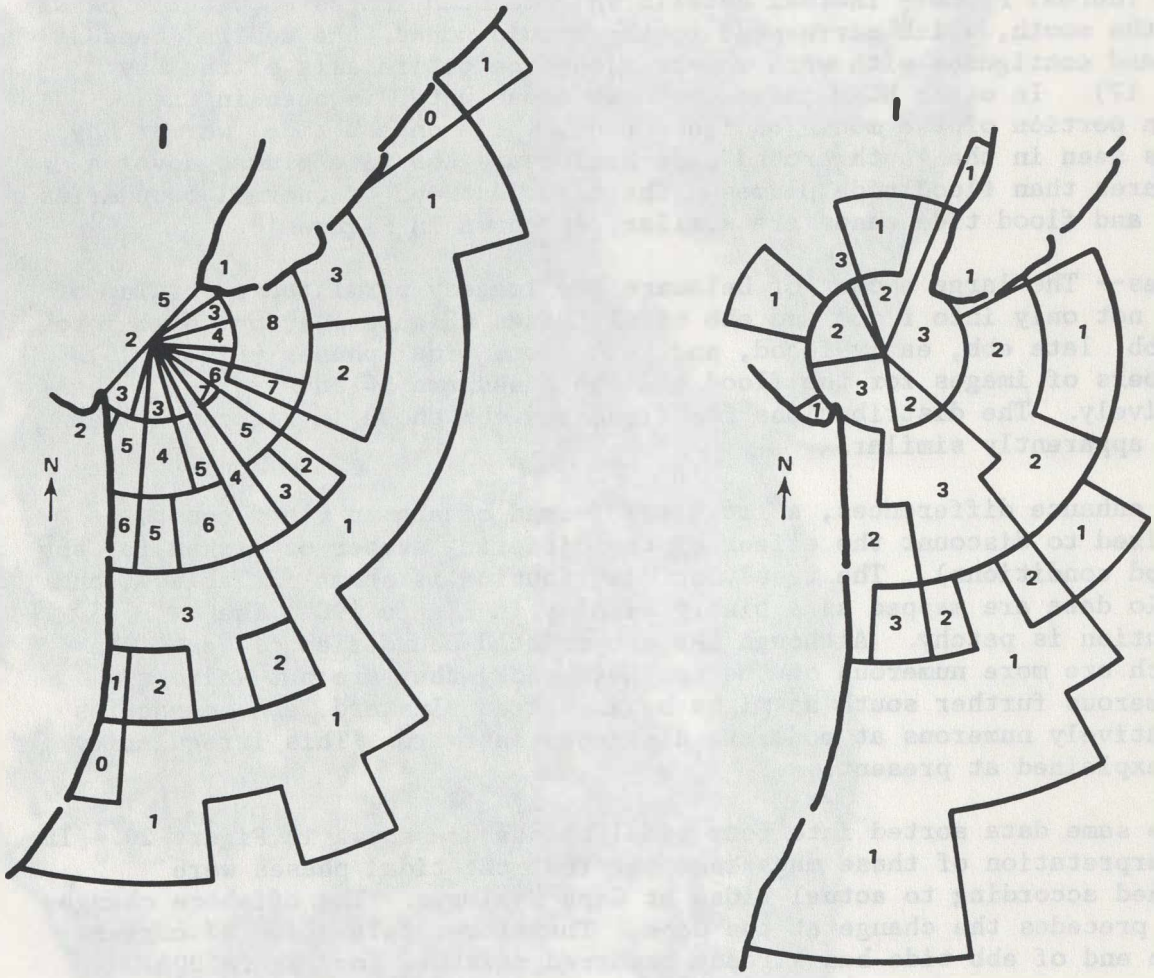

Landsat

HCMM

LEGEND

1	=	1–5 Counts
2	=	6–10 "
3	=	11–20 "
4	=	21–30 "
5	=	31–40 "
6	=	41–50 "
7	=	51–60 "
8	=	61–70 "

Figure 16. Composite of Turbidity and Thermal Boundaries from all Landsat and HCMM Images of Delaware Bay.

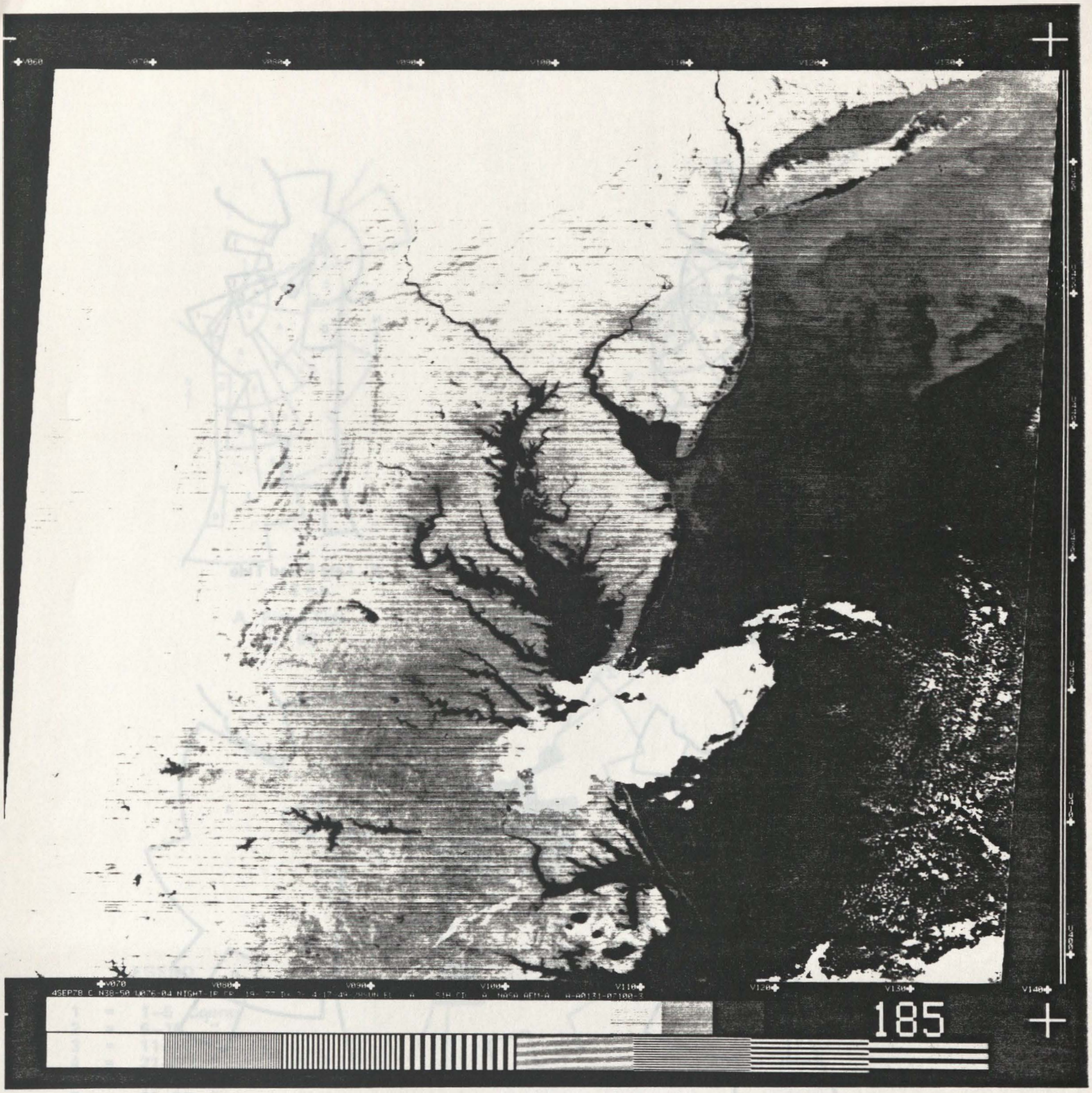

Figure 17. HCMM Image of Delaware Bay and New York Bight.

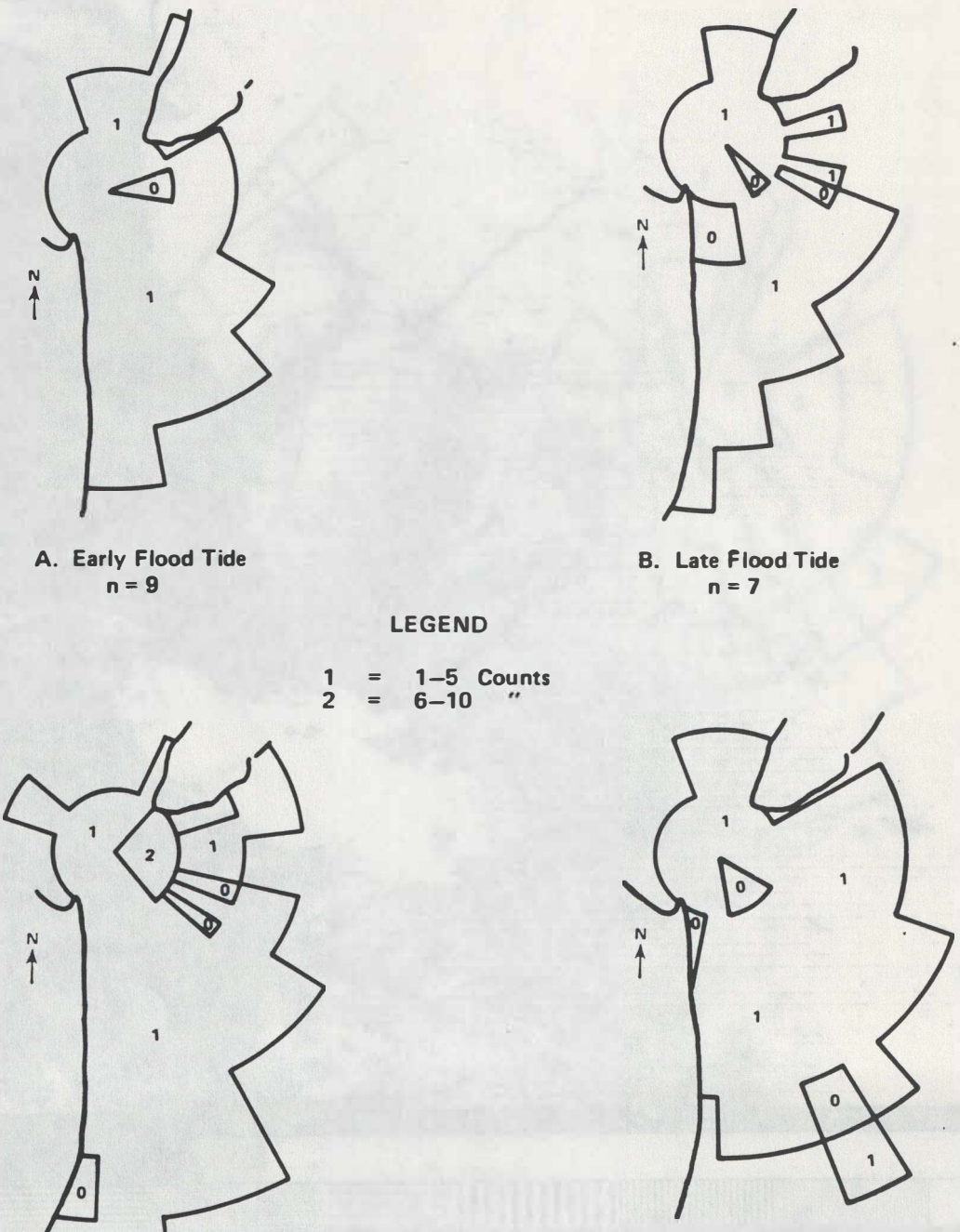

Figure 18. Areas Visited by Thermal Boundaries According to Tidal Phase from HCMM Images of Delaware Bay.

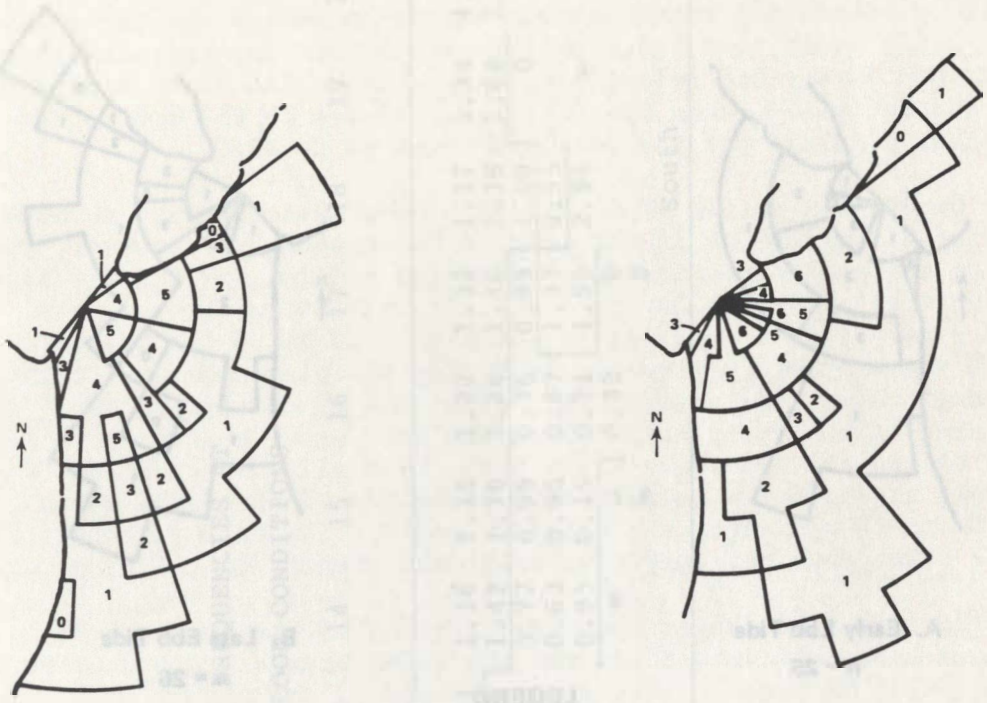

A. Flood Tide
n = 53

B. Ebb Tide
n = 59

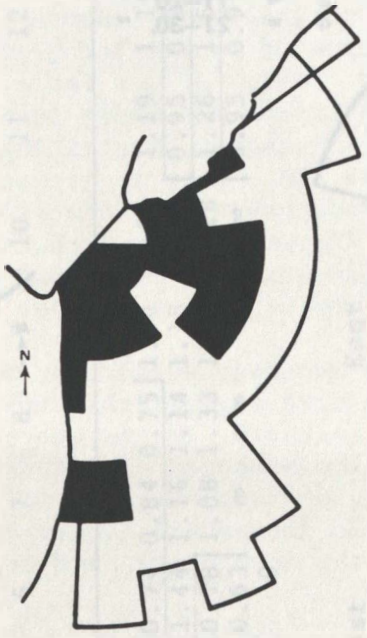

LEGEND

1 = 1–5 Counts
2 = 6–10 "
3 = 11–20 "
4 = 21–30 "
5 = 31–40 "
6 = 41–50 "

C. Normalized ratio of ebb to flood tide visits;
filled spaces = ratio exceeding unity

Figure 19. Areas Visited by Turbidity Boundaries, Delaware Bay, Sorted According to Binary Tidal Phase.

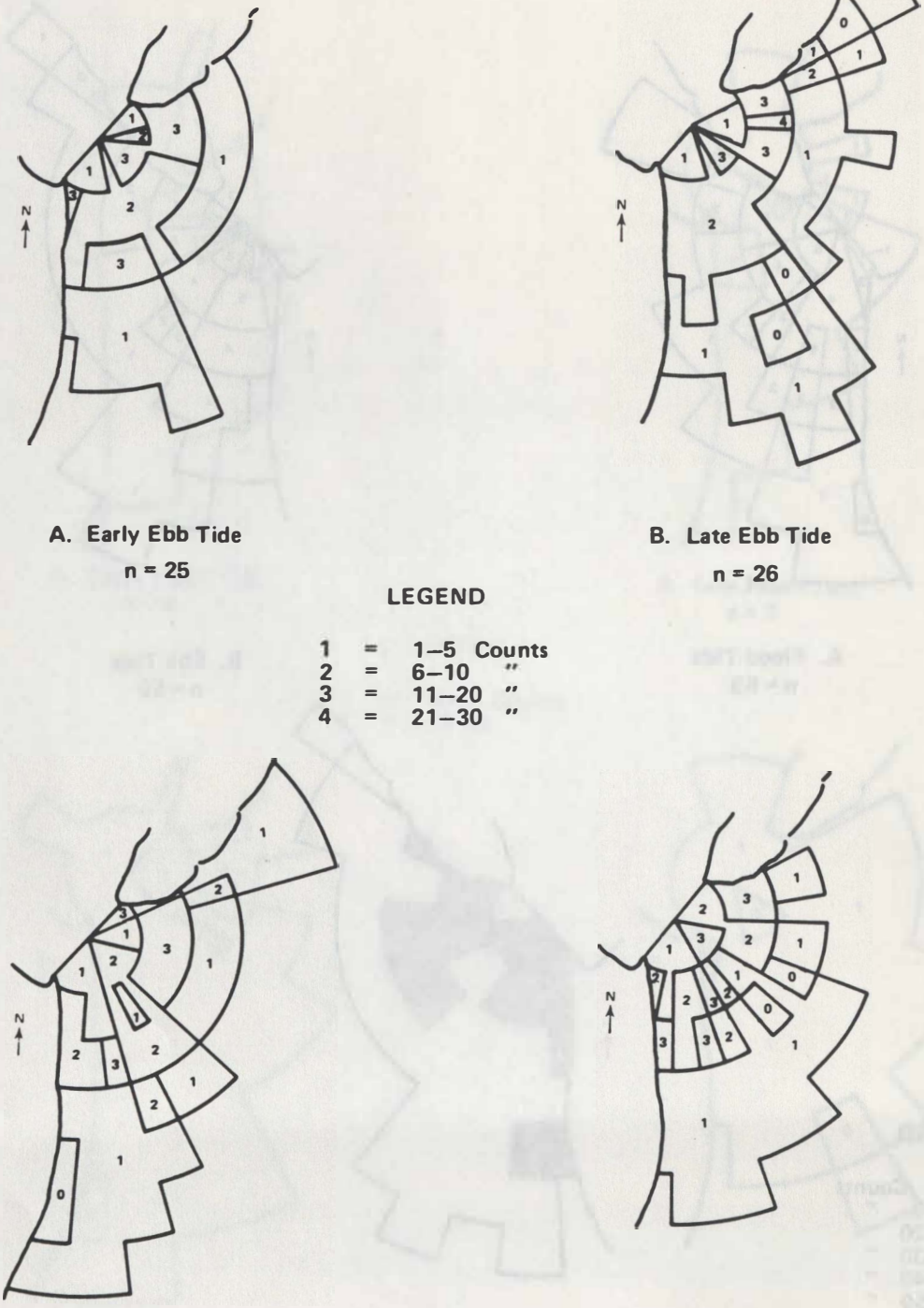

Figure 20. Areas Visited by Turbidity Boundaries, Delaware Bay, Sorted According to Quadrature Tidal Phase.

TABLE 4

NORMALIZED RATIOS OF TURBID BOUNDARY FREQUENCIES AT

DELAWARE BAY ENTRANCE FOR EBB OVER FLOOD CONDITIONS

Zone	Sector	4	5	6	7	8	9	10	11	12	13	14	15	16	17	18	19	20
A	Bay Entrance	0	0.58	0.74	0.84	0.75	1.04	1.21	1.19	1.15	1.21	1.16	1.15	1.22	1.32	1.17	1.34	4.26
B			1.54	1.44	1.16	1.14	1.15	1.07	0.95	0.99	0.99	1.42	1.30	1.24	1.46	1.38	1.68	2.37
C			1.08	0.78	1.08	1.33	1.89	1.18	1.26	1.58	0.74	0.77	0.99	0.76	0.95	1.08	0	
D			0.32	0.63	∞	∞	∞	∞	0.95	0.95	0.63	0.63	0.95	0.87	1.37	0.95		
E			0.95	0								0.95	0.19	0.71	1.58	2.84	∞	
F		∞										∞	∞	0.32	0			
G	Away From Entrance		Northeast				East						∞		0	South		

The turbid boundaries reach maximum extension beyond the bay mouth in late ebb to early flood, and these maximum extensions are confined to within 20 km of the New Jersey and Delaware coasts. During the other tidal phases, late flood and early ebb, when boundaries are closer to the mouth, the southern region slightly off the Delaware coast is favored.

Winds-- Seaward extension of turbidity plumes does not vary as much with different wind directions as in the case of Chesapeake Bay; however, the distributions for wind directions are otherwise similar for the two Bays. Figure 21 shows the Delaware Bay patterns for the four wind quadrants. The majority of plumes remain parallel to and within 20 km of the Delaware coast. With westerly and northwesterly winds, the plumes extend further south, although not as far seaward as in the case of Chesapeake Bay. The Cape May plumes often extend north along the New Jersey coast. In a few cases under strong northwesterly winds there is negligible turbidity along the New Jersey coast, and a large turbid plume the width of the mouth extends 40 km southward along the Delaware coast. The eastern extent of this type of plume does not vary regularly with respect to the tidal phase.

The large number of images permitted sorting of the images for different wind quadrants into flood and ebb tidal phases. The results are shown in Figure 21 (2 Pages). For wind quadrant 4, the number of images for each tidal phase is large. Turbid boundaries are seen very far south along the coast of Delaware in the case of flood tide.

To compare the impact of northeastern (quadrant 1) winds with western winds (quadrants 3 and 4), ratios of counts for Q1/Q3 and Q1/Q4 were prepared as explained earlier. Tables of the ratio data are presented in Tables 5 and 6, and the distributions are shown in Figures 22A and 22B. The three-part division of the bay discharge is strikingly shown in both figures, particularly in Figure 22A. Here it is seen that northeastern winds are more effective than southwestern winds (180 degrees opposite) in producing coastal turbidity. Figure 22B shows that northeastern winds are more effective than northwestern winds in producing turbidity at the Bay entrance, the Cape May shore, and far south but set off the Delaware coast.

Seasons-- Seasonal effects are even weaker for the Delaware plume than for the Chesapeake plume. The data suggest that turbidity zones are larger in area, and extended farther eastward, in the winter when north and northwest winds predominate. The seasonal distributions of turbidity boundaries are shown in Figure 23; those for thermal boundaries are shown in Figure 24. Plume fronts on HCMM images are closer to shore during summer, when winds are weak (but from the southwest), and fresh water discharge is low.

Disposal Site-- Sixty kilometres southeast of Delaware Bay is an acid waste disposal site. Of the 139 plume boundaries, none reach the area, the closest being 30 km away.

NEW YORK BAY

The Turbid Plume-- In the Landsat images of Lower New York Bay and the adjacent New York Bight there were 38 turbid plumes detected visually, and an additional 16 (30% of the total) discovered in the enhancements. The

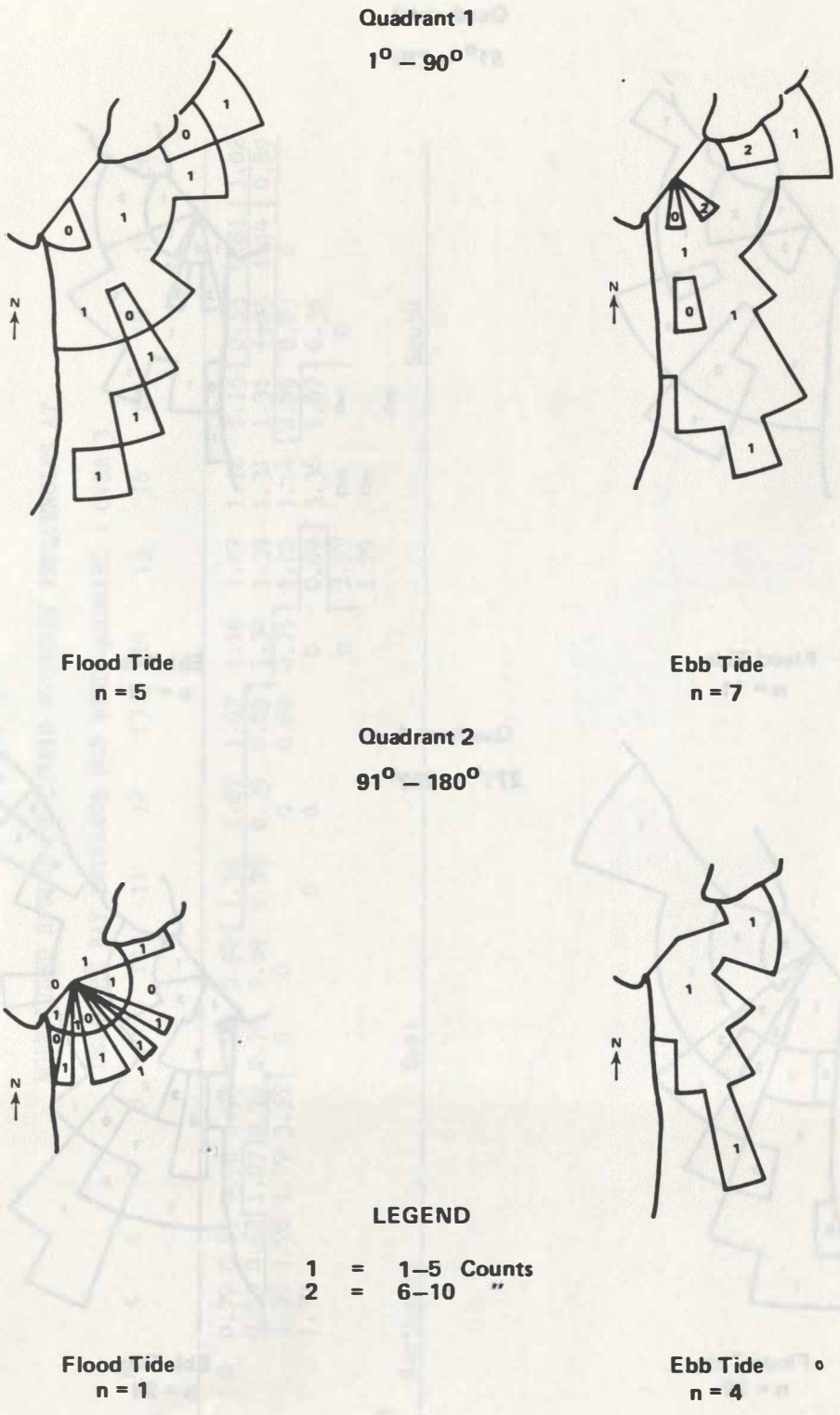

Figure 21. Areas Visited by Turbidity Boundaries, Delaware Bay, According to Wind Quadrant and Binary Tidal Phase.

Quadrant 3

$81^{o} - 270^{o}$

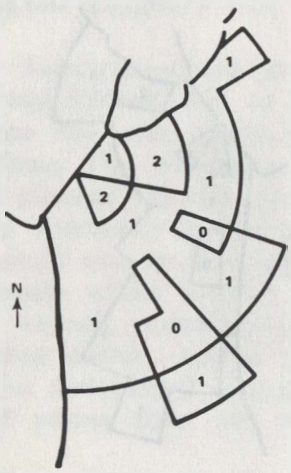

Flood Tide
n = 11

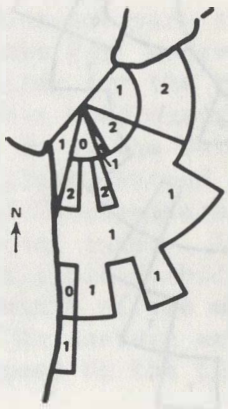

Ebb Tide
n = 11

Quadrant 4

$271^{o} - 360^{o}$

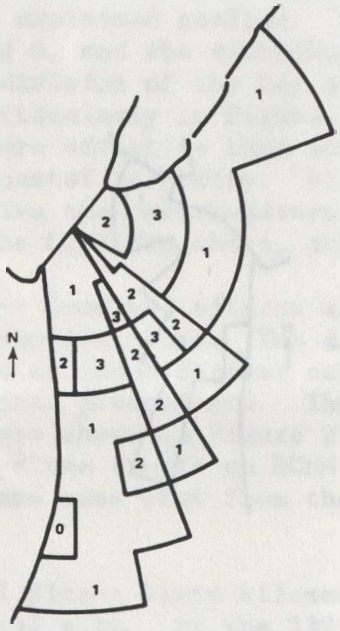

Flood Tide
n = 26

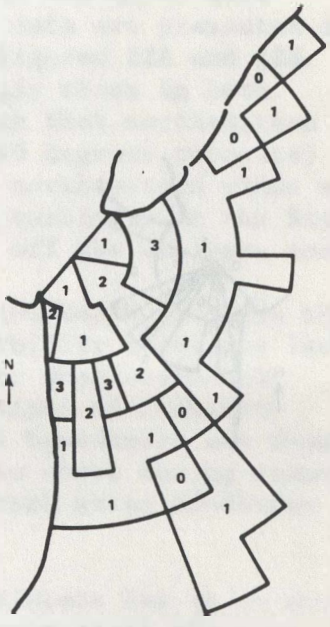

Ebb Tide
n = 24

Figure 21 (Cont.). Areas Visited by Turbidity Boundaries, Delaware Bay, According to Wind Quadrant and Binary Tidal Phase.

TABLE 5

NORMALIZED RATIOS OF TURBID BOUNDARY FREQUENCIES AT

DELAWARE BAY ENTRANCE FOR WIND QUADRANT 1 OVER 3

Zone	Sector	4	5	6	7	8	9	10	11	12	13	14	15	16	17	18	19	20
A	Bay Entrance	0	0.79	0.81	0.96	0.95	0.89	0.94	1.19	1.07	1.07	1.16	1.19	1.12	1.15	0.55	0.81	1.02
B			0.85	0.62	1.07	0.94	0.74	0.69	0.99	0.79	0.89	1.34	1.30	1.31	1.31	1.05	1.14	0.89
C			5.36	1.78	1.79	3.57	0	0		0	0.89	0.71	1.28	1.14	0.89	0.89	0	
D			1.79						0	0		0	0.89	5.36	1.07	0.36		
E												0	3.57	∞	∞	0		
F													1.79	∞				
G	Away From Entrance														∞			
		Northeast					East									South		

TABLE 6

NORMALIZED RATIOS OF TURBID BOUNDARY FREQUENCIES AT

DELAWARE BAY ENTRANCE FOR WIND QUADRANT 1 OVER 4

Zone	Sector	4	5	6	7	8	9	10	11	12	13	14	15	16	17	18	19	20
A	Bay Entrance	0	0.81	1.02	1.24	1.42	1.22	1.36	1.53	1.44	1.51	1.47	1.48	1.45	1.59	0.74	1.07	2.71
B			1.05	0.70	1.25	1.13	0.75	0.55	0.66	0.60	0.63	1.06	1.16	2.24	2.24	1.85	2.19	2.04
C			1.53	1.11	2.04	1.36	0	0	0	0	0.37	0.39	0.68	0.86	0.68	0.60	0	
D			2.04	1.02	0	0	0				0	0	0.37	0.80	1.11	0.81		
E			0	0								0	2.04	1.36	0.81	0	0	
F		0										0	4.07	1.36	0			
G	Away From Entrance												0		2.04			
		Northeast					East									South		

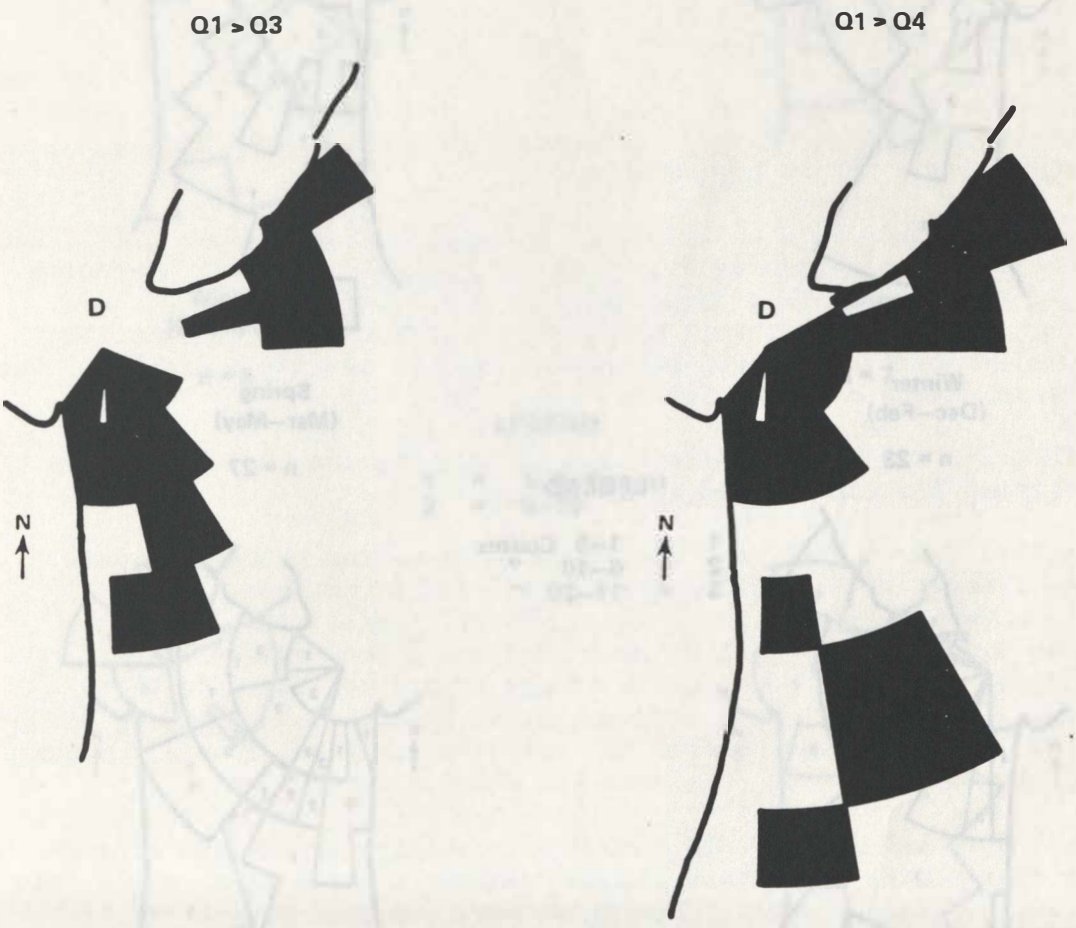

A: Quadrant 1 to Quadrant 3.

B: Quadrant 1 to Quadrant 4.

Figure 22. Ratios of Wind Quadrant Results for Delaware Bay Landsat Images.
Black areas indicate a higher occurrence of plume fronts during Quadrant 1 winds.

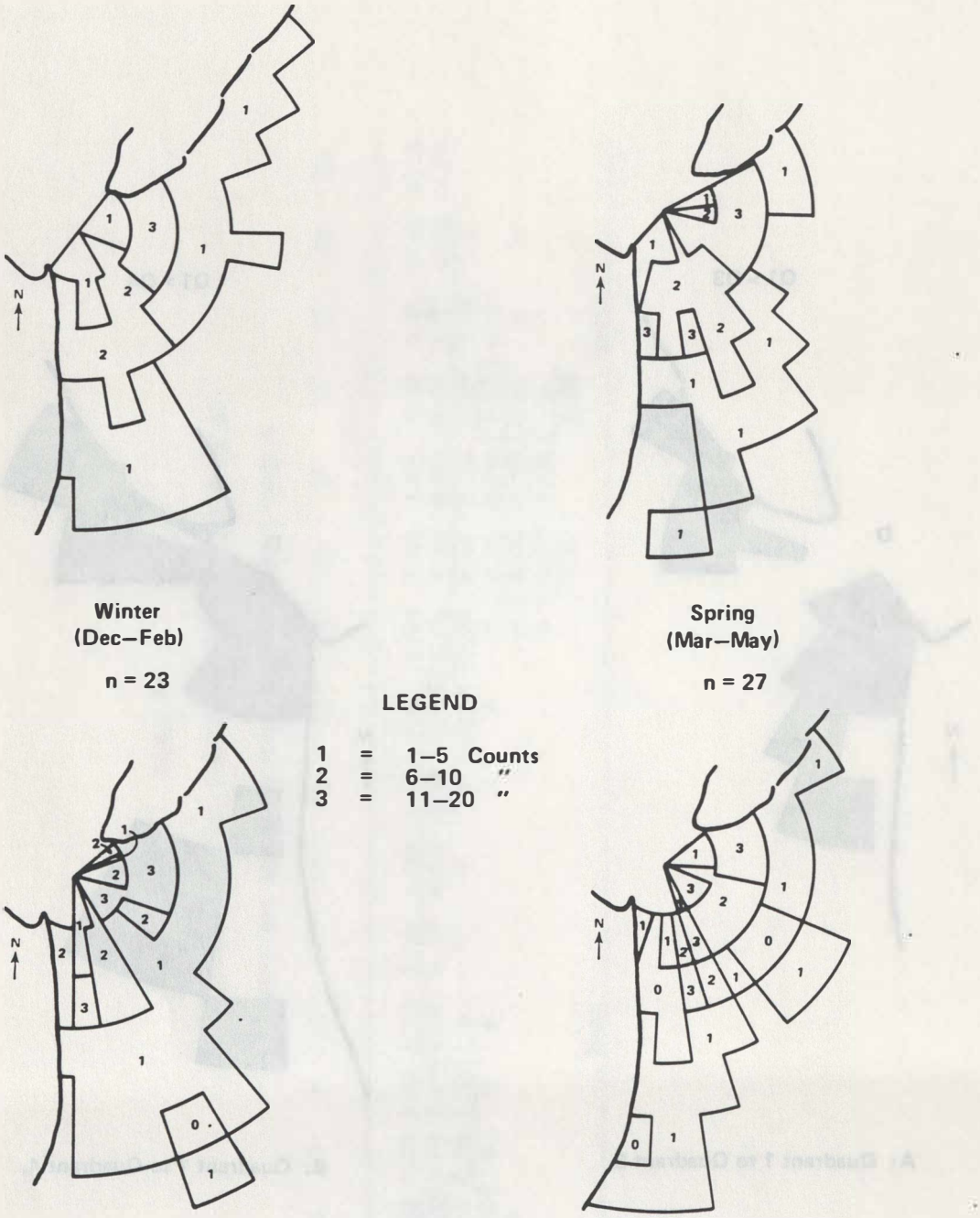

Figure 23. Areas Visited by Turbidity Boundaries, Delaware Bay, According to Season.

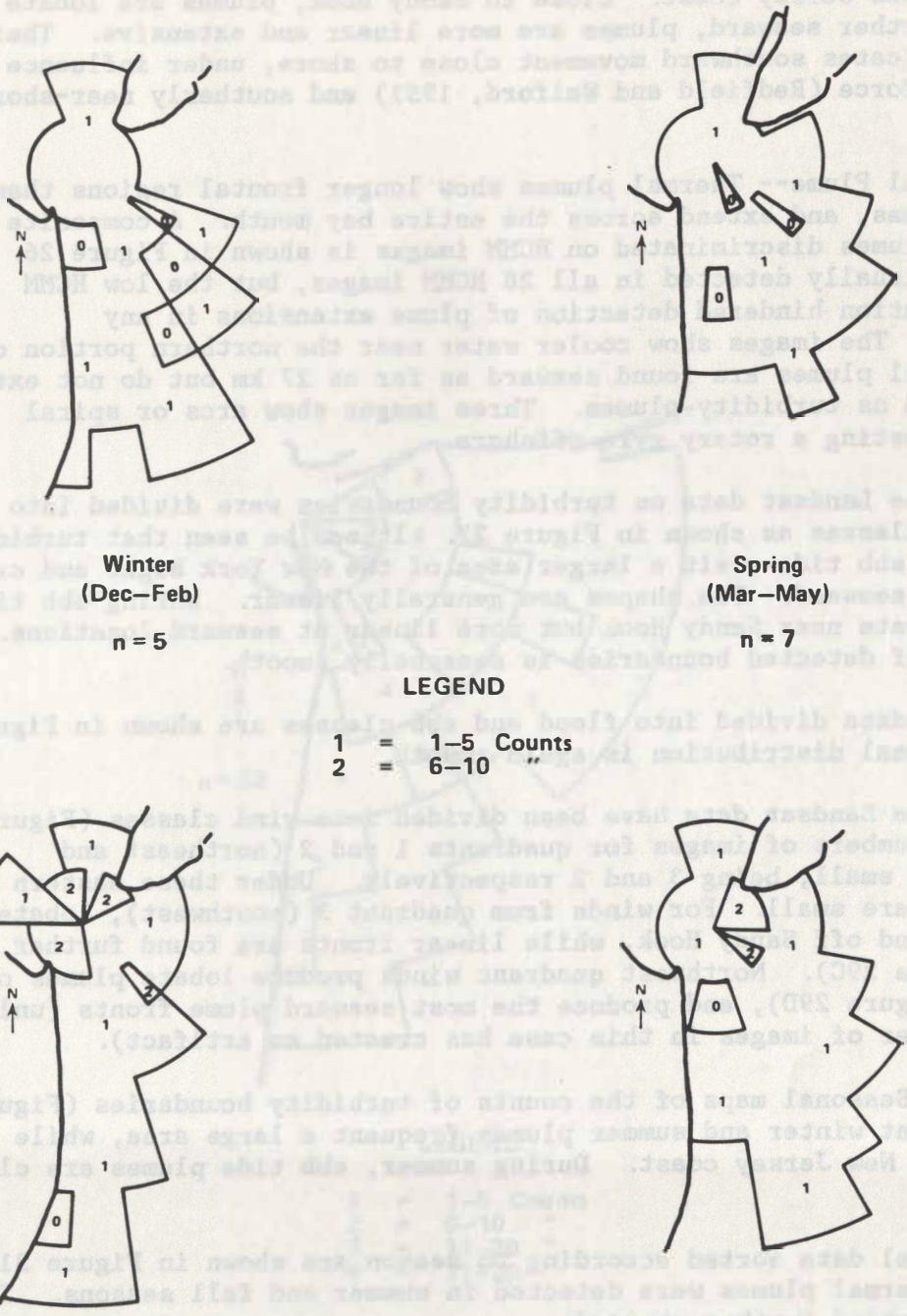

Figure 24. Areas Visited by Thermal Boundaries (HCMM), Delaware Bay, According to Season.

distribution of turbidity boundaries from all the images is shown in Figure 25. The pattern is dispersed, but the greater concentration of boundaries is along the New Jersey coast. Close to Sandy Hook, plumes are lobate in shape, but further seaward, plumes are more linear and extensive. Their curvature indicates southward movement close to shore, under influence of the Coriolis force (Redfield and Walford, 1951) and southerly near-shore currents.

The Thermal Plume-- Thermal plumes show longer frontal regions than the turbidity plumes, and extend across the entire bay mouth. A composite of the thermal plumes discriminated on HCMM images is shown in Figure 26. Plumes were visually detected in all 28 HCMM images, but the low HCMM spatial resolution hindered detection of plume extensions in any enhancements. The images show cooler water near the northern portion of the mouth. Thermal plumes are found seaward as far as 27 km but do not extend as far seaward as turbidity plumes. Three images show arcs or spiral features suggesting a rotary gyre offshore.

Tides-- The Landsat data on turbidity boundaries were divided into flood and ebb tide classes as shown in Figure 27. It can be seen that turbidity plumes during ebb tide visit a larger area of the New York Bight and are found farther seaward. The shapes are generally linear. During ebb tide, shapes are lobate near Sandy Hook but more linear at seaward locations. The distribution of detected boundaries is seasonally smooth.

The HCMM data divided into flood and ebb classes are shown in Figure 28. The seasonal distribution is again smooth.

Winds-- The Landsat data have been divided into wind classes (Figure 29), but the numbers of images for quadrants 1 and 2 (northeast and southeast) are small, being 3 and 2 respectively. Under these eastern winds, plumes are small. For winds from quadrant 3 (southwest), lobate plumes are found off Sandy Hook, while linear fronts are found further seaward (Figure 29C). Northwest quadrant winds produce lobate plumes off Sandy Hook (Figure 29D), and produce the most seaward plume fronts (unless the large number of images in this case has created an artifact).

Seasons-- Seasonal maps of the counts of turbidity boundaries (Figure 30) suggest that winter and summer plumes frequent a large area, while fall plumes hug the New Jersey coast. During summer, ebb tide plumes are close to Sandy Hook.

The thermal data sorted according to season are shown in Figure 31. Most of the thermal plumes were detected in summer and fall seasons. The summer cases extend further seaward.

The frequency distribution of plumes during the months of the year is smooth, as seen in Figures 32 and 33 for turbidity and thermal plumes respectively.

Disposal Sites-- Disposal sites for dredge spoil, sewage sludge, and acid waste are located roughly 25, 35, and 45 km southeast, respectively, from the New York Bay mouth, as shown in Figure 34. The sites and their exact locations are discussed by Gunnerson and Swanson (1975) and EPA

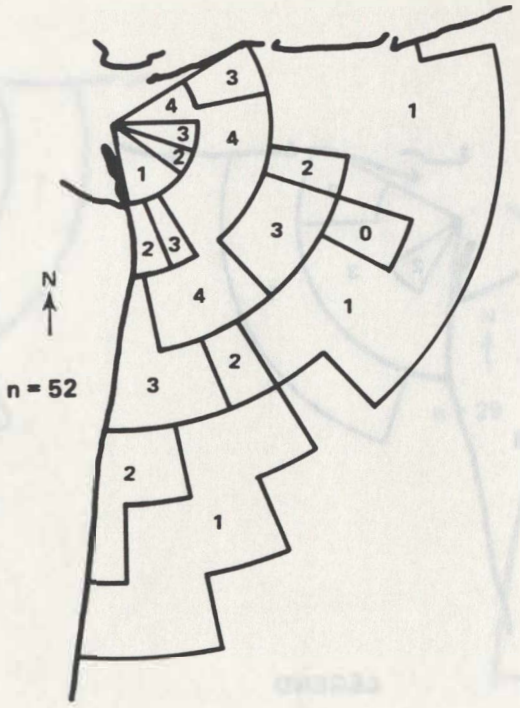

LEGEND

1 = 1–5 Counts
2 = 6–10 "
3 = 11–20 "
4 = 21–30 "

Figure 25. Composite of Turbidity Boundaries Extracted from All Landsat Images of New York Bight.

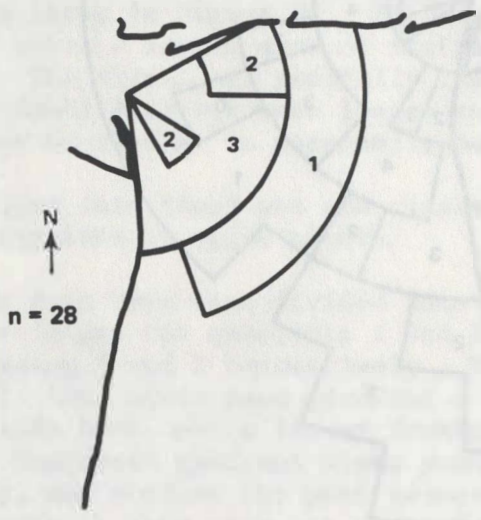

LEGEND

1 = 1–5 Counts
2 = 6–10 "
3 = 11–20 "

Figure 26. Composite of Thermal Boundaries Extracted from All HCMM Images of New York Bight.

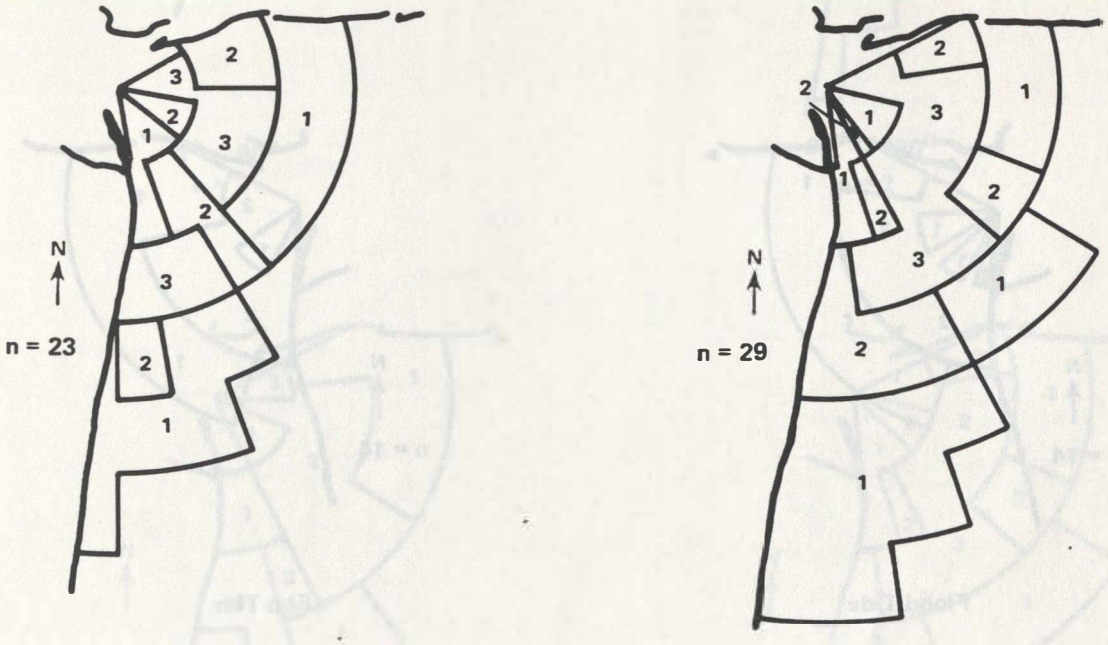

Figure 27. Areas Visited by Turbidity Boundaries, New York Bight, According to Tidal Phase.

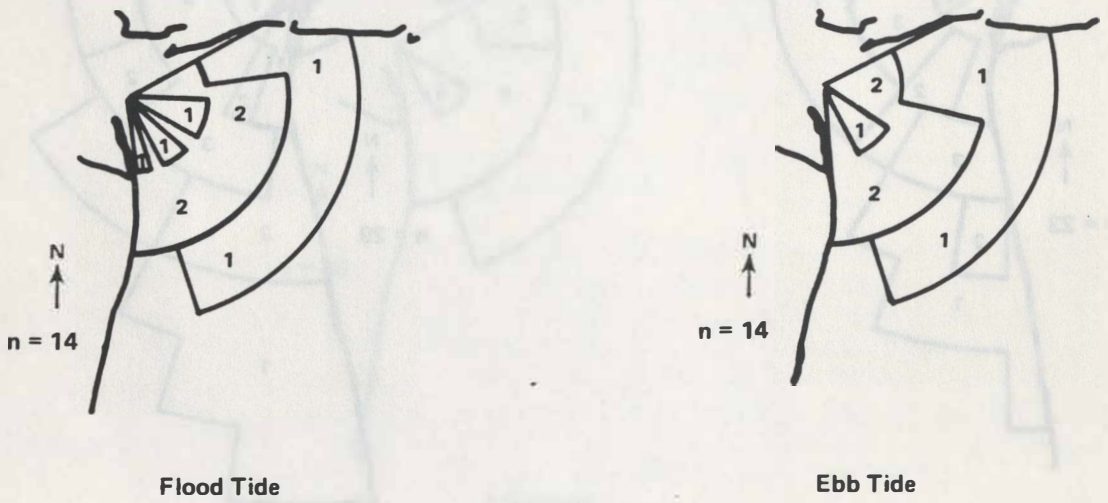

LEGEND

1 = 1–5 Counts
2 = 6–10 "

Figure 28. Areas Visited by Thermal Boundaries (HCMM), New York Bight, According to Tidal Phase.

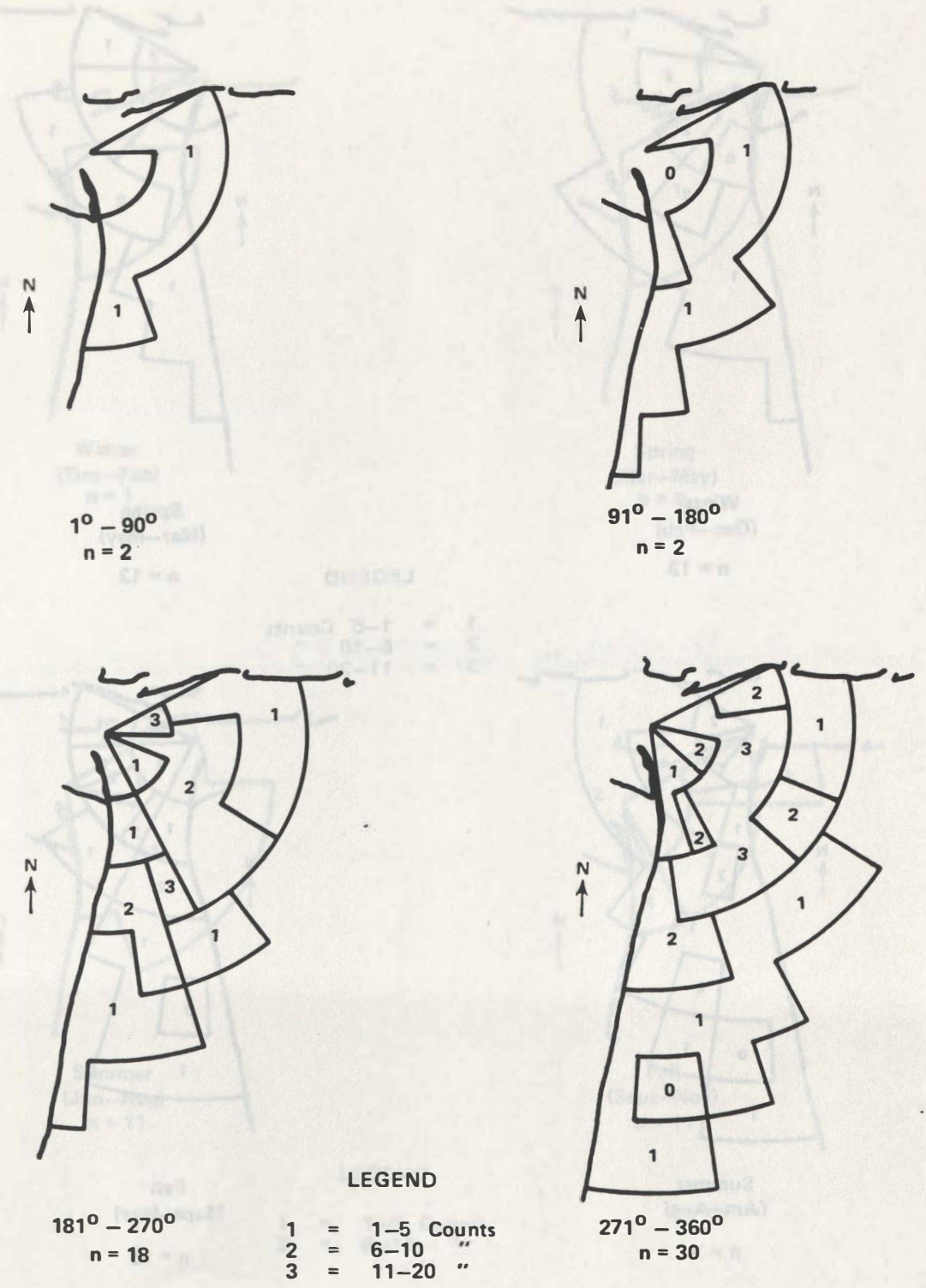

Figure 29. Areas Visited by Turbidity Boundaries, New York Bight, According to Wind Quadrant.

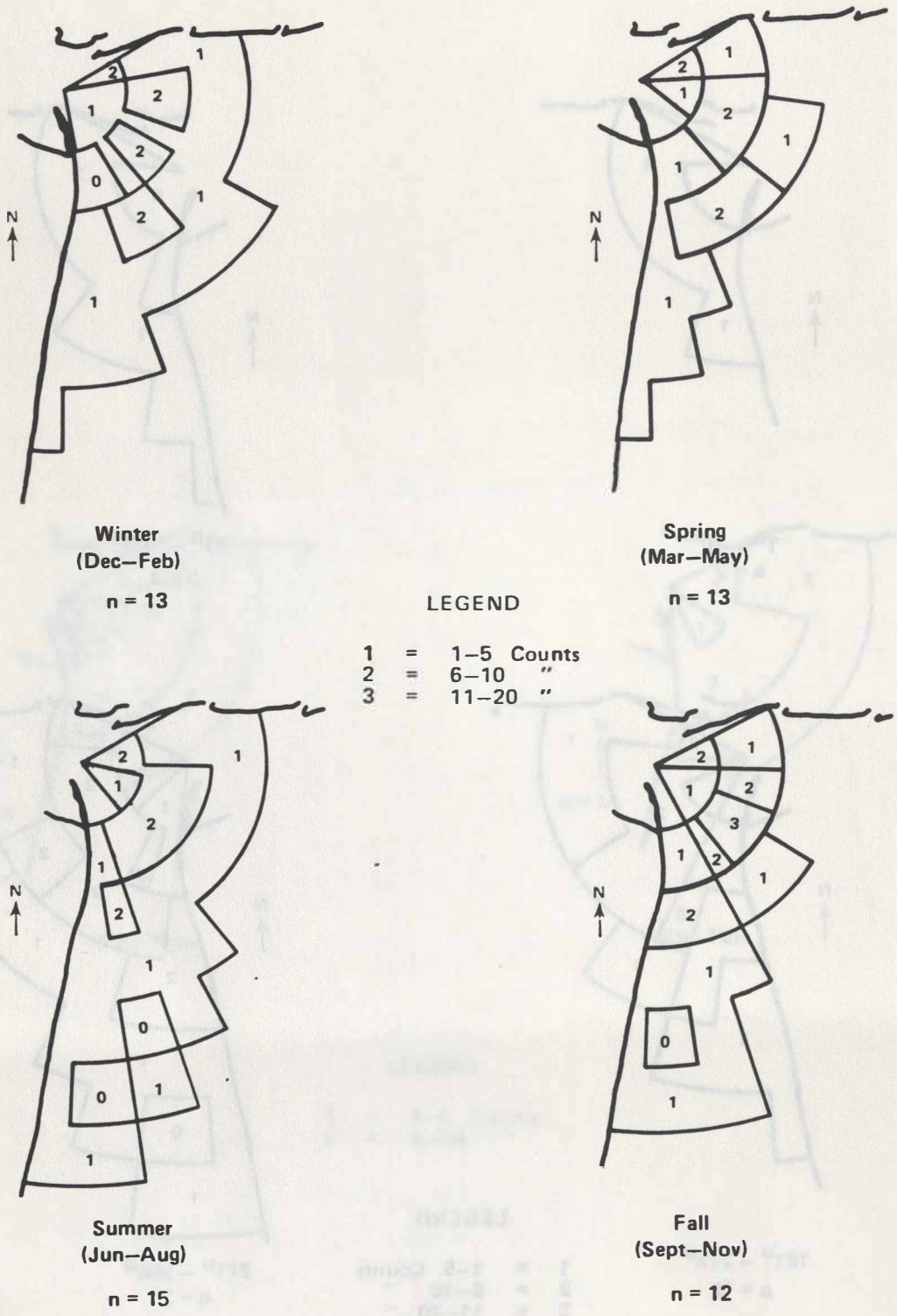

Figure 30. Areas Visited by Turbidity Boundaries, New York Bight, According to Season.

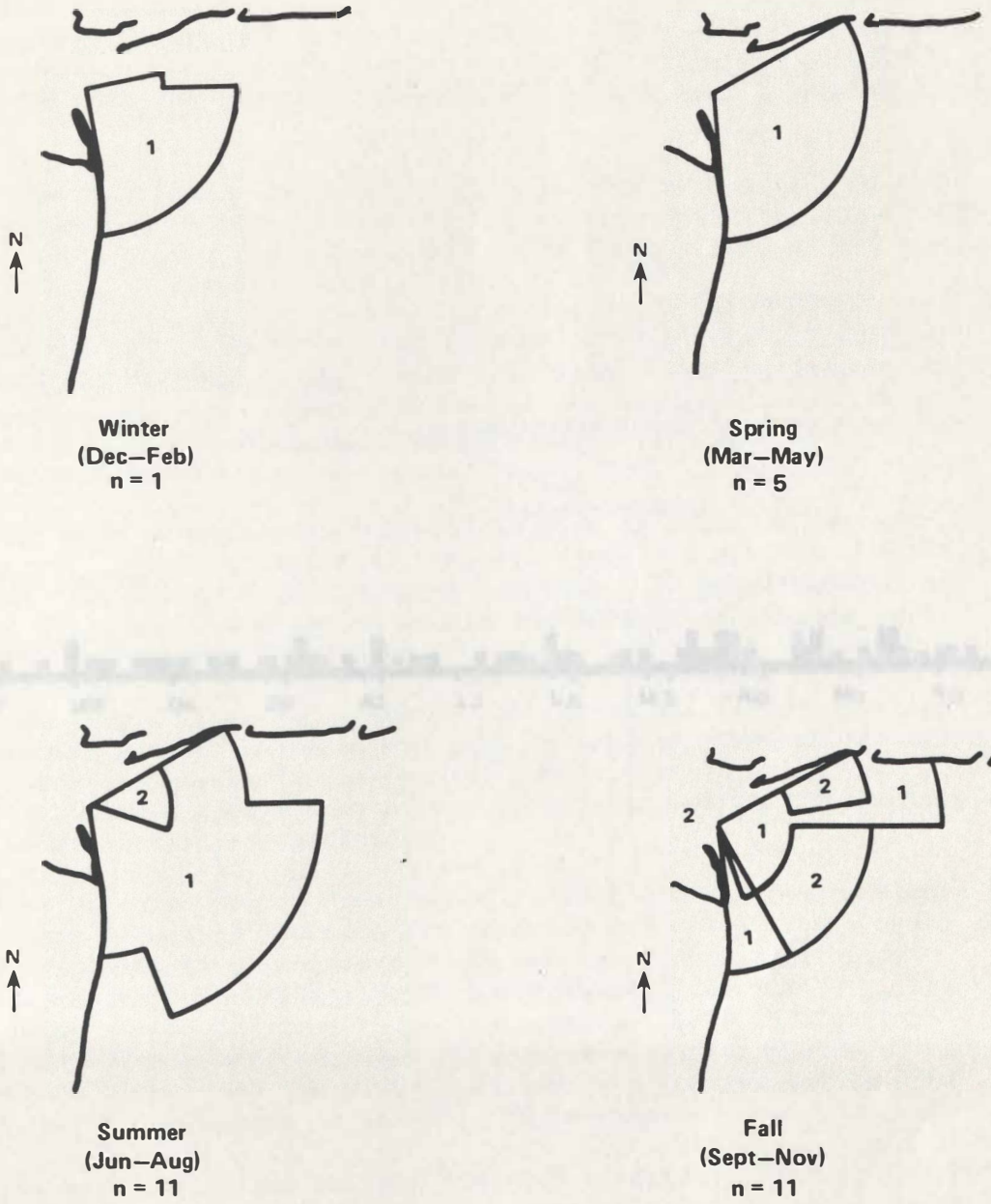

Figure 31. Areas Visited by Thermal Boundaries (HCMM), New York Bight, According to Season.

Figure 32. Seasonal Scatter of Detected Turbidity Plumes, New York Bight.

Figure 33. Seasonal Scatter of Detected Thermal Plumes (HCMM), New York Bight.

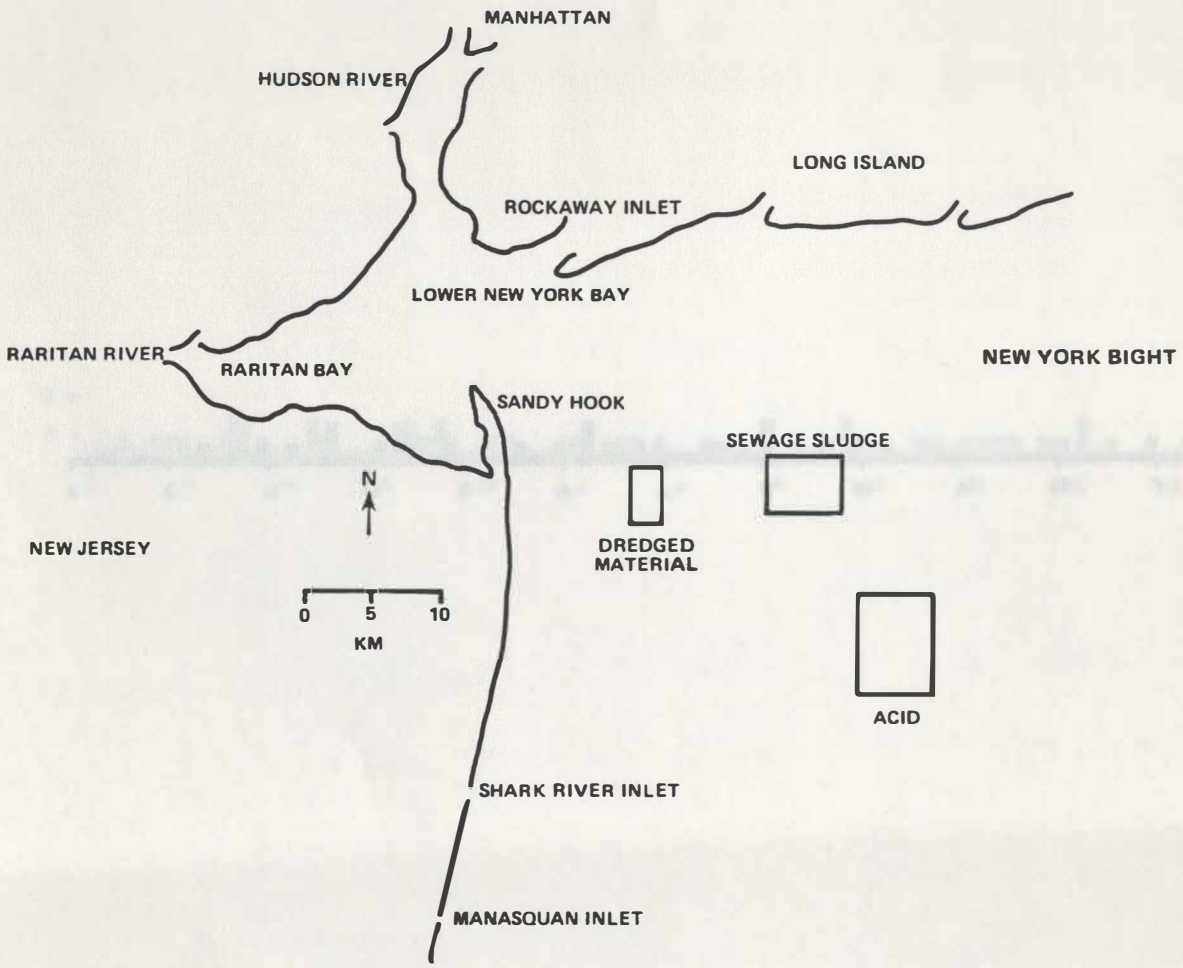

Figure 34. Waste Disposal Site Locations for the New York Bight.

(1982). Of the 82 naturally occurring turbidity boundaries detected in the New York Bight, 42 (51%) were in or beyond the dredge spoil area, 10 (12%) were in or beyond the sewage sludge area, while none reached the acid area. The totals can be seen in Table 7.

There were 57 waste disposal plumes detected on the Landsat images. According to their shapes and locations, and the known dumping protocols, the detected wastes were mainly of acid, the bright yellow-green color easily detected with the spectral band of Landsat MSS band 5 (Charnell and Maul, 1973).

Few of the dull plumes produced by brown sludge were seen. Unless their disposal occurs within one hour of the Landsat overpass, the sludge has time to settle beyond the penetration depth for the Landsat MSS spectral bands, and nothing is detected (EPA, 1978).

Acid wastes, which consist of 10% ferrous sulfate and 8.5% sulfuric acid (Redfield and Walford, 1951), react with ocean water to form a ferric hydroxide suspension. This suspension can be detected by Landsat from twelve hours (Charnell et al., 1974) to as many as five days (Vaccaro et al., 1972) after disposal.

Thus, the acid plumes would function as good circulation tracers (Freeland et al., 1976), except that disposal firms are not required to record actual coordinates of the dumping location. It would have to be assumed that all waste was disposed within the designated dumping area.

The feasibility of measuring disposed waste concentrations using Landsat may be judged from the extensive laboratory and field investigations of waste spectral properties performed by NASA Langely personnel in the early 1970s (see the review in Johnson and Munday, 1983); it may be concluded that Landsat measurement of concentrations would be moderately successful under restricted conditions.

Locations of waste plumes detected by Landsat are plotted in Figure 35, which shows many plumes far outside the designated dumping site. Under the presumption that with time a plume spreads and takes on an indistinct elliptical shape due to drifting, diffusion, and chemical reaction, the age of a waste plume may be inferred by its appearance. Data in Figure 35 reveal that the older plumes are more distant from the designated dumping sites. Analysis shows that the plume locations are not related to wind quadrants or seasons (Figures 36 and 37).

When the net circulation pattern sketched by Drake (1974) is overlain on the plume locations (Figure 38), the plume locations are found to be generally aligned with the western edge of the clockwise gyre which encompasses the acid disposal site. Diffuse (older) plumes were located in the gyre, but furthest from the disposal site. Those plumes northwest of the site might be explained on the basis that the currents of the gyre carried those plumes from the site. However, plumes seen southwest of the site, also seen by Polcyn and Sattinger (1979), cannot be so explained.

TABLE 7

NATURAL PLUME FREQUENCIES IN
NEW YORK BIGHT WASTE DISPOSAL AREAS

	No. of Plumes	In Dredge Spoil Area		In Sewage Sludge Area		In Acid Area
		No.	%	No.	%	No.
Landsat						
Visual	38	22	56	3	10	0
Visual+Enhanced	54	33	61	10	19	0
HCMM	28	9	32	0	0	0
TOTAL	82	42	51	10	12	0

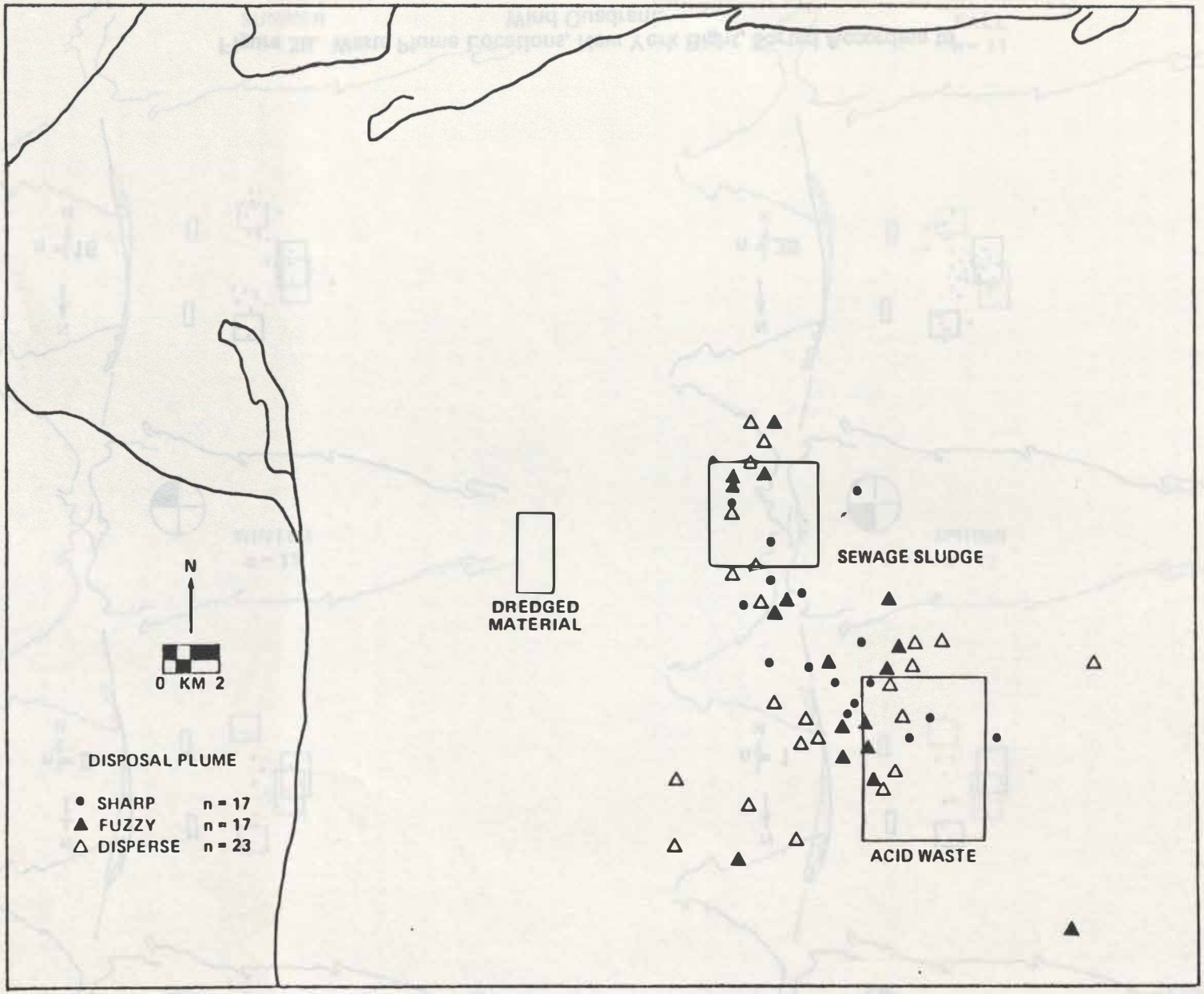

Figure 35. Locations of Waste Disposal Plumes Detected on Landsat Images of the New York Bight.

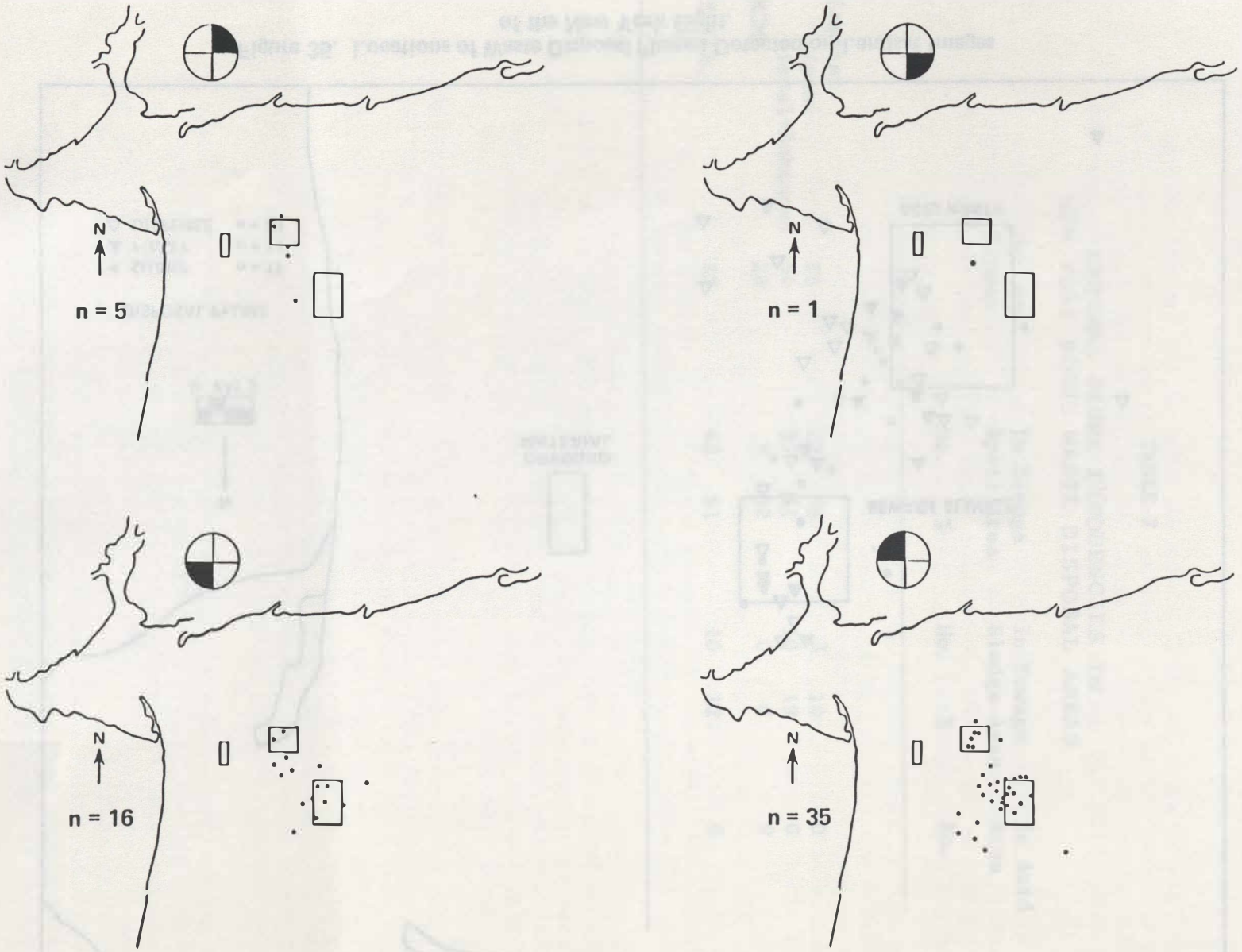

Figure 36. Waste Plume Locations, New York Bight, Sorted According to Wind Quadrant.

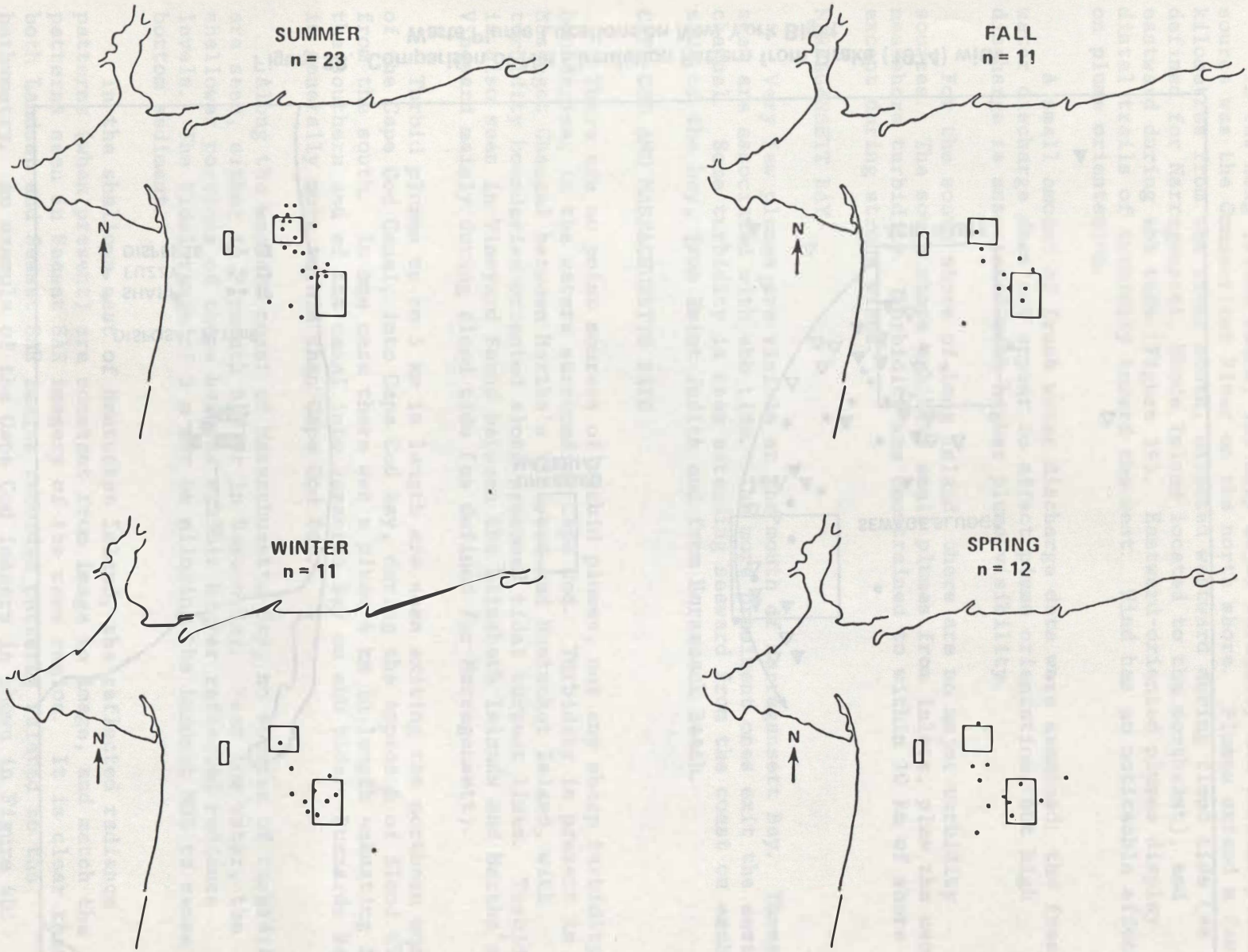

Figure 37. Waste Plume Locations, New York Bight, Sorted According to Season.

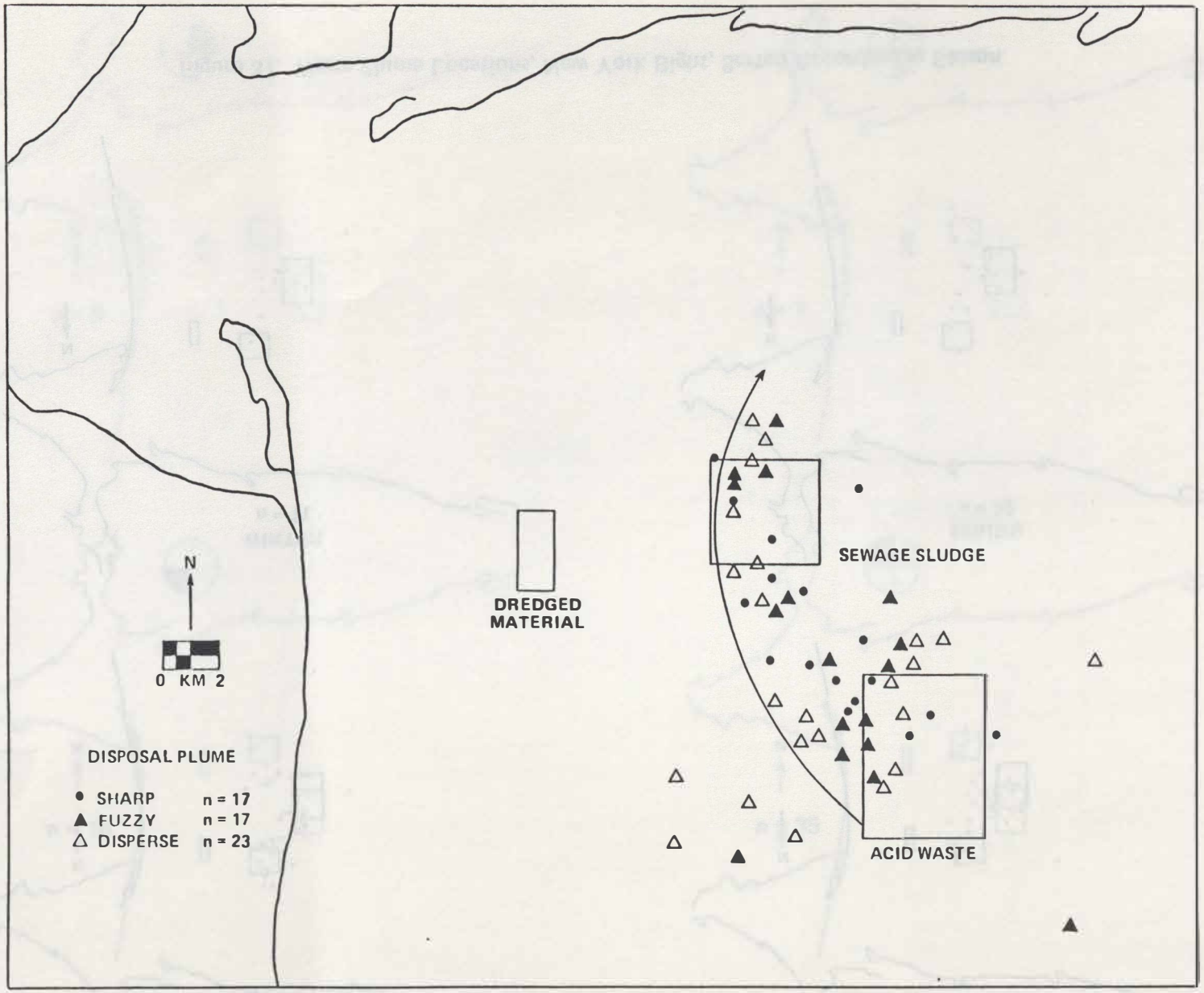

Figure 38. Comparison of Net Circulation Pattern from Drake (1974) with Waste Plume Locations on New York Bight.

LONG ISLAND SOUND AND SOUTH SHORE

In the Long Island Sound, the only major turbidity and thermal point source was the Connecticut River on the north shore. Plumes extend a few kilometres from the river mouth, directed westward during flood tide (as defined for Narragansett, Rhode Island located to the northeast), and eastward during ebb tide (Figure 39). Eastward-oriented plumes display distal trails of turbidity toward the west. Wind has no noticeable effect on plume orientation.

A small amount of fresh water discharge data were examined; the fresh water discharge does not appear to affect plume orientation, but high discharge is associated with higher plume visibility.

For the south shore of Long Island, there are no major turbidity sources. The south shore exhibits small plumes from inlets, plus the usual nearshore turbidity. Turbidity was constrained to within 10 km of shore except during strong winds.

NARRAGANSETT BAY

Very few plumes are visible at the mouth of Narragansett Bay. Those seen are associated with ebb tide. The more prominent ones exit the eastern channel. Some turbidity is seen extending seaward from the coast on each side of the bay, from Point Judith and from Horseneck Beach.

CAPE COD AND MASSACHUSETTS BAYS

There are no point sources of turbid plumes, nor any sharp turbidity boundaries, in the waters surrounding Cape Cod. Turbidity is present in Muskeget Channel between Martha's Vineyard and Nantucket Island, with turbidity boundaries oriented along presumed tidal current lines. Turbidity is also seen in Vineyard Sound between the Elizabeth Islands and Martha's Vineyard mainly during flood tide (as defined for Narragansett).

Turbid plumes up to 5 km in length are seen exiting the northern mouth of the Cape Cod Canal, into Cape Cod Bay, during the approach of flood tide from the south. In one case there was a plume 4 km in length emanating from the southern end of the canal into Buzzards Bay on ebb tide. Buzzards Bay is generally more turbid than Cape Cod Bay.

Along the western coast of Massachusetts Bay, no sources of turbidity are seen, either in Plymouth Bay or in Boston Bay. Near low water, the shallower portions of these harbors exhibit higher reflected radiance levels. The tidal range of 3 m may be allowing the Landsat MSS to sense bottom sediment.

In the shallows east of Nantucket Island, the reflected radiance patterns (when present) are constant from image to image, and match the patterns seen in Seasat SAR imagery of the same region. It is clear that both Landsat and Seasat SAR images recorded patterns related to the bathymetry. An example of the Cape Cod imagery is shown in Figure 40.

Figure 39. Connecticut River Turbid Plumes over a Tidal Cycle.

Figure 40. Landsat Image of Cape Cod and Massachusetts Bay.

DISCUSSION

Factors of Interest

Knowledge of general circulation in the Middle Atlantic Bight is important for understanding plume behavior. Obviously, the primary mechanisms affecting general circulation are net non-tidal flow, tidal currents, the Coriolis force, bay mouth morphology with resulting nearshore currents, density stratification, fresh water discharge, and winds. Complicating any interpretation of the Landsat imagery in terms of the above factors is the fact that plume features on any one image were generated during several tidal cycles; it was not unusual to see several plume boundaries in both ebb and flood tide images.

Net Non-Tidal Flow

The net non-tidal direction of water movement in the Middle Atlantic Bight is southerly (Bumpus, 1973; Boicourt, 1973; Beardsley et al., 1976). This southerly flow along the coast generally drives bay plumes southward. Southerly movement of the Chesapeake Bay plume was observed in the Superflux experiments (Campbell and Thomas, 1981). In the case of the New York Bay plume, southerly movement has been observed by various investigators (Ketchum et al., 1951; Costin et al., 1963; Charnell and Maul, 1973; Drake, 1974; Polcyn and Sattinger, 1979; Johnson et al., 1981).

The southerly flow of bay plumes is confirmed in the large number of images studied here, in that bands of uniform turbidity and temperature were frequently seen along the coasts south of all the bay mouths. Also, small plumes emanating from tidal inlets from Long Island south to North Carolina were seen to generally veer southward. The southerly flow according to Bumpus (1969) is not continuous, but experiences reversals, due to seasonal variations in fresh water discharge. Another cause of reversals is strong southern winds, which produce northward flow on the inner shelf (Boicourt, 1981). In the images, when small plumes from tidal inlets veered east or northeast, bay plumes also appeared to be oriented east or slightly northeast. Thus, the image analysis has provided direct confirmation of the prevailing southerly flow and its occasional reversals. Thus, the bay plumes in the overall sense passively follow the coastal flow.

Coriolis Effect

Estuarine water is assisted into the southerly flow through the Coriolis effect during ebb tide, when currents may typically exceed 2.3 knots (Brower et al., 1972). For all three bay mouths, plume features were prominent in the southern portion of the mouths during ebb tide, and features were prominent in the northern portion during flood, which implicates the Coriolis force as a large influence on water movement (Redfield and Walford, 1951; Ketchum et al., 1951; Ludwick and Melchor, 1972).

Rotary Flows and Gyres

The Coriolis force is joined by bay mouth morphology and resulting nearshore current patterns in affecting patterns of plume movement. The relatively linear ocean shorelines at the mouths of Chesapeake and Delaware Bays produce rotary flows and shear currents just beyond the Capes. Evidence for rotary flow adjacent to Cape Henry off Chesapeake Bay has been reported by Harrison et al. (1964), Johnson (1976), and Ruzecki et al. (1976). However, the images did not reveal any arcs or spiral features directly suggesting rotary flows adjacent to the Capes. The images revealed that plumes spread laterally, and turbidity boundaries were more linear, with increasing distance seaward. These features may be indirect evidence of rotary flow at the Capes.

Rotary flow north of Delaware Bay discussed by Ketchum (1953) may be responsible for the northward plume movement around Cape May seen in the images portraying ebb tide conditions. Drift bottles released in this area exhibited northward and southward motions (Ketchum, 1953), which were confirmed in current vector observations by DeAlteris and Keegan (1977). Kelly (1983) discussed evidence from sediment analysis that suspended material from inside the bay at Cape May eventually reaches the tidal inlets on the ocean side. These findings indicate that turbid plumes which on the images extend from Cape May to the inlets may be interpreted as showing bay-to-inlet transport of suspended material.

For the New York Bay, a more complicated situation has been observed. First, the apparent plume of Hudson River water did not always extend seaward from the river mouth. In some Landsat images, turbid water extended from the Hudson River to the southern Raritan Bay shore. Possibly these southward flows in the Bay were caused by high discharge from the Hudson River. The relationship of these flows to the Bay's general counterclockwise circulation pattern (Ayers et al., 1949; Jeffries, 1982) is unknown.

Second, flow through the mouth involves upwellings of shelf water. Studies by Kao (1975), Parker et al. (1976), and Hansen (1977) across the transect from Sandy Hook northward to Rockaway Point have revealed that Rockaway Channel exhibits a net flow into the Bay for the entire water column, while the net flow is inward only for bottom water in the Sandy Hook and Ambrose Channels. Those channels show a net outflow at the surface.

In the HCMM images, cold water plumes appeared to be coming from Rockaway Inlet. According to Stewart (1955) and Lavelle (1975), the cold water does not come from the inlet, but is incoming bottom water from the Hudson Canyon Valley. The cold water is upwelled in the Rockaway Channel area off Rockaway Inlet and becomes entrained by the Bay plume, producing the separate cold water plume which reaches the New York Bight. One HCMM image even showed entrained cold water reaching the lower Bight gyre and from there extending northward.

Third, the 90 degree change in shoreline orientation across the New York Bay mouth produces more complex local currents in the New York Bight than in the case of the Delaware and Chesapeake Bays. Shear currents and eddies 10-15 km offshore (Costin et al., 1963; Drake, 1974) disperse plume waters at the plume boundary toward the east and northeast. For locations further seaward, Drake (1974) postulated a large clockwise gyre, driven by

the offshore net non-tidal southerly flow situated far beyond reach of the plume fronts (Bumpus, 1973; Beardsley et al., 1976). The nearshore edge of the postulated gyre is located 20 km east of Sandy Hook (see Figure 38). The gyre should laterally spread abutting plume fronts due to entrainment. The images suggest that such spreading occurs: The turbidity boundaries in the New York Bight are more dispersed than for the other bays, and consist of linear segments as would be expected.

Direct evidence of the clockwise gyre was reported by Gunnerson and Swanson (1975) from studies using current meters. Some of the results are shown in Figures 41-43. Near-bottom flow shown in Figure 41 and flow in non-stratified conditions shown in Figure 42 together indicate that water leaving Raritan Bay will generally flow eastward. Southeast from Sandy Hook, flow of shelf water is northward. Thus, plume water (mixed to mid depth) generally cannot flow toward the southeast, as in the case of Chesapeake and Delaware Bays. Only in regions nearer shore is flow permitted toward the south, along the Sandy Hook coastline.

The generalized flow diagram for fine sediment transport shown by Gunnerson and Swanson is shown in Figure 43. In other investigations of New York Bight circulation patterns, an overall pattern did not emerge due to the variability of inner Bight currents (Gunnerson and Swanson, 1975; Hansen, 1977). This variability is affected by the angular coastline, the Lower New York Bay estuary, winds, tidal and river flow, and the Hudson Canyon and other bathymetric features. The relative importance of each variable is difficult to assess, having led Redfield and Walford (1951) to state that they could not quantitatively determine wind effects on circulation.

In other studies, it was concluded that net circulation was strongly affected by tides and winds (Gunnerson and Swanson, 1975), with plume movement sensitive to wind stress and reversals in net non-tidal shelf flow (Bowman and Wunderlich, 1976). Hansen (1977) cautioned that the currents were so random that statistical patterns only, not individual data sets, are useful for elucidating features of circulation.

Tidal Currents

Tidal currents are the primary determinants of plume movements near bay mouths, but this influence diminishes with distance offshore, and the influence of shelf non-tidal currents increases. For Chesapeake Bay, the tidal excursion is negligible at the Chesapeake Light Station 23 km offshore. Farther north, the tidal currents are stronger, as indicated in NOAA tidal current tables, due to a greater tidal range. Therefore, tidal current-related effects might be expected at greater distances offshore at the more northerly locations. The Cape Cod images, as noted earlier, did exhibit current-related effects between Nantucket Sound islands.

According to NOAA tide and tidal current tables, the tidal wave has nearly perfect progressive wave characteristics at the Chesapeake Bay entrance, where maximum currents occur near high and low water. Farther north in Long Island Sound and off Cape Cod, the tidal wave changes to near-standing wave characteristics, with maximum currents occurring nearly three hours after high and low water. The tidal range also increases with

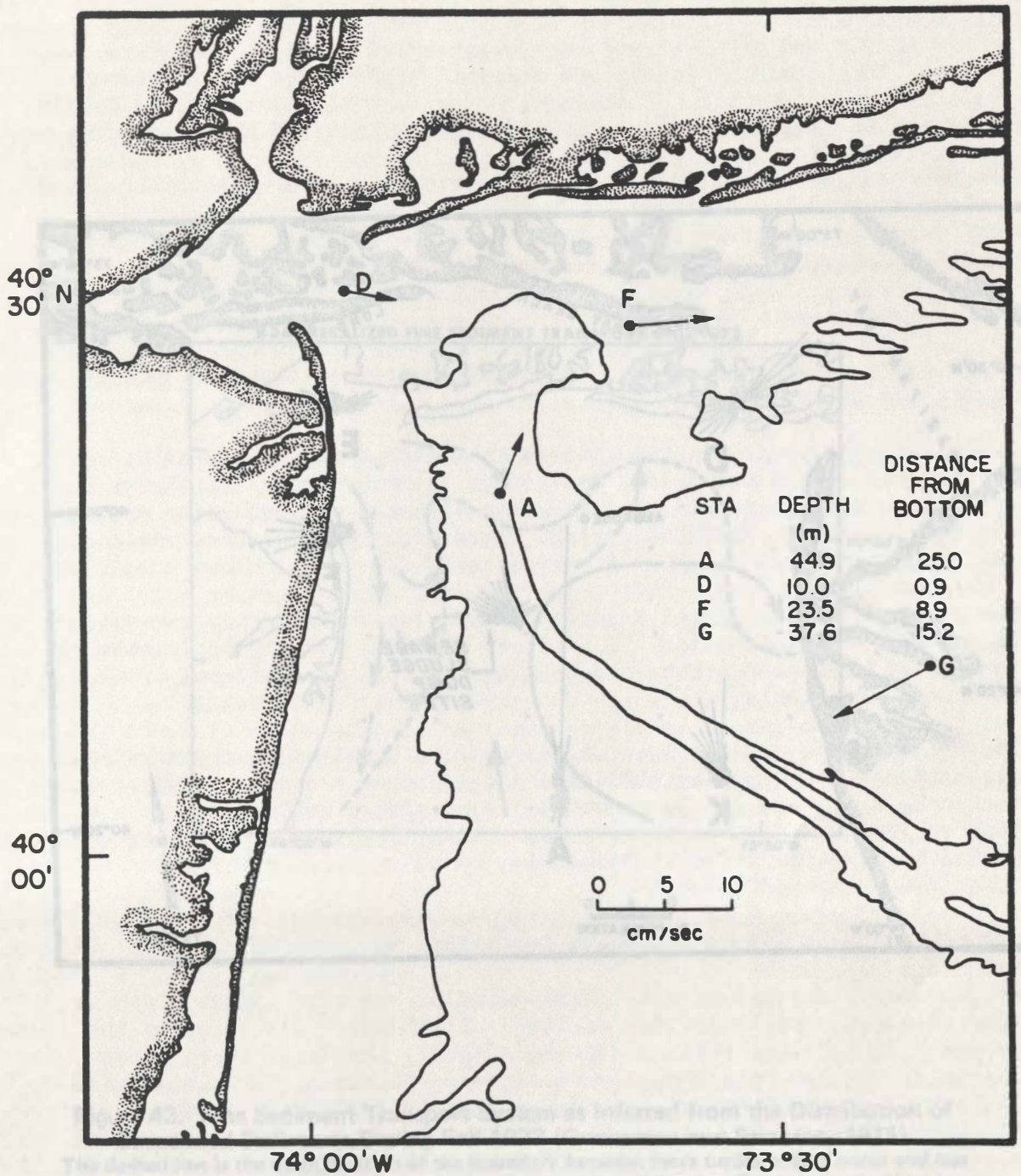

Figure 41. Mean Near-Bottom Current Vectors for Observations During the Period Aug-Sept 1973 (Gunnerson and Swanson, 1975).

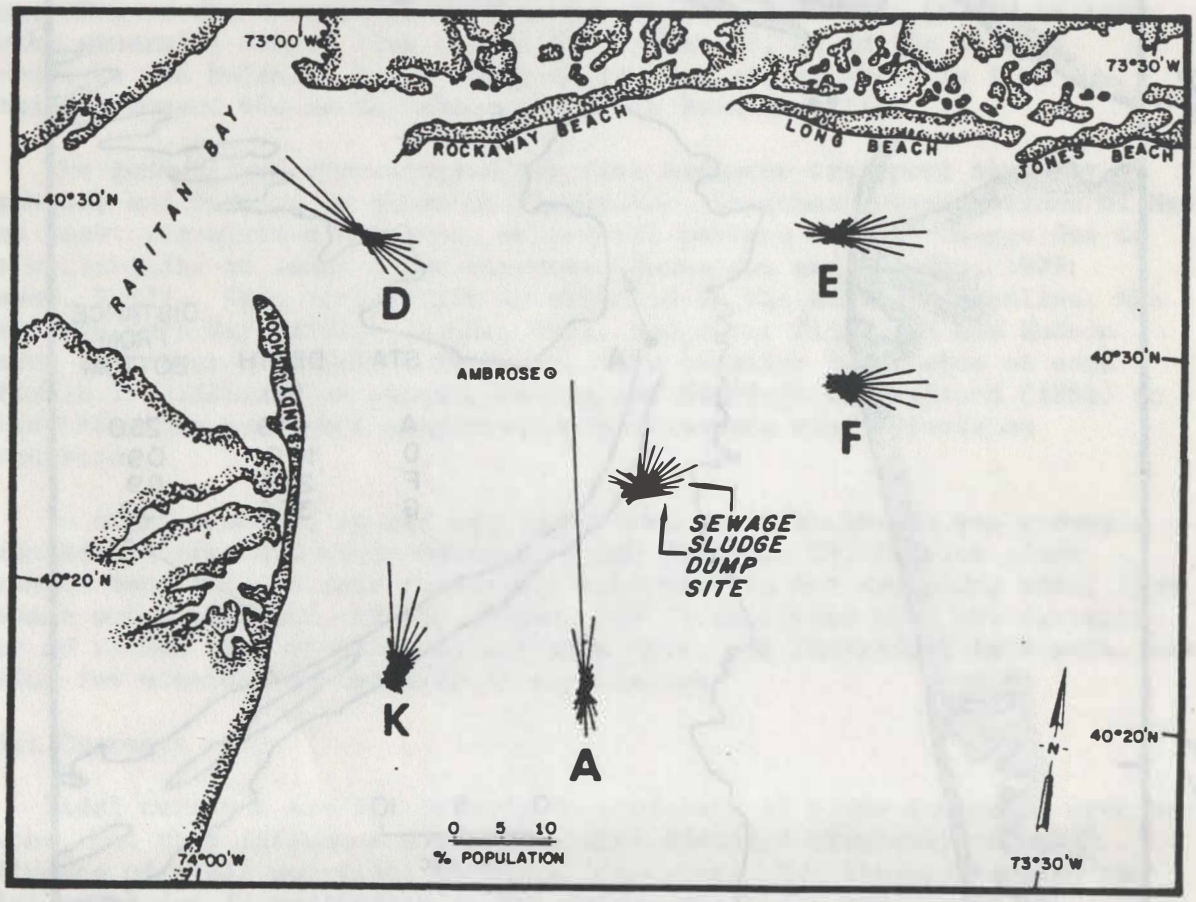

Figure 42. Polar Histograms of Frequency of Current Direction During the Period Oct-Nov 1973 (Gunnerson and Swanson, 1975).

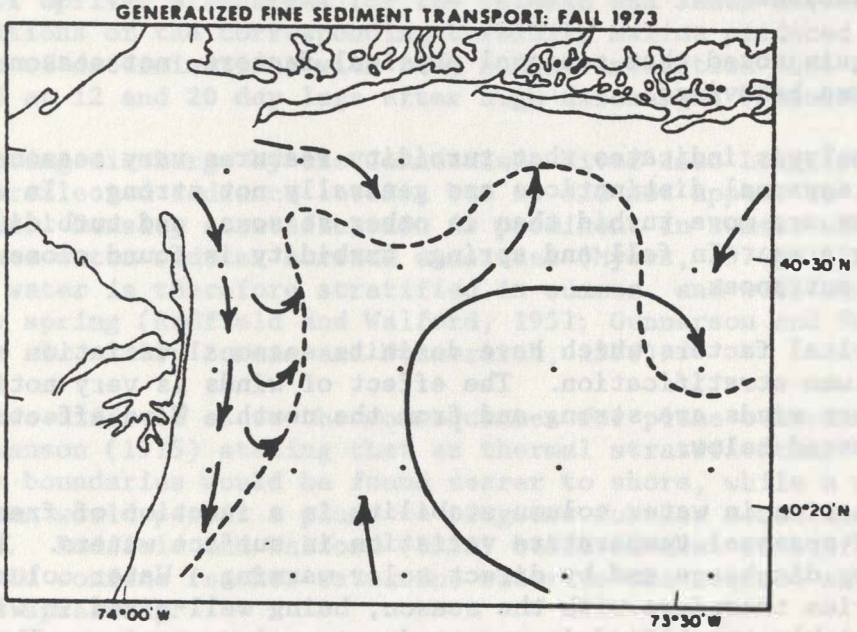

Figure 43. Fine Sediment Transport System as Inferred from the Distribution of Suspended Sediments During Fall 1973 (Gunnerson and Swanson, 1975).
The dashed line is the mean position of the boundary between more turbid coastal water and less turbid off-shore water. Turbid, brackish, surface effluent from the harbor flows down the New Jersey shore. The clockwise gyre is driven by southwesterly drift of off-shore shelf water, and, on bottom, by the influx of saline water into the harbor. Regional currents which appear to be persistent are indicated by solid arrows.

distance northward from about 0.5 m at Chesapeake Bay to almost 3.0 m at Boston Bay, with correspondingly stronger tidal currents. The stronger currents tend to produce greater bottom resuspension, which is seen at low tide in images of Boston and Plymouth Bays. The greater bottom resuspension in the northern nearshore waters tends to balance the fact that such waters have fewer point sources of suspended sediment.

In the middle and southern portions of the Middle Atlantic Bight, nevertheless, the turbidity levels are somewhat higher, due to the strength of turbidity in plume waters. Therefore, water mass movement is more easily tracked by visible spectrum sensors in the southern half of the study area.

The HCMM imagery revealed thermal contrasts in the northern waters, and showed thermal plumes at river and harbor mouths, but thermally distinct water could not be traced very far seaward. The well-known upwelling east of Cape Cod and Nantuckett Shoals was recognizable.

Seasonal Variations

It is again noted that seasonal physical factors, not seasons per se, influence plume behaviors.

Image analysis indicates that turbidity features vary seasonally; however, the seasonal distinctions are generally not strong. In winter and summer, waters are more turbid than in other seasons, and turbidity is noted over a larger area. In fall and spring, turbidity is found closer to coasts south of bay entrances.

Two physical factors which have definite seasonal variation are winds and water column stratification. The effect of winds is very noticeable in the winter when winds are strong and from the north. Wind effects are further discussed below.

The variation in water column stability is a function of fresh water discharge and seasonal temperature variation in surface waters. Temperature is affected by discharge and by direct solar warming. Water column stability varies therefore with the season, being well-mixed in winter and spring, and highly stratified in summer due to solar warming. These influences are discussed below.

Fresh Water Discharge and Water Column Stability

Fresh water discharge affects plume behavior, as high spring discharge can cause plumes to spread further seaward. Fresh water discharge by the Raritan and Hudson Rivers reaches a peak in April, the large fresh water volume causing the New York Bay plume to spread and extend farther seaward than under low discharge (Redfield and Walford, 1951; Jeffries, 1962; Duedall et al., 1979). There has been disagreement over whether increased volumes cause faster plume velocities (Jeffries, 1962; Redfield and Walford, 1951). As previously mentioned, low discharge can reverse the southerly non-tidal flow (Bumpus, 1969).

The fresh water flow from the Lower New York Bay estuary (primarily from the Hudson River) was anomalously high in the October- April period during 1977-1978, and higher than for any other year since 1946-1947. Conversely, the fresh water flow for October to April in 1980-1981 was anomalously low, lower than for any other year since 1946-1947 (Stanford, 1981). Unfortunately, image analysis has not yet revealed any plume responses specifically related to discharge variations. In this regard, one can examine Figures 12, 23, 24, 30, and 31.

Further analysis involving careful examination of daily discharge data for periods preceding each Landsat pass might prove worthwhile, as it has not been possible to carry out an extensive analysis of discharge effects in this study.

It is noted, however, that time-consuming analysis of the discharge-turbidity relationship for Chesapeake Bay waters (waters in the Bay itself, not in the mouth nor in the plume) disclosed little of high significance. An examination of upriver discharges for the Potomac and James Rivers relative to positions of the corresponding turbidity maxima produced very low coefficients of determination, with only slight indication that the maxima responded at 12 and 20 day lags after high discharges (Fedosh, 1984).

A higher spring discharge by the Connecticut River into Long Island Sound increased reflected radiance levels, but it did not appear to affect plume orientation. Density stratification is prominent in summer when solar warming of surface water reduces surface densities (Myers, 1974). In the New York Bight, water is therefore stratified in summer, and well mixed in winter and early spring (Redfield and Walford, 1951; Gunnerson and Swanson, 1975; Lavelle et al., 1975; Bowman and Wunderlich, 1976).

Opinions have differed as to the consequences for plume behavior, Gunnerson and Swanson (1975) stating that as thermal stratification increased, plume boundaries would be found nearer to shore, while a well-mixed water column would permit a plume to progress further south along the New Jersey coast. Redfield and Walford (1951) believed that stratification, in contrast, would confine fresher estuarine water to the surface and facilitate plume spreading.

In the HCMM images for the New York Bight studied here, summer thermal plumes were found farther seaward, compared to fall plumes when the water column was in transition toward a mixed state, in agreement with Redfield and Walford (1951) (see Figure 31).

Winds

Local winds are important forces which may temporarily overpower other plume-driving mechanisms. Along the Mid-Atlantic coast, third and fourth quadrant winds are dominant in summer and winter respectively. Westerly winds drive the plumes seaward away from bay mouths. In the New York Bight, such winds appear to drive the plume fronts into the offshore gyre.

First and fourth quadrant winds, that is, generally northern winds, confine the plumes to nearshore regions, and accentuate the effects of the Coriolis force and net non-tidal southerly flow in causing plume movements toward the south, parallel to the coast.

Second quadrant winds occur too seldom for the images examined to make any conclusions.

The less than distinct seasonal results noted earlier may have resulted from the seasonal distribution of winds. For example, in the New York Bay, winds are northwest in the winter, and change during the spring to south winds for the summer (Brower et al., 1972). However, the wind distribution of the Landsat images did not match the seasonal trend as can be seen in Table 8.

Because third and fourth quadrant winds drove plumes seaward, and for the images studied were evenly distributed across the seasons, the seasonal differences were minimized. Perhaps the majority of Landsat images had third and fourth quadrant winds because such winds are related to dry Canadian air which produces few clouds and therefore more usable images.

The Delaware Bay plume is less affected by winds than the other bay plumes. The only easily-discerned effects are during strong north winds, which produce a large turbid plume as wide as the mouth which extends 60 km toward the south. Northwesterly winds in general tend to orient turbidity streamlines along the wind direction.

Wind-driven currents become significant on open water when winds greater than 6 knots blow for more than 36 hours (Lavelle et al., 1975). The majority of Landsat images for the New York Bight had wind speeds above this minimum for at least 24 hours. For third and fourth quadrant winds, the number of turbid boundaries seaward of New York Bay was large. These results of image analysis are compatible with the conclusions by Redfield and Ketchum (1951) and Ketchum et al. (1951) that third quadrant winds spread plumes eastward.

These investigators also stated that northern winds confined plumes along the New Jersey coast. Concerning this conclusion, there was too small a number of images with first quadrant winds to permit comment. Northwest winds produced the most seaward plume fronts.

Unlike water masses on the shelf which manifest an Ekman transport effect (Doebler, 1966), the plumes in the images are usually oriented downwind. It would, however, be difficult to see Ekman effects in the images because of the lack of specificity in determining the direction of plume movement. One exception might be eastward moving plumes under southwest winds, suggested by Ruzecki (1981).

Sources of Suspended Sediment

In waters surrounding Cape Cod, tidal resuspension of bottom sediment is the primary source of surficial suspended sediment. In Long Island Sound, sediment sources are river discharge and local resuspension. Sediment sources for the New York Bay plume include the Hudson River and bottom resuspension. Kelly (1983) summarizes earlier studies of the Delaware Bay, and identifies its suspended sediment sources as primarily bottom resuspension, with a minor contribution from the Delaware River (see Oostdam, 1971). In the Chesapeake Bay, the sources include resuspension and James River sediment (Ludwick and Melchor, 1972; Nichols, 1972).

TABLE 8

SEASONAL DISTRIBUTION OF WIND QUADRANTS
FOR AVAILABLE LANDSAT IMAGES OF NEW YORK BIGHT

Season	Quadrant			
	First	Second	Third	Fourth
Winter			3	9
Spring	1	2	5	5
Summer	2		2	9
Fall			7	5

For each bay, the exact origin of sediment varies with geomorphology. The mouths of the Delaware and Chesapeake Bays are similar, but for Delaware Bay there is no fluvial source close to the mouth, such as the James River in Chesapeake Bay. The sediment source is instead a shallow embayment in the northern region of the bay.

The Chesapeake Bay orientation makes it sensitive to northern winds, but the axis of the mouth is nearly eastward. In contrast, both the Delaware Bay mouth and Bay orientation are aligned northwest and the system is therefore very sensitive to northwest winds. The Lower New York Bay has minimal fetch in comparison, and an angular configuration at its mouth.

Because resuspension is identified as the dominant source of plume sediment in all bays, it is expected that the stronger northwesterly winds in winter would produce greater turbidities, due to appropriate orientation of the wind vector along bay axes, producing a greater likelihood of bottom resuspension. As expected, the images show greater turbidities under these conditions.

Ludwick and Melchor (1972) have previously stated that Chesapeake Bay turbidity increases during winter because of the greater frequency of strong northerly winds. However, less turbid water is still found over channels (Munday and Fedosh, 1981b) where wind waves cannot resuspend sediment due to the greater depths.

Cooler winter water has a greater viscosity, which slows settling velocities (Oostdam, 1971); consequently, particles remain in suspension longer. There may be some evidence of this effect in winter Landsat images of the New York Bight and Delaware Bay, which show plumes farther southward. The greater size of winter plumes could also be attributed to the stronger northerly winds in winter.

Waste Disposal

The dredge spoil and sewage sludge disposal sites off Chesapeake Bay and in the New York Bight are frequently visited by turbidity boundaries when winds blow from the southwest quadrant. In contrast, the acid disposal sites off Delaware Bay and in the New York Bight are situated far enough seaward not to be reached under conditions prevailing with the images studied.

Drift directions for 7 acid plumes off Delaware Bay (Klemas and Philpot, 1981) are an average of 60 degrees to the right of the wind direction (water depth 38-48 m; Ekman theory for infinite depth predicts deviations of 45 degrees). The discrepancy from Ekman theory may indicate that 1-day wind vector averages have low correlations with shelf surface currents, or that shore-derived wind data are inappropriate for analysis of shelf water movement.

The locations of acid plumes in the New York Bight roughly follow a northwest-to-southeast line from the acid disposal site. The lack of information on the exact location and time of dumping precludes calculation of drift rates, but a rough age could be inferred if desired by study of the dump-time and image data of Klemas and Philpot (1981), which reveal in

general the spreading of waste plumes with time since release. Also, the more dispersed acid plumes are farther west from the disposal site. The result moderately confirms expectations: An overlay of the clockwise gyre (Drake, 1974) on the acid plume locations shows that the current in the disposal site should be toward the northwest.

REGIONAL OVERVIEW

The collection of cloud-free Landsat imagery for the Middle Atlantic Bight between 1972 and 1981 provides for a quasi-synoptic view of the entire Bight. Seven scenes, acquired in four orbital paths over four successive days, provide the coverage shown in Figure 1. The chart in Figure 44 portrays the calendar distribution of all images acquired for this study, and can be used to determine the combinations of scenes which produce a 4-day quasi-synoptic view. Over such 4-day periods, meteorological and oceanographic conditions change, but examination of the appropriate data may reveal some 4-day sets of scenes in which such conditions vary only slightly. An examination of the data in this regard has not been performed here.

Truly synoptic coverage can be obtained from orbiting sensors with greater areal coverage, such as HCMM, but at a loss of spatial resolution. A study of all available satellite data sets will provide the most comprehensive view with regard to both spatial and temporal resolution.

CONCLUSIONS

In the southern and central portions of the Middle Atlantic Bight, the Chesapeake, Delaware, and New York Bays are the principal sources for turbidity and thermal plumes. The dynamic behavior of these plumes has been examined, with respect to tidal currents, the Coriolis force, shelf and nearshore circulation, fresh water discharge, and local winds as the plume driving mechanisms. The usual effect of the forces apart from winds is to drive plumes southeasterly along the coasts from the bay mouths.

During northern winds, this southeastern movement is enhanced. During strong southwest and westerly winds, plumes move more seaward and spread laterally, sometimes entering or going beyond waste disposal areas.

In the northern portion of the Middle Atlantic Bight, from Long Island to Cape Cod, a lack of distinct sediment and thermal sources makes it difficult to discern turbid plumes or other water masses significant in exchange processes between near-shore and off-shore waters.

REFERENCES

Ayers, J.C., B.H. Ketchum, and A.C. Redfield. 1949. Hydrographic consideration relative to the location of sewer outfalls in Raritan Bay. Woods Hole Oceanogr. Inst., Ref. No. 29-13 (unpubl. manuscr.).

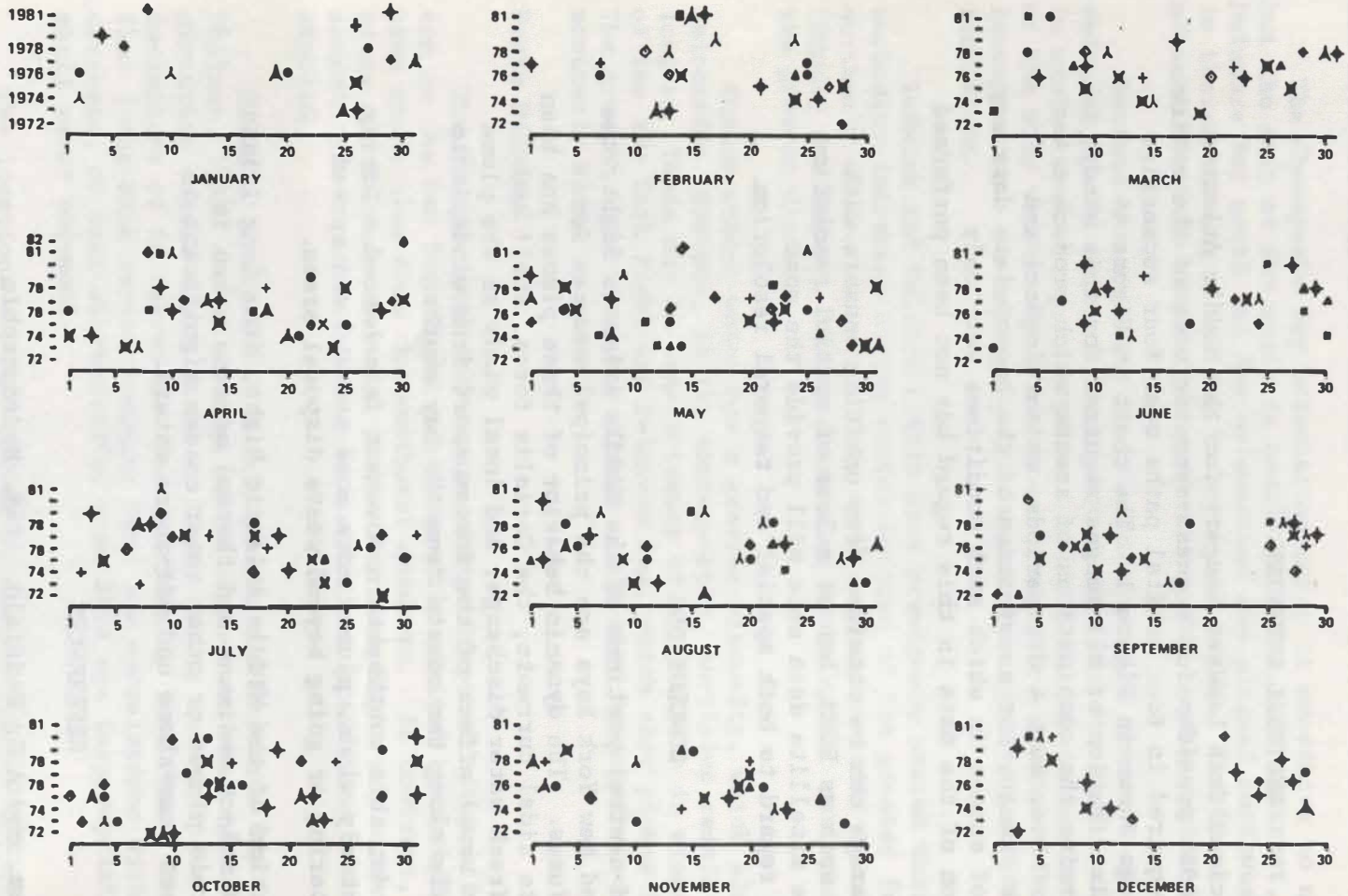

Figure 44. Calendar Distribution of Landsat Scenes, All Scenes in Region of Study, Over the Years 1972 to 1981.

Beal, R., P. DeLeonibus, and I. Katz. 1981. Spaceborne synthetic aperture radar for oceanography. Johns Hopkins Univ. Press, Baltimore, Md., 215 p.

Beardsley, R.C., W.C. Boicourt, and D.V. Hansen. 1976. Physical oceanography of the Middle Atlantic Bight. In Middle Atlantic Continental Shelf and the New York Bight (ed. M.G. Gross), Amer. Soc. Lminol. Oceanogr. Spec. Symp. 2:20-34.

Boicourt, W.C. 1973. The circulation of water on the continental shelf from Chesapeake Bay to Cape Hatteras. Ph.D. Thesis. The Johns Hopkins Univ., Baltimore, Md., 183 p.

Boicourt, W.C. 1981. Circulation in the Chesapeake Bay entrance region: estuary-shelf interaction. In Chesapeake Bay Plume Study-Superflux 1980 (eds. J.W. Campbell and J.P. Thomas), NASA Conf. Publ. 2188, p. 61-78.

Bowker, D.E., W.G. Witte, P. Fleischer, T.A. Gosink, W.J. Hanna, and J.C. Ludwick. 1975. An investigation of the waters in the lower Chesapeake Bay. Proc. 10th Intl. Symp. Remote Sensing of Env., Ann Arbor, Mich., p. 411-420.

Bowman, M.J. and L.D. Wunderlich. 1976. Distribution of hydrographic properties in the New York Bight Apex. In Middle Atlantic Continental Shelf and the New York Bight (ed. M.G. Gross), Amer. Soc. Limnol. Oceanogr. Spec. Symp. 2:58-68.

Brower, W.A., D.D. Sick, and R.G. Quayle. 1972. Environmental guide for seven U.S. ports and harbor approaches. NOAA National Climatic Center COM-72-11258, Asheville, N.C. 22801, 165 p.

Bumpus, D.F. 1969. Reversals in the surface drift in the Middle Atlantic Bight area. Deep-Sea Res. suppl. 16:17-23.

Bumpus, D.F. 1973. A description of the circulation on the continental shelf of the east coast of the United States. In Progress in Oceanography (ed. B.F. Warren), Pergamon Press, N.Y., 6:111-156.

Campbell, J.W. and J.P. Thomas (eds.). 1981. Chesapeake Bay plume study-Superflux 1980. NASA Conf. Publ. 2188, Wash. D.C., 522 p.

Charnell, R.L. and G.A. Maul. 1973. Oceanic observations of New York Bight by ERTS-1. Nature 242:451-452.

Charnell, R.L., J.R. Apel, W. Manning III, and R.H. Qualset. 1974. Utility of ERTS-1 for coastal ocean observations: the New York Bight example. Mar. Techn. Soc. J. 8(3):42-47.

Costin, M., P. Davis, R. Gerard, and B. Katz. 1963. Dye diffusion experiments in New York Bight. Columbia Univ., Lamont Geol. Obs. Techn. Rept. CU-2-63.

DeAlteris, J.T. and R.T. Keegan. 1977. Advective transport processes related to the design of wastewater outfalls for the New Jersey coast. In Transport Processes in Lakes and Oceans (ed. R. Gibbs), Plenum Press, N.Y., p. 63-89.

Doebler, H.J. 1966. A study of shallow water drift currents at two stations off the east coast of the United States. U.S. Navy Underwater Sound Lab. Rept. 755, New London, Conn., 78 p.

Drake, D.E. 1974. Suspended particulate matter in the New York Bight apex: September-November 1973. NOAA Techn. Rept. ERL318-MESA-1.

Duedall, I.W., H.B. O'Connors, R.E. Wilson, and J.H. Parker. 1979. The lower bay complex. MESA New York Bight Atlas Monograph 29, N.Y. Sea Grant Institute, Albany, N.Y.

Elder, R.B. 1971. The effect of run-off from Hurrican Camille on the continental shelf waters of the Chesapeake Bight. M.A. Thesis, Virginia Inst. Mar. Sci., Gloucester Point, Va., 80 p.

Environmental Protection Agency. 1978. Final environmental impact statement on the ocean dumping of sewage sludge in the New York Bight. U.S.E.P.A., Region II, New York. 226 p., 11 app.

Environmental Protection Agency. 1982. Environmental impact statement (EIS) for the New York dredged material disposal site designation. U.S.E.P.A., Washington, D.C.

Fedosh, M. 1984. Lower Chesapeake Bay surface turbidity variations as detected from Landsat images. M.S. Thesis, Virginia Inst. Mar. Sci., Gloucester Point, Va., 191 pp.+app.

Fedosh, M. and J.C. Munday Jr. 1982. Satellite analysis of estuarine plume behavior. Oceans 82, Washington, D.C., IEEE, New York, p. 563-571.

Freeland, G.L., D.J.P. Swift, and W.L. Stubblefield. 1976. Surficial sediments of the NOAA-MESA study areas in the New York Bight. In Middle Atlantic Continental Shelf and the New York Bight (ed. M.G. Gross), Amer. Soc. Limnol. Oceanogr. Spec. Symp. 2:90-101.

Gross, M.G. 1976. Sources of urban wastes. In Middle Atlantic Continental Shelf and the New York Bight (ed. M.G. Gross), Amer. Soc. Limnol. Oceanogr. Spec. Symp. 2:150-161.

Gunnerson, C.G. and R.L. Swanson. 1975. Ocean dumping in the New York Bight. NOAA Techn. Rept. ERL321-MESA-2, 78 p.

Hansen, D.V. 1977. Circulation. MESA New York Bight Atlas Monograph 3, N.Y. Sea Grant Institute, Albany, N.Y. 23 p.

Harrison, W., J.J. Norcross, N.A. Pore, and E.M. Stanley. 1967. Circulation of shelf waters off the Chesapeake Bight: surface and bottom drift of continental shelf waters between Cape Henlopen, Delaware, and Cape Hatteras, North Carolina, June 1963-December 1964. U.S. Environm. Science Services Admin., Professional Paper No. 3, Washington, D.C., 82 p.

Harrison, W., M.L. Brehmer, and R.B. Stone. 1964. Nearshore tidal and non-tidal currents, Virginia Beach, Virginia. U.S. Army Coastal Eng. Res. Center Techn. Memor. 5.

Hovis, W.A., D.K. Clark, F. Anderson, R.W. Austin, W.H. Wilson, E.T. Baker, D. Ball, H.R. Gordon, J.L. Mueller, S.Z. El-Sayed, B. Sturm, R.C. Wrigley, and C.S. Yentsch. 1980. Nimbus-7 Coastal Zone Color Scanner: system description and initial imagery. Science 210:60-63.

Howe, M.R. 1962. Some direct measurements of the non-tidal drift on the continental shelf between Cape Cod and Cape Hatteras. Deep-Sea Research 9:445-455.

Jeffries, H.P. 1962. Environmental characteristics of Raritan Bay, a polluted estuary. Limnol. Oceanogr. 7:21-31.

Johnson, R.E. 1976. Circulation study near Cape Henry, Virginia, using Lagrangian techniques. Inst. Oceanography Techn. Rept. 21, Old Dominion Univ., Norfolk, Va., 80 p.

Johnson, R.W. and R.C. Harriss. 1980. Remote sensing for water quality and biological measurements in coastal waters. Photogramm. Eng. Remote Sensing 46(1):77-85.

Johnson, R.W., G.S. Bahn, and J.P. Thomas. 1981. Synoptic thermal and oceanographic parameter distributions in the New York Bight Apex. Photogramm. Eng. Remote Sensing 48(11):1593-1598.

Johnson, R.W. and J.C. Munday Jr. 1983. The marine environment. Chapter 28, in Manual of Remote Sensing, 2nd edition (ed. R.N. Colwell), Amer. Soc. Photogramm., Falls Church, Va., p. 1371-1496.

Kao, A. 1975. Current structure in the Sandy Hook to Rockaway Point transect. State Univ. New York Mar. Sci. Center, Mar. Sci. Res. Papers, Stoney Brook, N.Y.

Kelley, J. 1983. Composition and origin of the inorganic fraction of southern New Jersey inner continental shelf suspended sediment. Geol. Soc. Amer. Bull. 94(6):689-699.

Ketchum, B.H. 1953. Preliminary evaluation of the coastal water off Delaware Bay for the disposal of industrial wastes. Woods Hole Oceanogr. Inst. ref. no. 53-31, 53 pp.+app.

Ketchum, B.H., A.C. Redfield, and J.C. Ayers. 1951. The oceanography of the New York Bight. Pap. Phys. Oceanogr. Meteorol. 12(1):46p.

Klemas, V. and D.F. Polis. 1977. A study of density fronts and their effects on coastal pollutants. Remote Sensing of Env. 6:95-126.

Klemas, V. and W.D. Philpot. 1981. Remote sensing of ocean-dumped waste drift and dispersion. In Ocean Dumping of Industrial Wastes (eds. B.H. Ketchum, D.R. Kester, and P.K. Park), Marine Science vol. 12, Plenum Press, N.Y., p. 193-211.

Lavelle, J.W., G.H. Keller, and T.L. Clark. 1975. Possible bottom current response to surface winds in the Hudson Shelf Channel. J. Geophys. Res. 80(15):1953-1956.

Ludwick, J.C. 1973. Tidal currents, sediment transport, and sand banks in Chesa- peake Bay entrance, Virginia. Inst. Oceanography Techn. Rept. 16, Old Dominion Univ., Norfolk, Va., 13 p.

Ludwick, J.C. and J.R. Melchor. 1972. Surface water turbidity in the entrance to Chesapeake Bay, Virginia. Inst. Oceanography Techn. Rept. 5, Old Dominion Univ., Norfolk, Va., 67 p.

Mairs, R.L. and D.K. Clark. 1973. Remote sensing of estuarine circulation dynamics. Photogramm. Eng. 39(9):927-938.

Munday, J.C., Jr. 1983. Chromaticity of path radiance and atmospheric correction of Landsat data. Remote Sens. of Env. 13:525-538.

Munday, J.C., Jr., T.T. Alfoldi, and C.L. Amos. 1979. Bay of Fundy verification of a system for multidate Landsat measurement of suspended sediment. In Satellite Hydrology, Amer. Water Res. Assoc., Minneapolis, Minn., p. 622-640.

Munday, J.C., Jr. and M.S. Fedosh. 1980. Southern Chesapeake Bay circulation and suspended sediment transport analyzed using Landsat imagery. Proc. Amer. Soc. Photogr. Fall Techn. Mtg., Niagara Falls, N.Y., p. RS-3-F:1-5.

Munday, J.C., Jr. and M.S. Fedosh. 1981a. Chesapeake Bay plume dynamics from Landsat. In Chesapeake Bay Plume Study-Superflux 1980 (eds. J.W. Campbell and J.P. Thomas), NASA Conf. Publ. 2188, p. 79-92.

Munday, J.C., Jr. and M.S. Fedosh. 1981b. Landsat analysis of the dynamics of the Chesapeake Bay plume on the continental shelf. Final Rept. contract NA-80-FA-C-00051 NOAA NMFS. Virginia Inst. Mar. Sci., Gloucester Point, 59 p.

Myers, T.D. 1974. An observation of rapid thermocline formation in the Middle Atlantic Bight. Estuarine and Coastal Mar. Sci. 2:75-82.

NASA Goddard Space Flight Center. 1973. Proc. Symp. Significant Results Obtained from ERTS-1. Greenbelt, Md., publ. SP-327.

Nichols, M.M. 1972. Sediments of the James River estuary, Virginia. Geol. Soc. Amer. Memoir 133, p. 169-210.

Oostdam, B. 1971. Suspended sediment transport in Delaware Bay. Ph.D. Thesis. Univ. Delaware, Newark, 316 p.

Parker, J.H., I.W. Duedall, H.B. O'Connors, and R.E. Wilson. 1976. Raritan Bay as a source of ammonium and chlorophyll a for the New York Bight Apex. In Middle Atlantic Continental Shelf and the New York Bight (ed. M.G. Gross), Amer. Soc. Limnol. Oceanogr. Spec. Symp. 2:212-219.

Polcyn, F.C. and I.J. Sattinger. 1979. Marine ecosystem analysis program: a summary of remote sensing investigations in the New York Bight. Env. Res. Inst. Michigan Rept. 131200-1-F, Ann Arbor, Mich., 157 p.

Redfield, A.C. and L.A. Walford. 1951. A study of the disposal of chemical waste at sea. W.H.O.I. Contrib. No. 586, 49 p.

Ruzecki, E.P. 1981. Temporal and spatial variations of the Chesapeake Bay plume. In Chesapeake Bay plume study-Superflux 1980 (eds. J.W. Campbell and J.P. Thomas), NASA Conf. Publ. 2188, p. 111-130.

Ruzecki, E.P., C. Welch, J. Usry, and J. Wallace. 1976. The use of the EOLE satellite system to observe continental shelf circulation. Eighth Ann. Offshore Technol. Conf., Houston, Tx., p. 697-708.

Stanford, H.M. 1981. FY1981 NEMP water column characterization cruises in the New York Bight. Unpubl. letter, National Marine Fisheries Service.

Stewart, H.B., Jr. 1955. Upstream bottom currents in New York Harbor. Science 127:1113-1114.

Vaccaro, R.F., G.D. Grice, G.T. Rowe, and P.H. Wiebe. 1972. Acid-iron waste disposal and the summer distribution of standing crops in the New York Bight. Water Res. 6:231-256.

Whitlock, C.H. 1976. An estimate of the influence of sediment concentration and type on remote sensing penetration depth for various coastal waters. Techn. Memor. X-73906, NASA Langley Res. Center, Hampton, Va., 17 p.

Wiesnet, D.R., D.F. McGinnis, Jr., M. Matson, and J.A. Pritchard. 1980. Preliminary survey of HCMM satellite thermal imagery as applied to hydrospherics. Amer. Soc. Photogramm. Fall Convention (Niagara Falls, N.Y.), Falls Church, Va., p. RS-3-E-1 to RS-3-E-12.

APPENDIX 1

TIDE AND WIND DATA FOR LANDSAT PASSES

Overpass Times are Before (-) or After (+) Actual High Tide at the Nearest Tide Recording Station

Chesapeake Bay

	Date	Overpass Time Sewells Point, VA	12-Hour Wind Average Norfolk, VA Dir (°)	Speed (kts)
94	3 Dec 79	+1:18	10	13
93	15 Nov 79	+4:18	330	6
92	28 Oct 79	-5:00	250	10
91	19 Oct 79	+2:10	80	5
90	3 Jul 79	-5:35	10	10
89	1 May 79	-2:09	30	16
88	22 Apr 79	+4:41	220	13
87	17 Mar 79	-1:26	280	9
86	4 Jan 79	-3:59	250	6
85	26 Dec 78	+4:33	240	10
84	27 Sep 78	+4:45	60	10
83	18 Sep 78	-0:10	260	6
82	22 Aug 78	-1:57	30	8
81	4 Aug 78	+0:51	210	7
80	17 Jul 78	+4:08	30	9
79	8 Jul 78	-1:13	200	6
78	29 Jun 78	+5:50	0	11
77	20 Jun 78	+1:28	280	5
76	11 Jun 78	-2:46	140	8
75	9 Apr 78	-0:17	30	10
74	31 Mar 78	-4:23	160	8
73	4 Mar 78	+5:11	340	18
72	27 Jan 78	-1:52	260	22
71	28 Dec 77	-2:07	30	11
70	22 Dec 77	+2:44	270	13
69	11 Oct 77	+2:05	0	0
68	29 Sep 77	-1:09	0	13
67	11 Sep 77	+1:53	0	13
66	5 Sep 77	-4:41	220	10
65	6 Aug 77	-5:27	250	13
64	19 Jul 77	-2:01	290	5
63	7 Jun 77	-3:54	320	12
62	8 May 77	-3:36	50	10
61	14 Apr 77	+4:39	290	7
60	9 Mar 77	-1:56	220	11
59	25 Feb 77	-4:47	250	16
58	1 Feb 77	+2:24	290	14
57	27 Dec 76	-4:11	310	15
56	9 Dec 76	-0:58	280	6
55	21 Nov 76	+1:21	40	7
54	3 Nov 76	+3:22	200	5

Chesapeake Bay

	Date	Overpass Time Sewells Point, VA	12-Hour Wind Average Norfolk, VA Dir (°)	Speed (kts)
53	16 Oct 76	-4:32	0	11
52	23 Aug 76	+2:48	290	8
51	5 Aug 76	-5:30	310	4
50	27 Jul 76	+0:25	240	15
49	12 Jun 76	+1:02	360	6
48	25 May 76	+3:50	60	10
47	28 Apr 76	+1:02	320	10
46	10 Apr 76	+4:15	0	13
45	1 Apr 76	+0:10	350	14
44	23 Mar 76	-5:56	40	10
43	5 Mar 76	-2:01	250	18
42	25 Feb 76	+4:17	250	12
41	7 Feb 76	-3:25	0	14
40	20 Jan 76	-1:24	240	13
39	2 Jan 76	+0:24	50	7
38	24 Dec 75	-3:20	20	15
37	18 Nov 75	+1:30	0	7
36	31 Oct 75	+3:49	0	13
35	22 Oct 75	+0:07	280	7
34	13 Oct 75	-6:21	0	11
33	4 Oct 75	+2:01	30	10
32	29 Aug 75	-3:41	110	8
31	20 Aug 75	+1:54	40	6
30	11 Aug 75	-2:05	220	7
29	2 Aug 75	+6:41	40	4
28	18 Jun 75	+5:38	180	7
27	9 Jun 75	+1:34	320	9
26	22 May 75	+3:17	220	11
25	13 May 75	-0:16	270	11
24	25 Apr 75	+1:20	240	10
23	21 Feb 75	+5:15	10	15
22	11 Dec 74	+2:48	0	0
21	23 Nov 74	+5:32	50	6
20	18 Oct 74	-1:04	0	18
19	12 Sep 74	+5:09	250	10
18	20 Jul 74	+0:17	0	12
17	21 Apr 74	+2:02	230	7
16	3 Apr 74	+4:38	200	12
15	26 Feb 74	-1:15	0	14
14	28 Nov 73	-1:01	220	17
13	10 Nov 73	+1:47	360	16
12	23 Oct 73	+3:30	60	8
11	5 Oct 73	-6:06	250	7
10	17 Sep 73	-1:29	80	12
9	30 Aug 73	-0:11	10	4

Chesapeake Bay

	Date	Overpass Time Sewells Point, VA	12-Hour Wind Average Norfolk, VA Dir (°)	Speed (kts)
8	12 Aug 73	+2:19	210	12
7	25 Jul 73	+6:011	150	4
6	1 Jun 73	+1:26	40	11
5	14 May 73	+3:141	70	14
4	13 Feb 73	+5:081	230	3
3	26 Jan 73	-4:161	10	51
2	3 Dec 72	+2:321	210	16
1	10 Oct 72	-0:161	10	15

Delaware Bay

	Date	Overpass Time Cape Henlopen, DE	24-Hour Wind Average Cape May, NJ Dir (°)	Speed (kts)
128	16 Feb 81	+3:301	75	5
127	15 Feb 81	+4:181	331	2
126	29 Jan 81	-5:181	260	5
125	6 Dec 80	+2:011	351	11
124	31 Oct 80	-4:59	339	7
123	2 Aug 80	-3:23	249	10
122[1]	27 Jun 80	+2:111	87	4
121	9 Jun 80	+4:301	310	20
120	26 Jan 80	+5:561	23	6
119	3 Dec 79	-1:591	273	16
118	19 Oct 79	-2:39	166	2
117	3 Jul 79	-5:35	273	14
116	14 Jun 79	-1:531	334	2
115	1 May 79	-1:58	227	3
114	17 Mar 79	-0:511	235	8
113	4 Jan 79	-3:05	313	10
112	26 Dec 78	+4:151	274	14
111	20 Nov 78	-1:571	343	7
110	2 Nov 78	+0:391	30	3
109	1 Nov 78	+1:091	332	3
108	24 Oct 78	-4:44	343	11
107	15 Oct 78	+2:151	316	10
106	27 Sep 78	-5:15	78	4
105	8 Jul 78	-0:44	174	8
104	7 Jul 78	-0:191	218	4
103	29 Jun 78	+6:021	313	9
102	28 Jun 78	-5:341	260	7
101	20 Jun 78	+2:041	221	5
100	11 Jun 78	-2:35	221	5
991	10 Jun 78	-1:281	301	6
981	18 Apr 78	+5:131	156	6
971	9 Apr 78	-0:181	295	8

Delaware Bay

	Date	Overpass Time Cape Henlopen, DE	24-Hour Wind Average Cape May, NJ Dir (°)	Speed (kts)
96	31 Mar 78	-3:59	289	5
95	30 Mar 78	-2:59	336	8
94	28 Dec 77	-1:26	309	3
93	22 Dec 77	+2:20	175	5
92	29 Sep 77	-0:39	328	10
91	11 Sep 77	+1:41	313	7
90	6 Aug 77	-4:33	0	0
89	31 Jul 77	+0:39	0	0
88	19 Jul 77	-1:49	295	3
87	13 Jul 77	+3:34	186	9
86	30 Jun 77	+1:25	217	4
85	26 May 77	-5:44	286	1
84	20 May 77	-0:30	51	7
83	8 May 77	-3:18	337	6
82	1 May 77	+3:02	200	6
81	14 Apr 77	-4:02	229	5
80	13 Apr 77	-4:57	267	9
79	27 Mar 77	-3:57	278	9
78	26 Mar 77	-3:08	307	18
77	9 Mar 77	-1:08	261	6
76	8 Mar 77	-0:21	322	5
75	7 Feb 77	-1:16	0	0
74	1 Feb 77	+3:24	209	12
73	31 Jan 77	+4:24	0	0
72	27 Dec 76	-3:23	307	15
71	9 Dec 76	+0:20	319	12
70	20 Nov 76	+2:51	0	0
69	2 Nov 76	+4:21	319	9
68	15 Oct 76	-3:14	268	7
67	28 Sep 76	-2:20	336	6
66	9 Sep 76	+0:53	311	3
65	31 Aug 76	-3:56	0	0
64	23 Aug 76	+3:11	0	0
63	22 Aug 76	+4:18	0	0
62	4 Aug 76	-6:06	0	0
61	18 Jul 76	-4:06	0	0
60	17 Jul 76	-2:53	0	0
59	12 Jun 76	+1:25	0	0
58	28 Apr 76	+1:19	314	15
57	18 Apr 76	-1:17	148	6
56	10 Apr 76	+4:57	8	8
55	23 Mar 76	-5:50	284	4
54	14 Mar 76	+3:04	266	6
53	5 Mar 76	-1:31	222	5
52	24 Feb 76	+5:53	0	0

	Date	Delaware Bay Overpass Time Cape Henlopen, DE	24-Hour Wind Average Cape May, NJ Dir (°)	Speed (kts)
51	19 Jan 76	+0:01	0	0
50	24 Dec 75	-3:082	318	11
49	26 Nov 75	-4:122	351	5
48	18 Nov 75	+1:422	293	5
47	31 Oct 75	+4:13	353	16
46	22 Oct 75	+0:242	241	8
45	21 Oct 75	+1:072	269	7
44	13 Oct 75	-5:462	329	15
43	3 Oct 752	+3:312	347	15
42	29 Aug 75	-3:292	0	0
41	2 Aug 75	+6:18	245	4
40	1 Aug 75	-5:29	237	4
39	23 Jul 75	+1:02	225	1
38	9 Jun 75	+1:522	318	6
37	22 May 74	+3:472	161	1
36	21 Feb 75	+6:022	299	4
35	28 Dec 74	+2:25	222	5
34	11 Dec 74	+3:292	279	6
33	23 Nov 742	-5:342	0	0
32	4 Nov 74	-1:14	190	0
31	18 Oct 74	-0:082	308	7
30	12 Sep 74	+5:292	231	6
29	20 Jul 74	+1:142	0	0
28	2 Jul 74	+3:082	0	0
27	26 May 74	-2:11	0	0
26	8 May 74	+0:132	338	0
25	21 Apr 74	+2:262	0	0
24	20 Apr 74	+2:56	25	2
23	3 Apr 74	+4:562	188	2
22	26 Feb 74	-1:032	0	0
21	23 Oct 73	+4:052	0	02
20	22 Oct 73	+4:532	60	3
19	16 Sep 73	-0:332	0	0
18	30 Aug 73	0:00	0	0
17	29 Aug 73	+0:43	0	0
16	12 Aug 73	+2:432	203	4
15	7 Jul 73	-4:14	0	0
14	31 May 73	+2:56	90	1
13	13 May 73	+2:02	175	5
12	7 Apr 73	-0:362	02	0
11	13 Feb 73	+5:382	20	14
10	12 Feb 73	-6:16	0	0
9	26 Jan 73	-4:02	322	7
8	25 Jan 73	-3:34	0	0
7	3 Dec 72	+3:142	0	0

Delaware Bay

	Date	Overpass Time Cape Henlopen, DE	24-Hour Wind Average Cape May, NJ Dir (°)	Speed (kts)
6	2 Dec 72	+3:56	0	0
5	27 Oct 72	-1:58	332	5
4	10 Oct 72	+0:07	339	9
3	9 Oct 72	+0:55	319	5
2	3 Sep 72	-5:25	0	0
1	16 Aug 72	-3:41	56	8

New York Bight

	Date	Overpass Time Sandy Hook, NJ	24-Hour Wind Average Sandy Hook, NJ Dir (°)	Speed (kts)
58	9 Jul 81	-4:00	350	3
57	25 May 81	-2:22	251	2
56	10 Apr 81	-2:41	239	9
55	15 Feb 81	+5:01	255	4
54	5 Dec 80	+2:24	295	15
53	12 Oct 80	+0:49	237	9
52	12 Sep 79	-2:50	321	5
51	16 Aug 79	-4:59	292	12
50	7 Aug 79	+3:01	300	6
49	9 May 79	+4:23	163	8
48	17 Feb 79	-0:57	350	12
47	10 Nov 78	+6:22	270	6
46	1 Nov 78	+1:57	263	3
45	26 Sep 78	-5:21	329	8
44	21 Aug 78	+0:09	0	0
43	7 Jul 78	+0:37	357	5
42	10 Jun 78	-0:53	273	7
41	30 Mar 78	-2:17	311	6
40	11 Mar 78	+0:34	11	5
39	13 Feb 78	-3:45	273	13
38	28 Sep 77	+0:45	271	8
37	30 Jun 77	+2:48	260	10
36	24 Jun 77	-4:02	195	4
35	1 May 77	+3:43	184	5
34	13 Apr 77	+5:38	280	10
33	8 Mar 77	+0:04	334	4
32	18 Feb 77	+1:53	276	14
31	31 Jan 77	+4:52	283	19
30	2 Nov 76	+5:39	280	16
29	31 Aug 76	-3:26	338	14
28	22 Aug 76	+4:59	286	8
27	4 Aug 76	-5:00	188	1
26	26 Jul 76	+2:13	352	9

New York Bight

	Date	Overpass Time Sandy Hook, NJ	24-Hour Wind Average Sandy Hook, NJ Dir (°)	Speed (kts)
25	18 Apr 76	-1:15	211	5
24	24 Feb 76	-5:56	315	12
23	19 Jan 76	+0:35	337	13
22	10 Jan 76	+0:35	297	20
21	21 Oct 75	+1:54	329	8
20	3 Oct 75	+4:18	317	14
19	28 Aug 75	-2:06	315	10
18	19 Aug 75	+3:35	316	6
17	28 Dec 74	+2:53	242	12
16	22 Nov 74	-3:53	265	27
15	13 Jun 74	-3:24	58	3
14	8 May 74	+0:43	257	7
13	20 Apr 74	+3:56	325	6
12	15 Mar 74	-2:52	289	14
11	2 Jan 74	-3:44	301	14
10	22 Oct 73	+5:41	240	3
9	4 Oct 73	-3:12	232	4
8	16 Sep 73	0:00	241	5
7	29 Aug 73	+1:36	266	6
6	31 May 73	+3:44	157	5
5	7 Apr 73	-0:34	243	15
4	12 Feb 73	-5:04	318	23
3	25 Jan 73	-2:41	268	20
2	9 Oct 72	+1:43	298	12
1	16 Aug 72	-2:29	73	2

Long Island Sound

	Date	Overpass Time Narragansett, RI
66	9 Apr 81	-1:36
65	4 Mar 81	+3:48
64	14 Feb 81	+6:06
63	4 Dec 80	+3:49
62	25 Jun 80	+4:24
61	4 Nov 79	+2:22
60	15 Aug 79	-4:17
59	6 Dec 78	-2:39
58	31 Oct 78	+2:39
57	13 Oct 78	+5:01
56	25 Sep 78	-4:45
55	31 May 78	+5:57
54	22 May 78	+2:07
53	4 May 78	+3:37
52	25 Apr 78	-0:05

Long Island Sound

	Date	Overpass Time Narragansett, RI
51	20 Nov 77	+5:037
50	27 Sep 77	+1:157
49	9 Sep 77	+4:297
48	17 Jul 77	+0:177
47	11 Jul 77	-7:087
46	23 Jun 77	-3:317
45	30 Apr 77	+5:08
44	25 Mar 77	-1:45
43	19 Nov 76	+4:157
42	14 Oct 76	-1:207
41	8 Sep 76	+1:597
40	28 Jun 76	+1:507
39	10 Jun 76	+4:08
38	23 May 76	-5:587
37	5 May 76	-2:347
36	17 Apr 76	-0:09
35	8 Apr 76	-5:037
34	12 Mar 76	+5:10
33	14 Feb 767	+3:247
32	16 Nov 75	+3:367
31	14 Sep 75	-5:177
30	5 Sep 75	+2:467
29	9 Aug 75	+1:017
28	22 Jul 75	+2:447
27	4 Jul 75	-5:347
26	20 May 75	-5:37
25	11 May 75	+2:087
24	14 Apr 75	+0:377
23	27 Mar 75	+2:207
22	9 Mar 75	+4:207
21	28 Feb 75	+0:387
20	26 Jan 75	+3:03
19	9 Dec 74	+5:487
18	10 Sep 74	-3:57
17	23 Aug 74	-2:047
16	30 Jun 74	+5:43
15	12 Jun 74	-3:09
14	7 May 74	+1:52
13	1 Apr 74	-5:057
12	14 Mar 74	-2:27
11	24 Feb 74	+1:03
10	10 Aug 73	+4:55
9	23 Jul 73	-3:05
8	30 May 73	+4:327
7	12 May 73	-6:347

Long Island Sound

	Date	Overpass Time Narragansett, RI
6	24 Apr 73	-2:29
5	6 Apr 73	+0:197
4	19 Mar 73	+2:187
3	1 Mar 73	+4:507
2	8 Oct 72	+1:557
1	28 Jul 72	+1:017

Narragansett Bay

	Date	Overpass Time Narragansett, RI
100	30 Apr 82	-3:48
99	14 May 81	+5:207
98	8 Apr 81	-0:487
97	8 Jan 81	+0:417
96	21 Dec 80	+2:467
95	10 Oct 80	+1:317
94	4 Sep 80	+6:187
93	4 Nov 79	+2:257
92	9 Jul 79	+2:417
91	6 Dec 78	-2:407
90	31 Oct 78	+2:397
89	21 Oct 78	-1:377
88	13 Oct 78	+5:01
87	31 May 78	-6:28
86	4 May 78	+3:377
85	25 Apr 78	-0:057
84	28 Mar 78	-0:397
83	9 Mar 78	+2:047
82	11 Feb 78	-1:107
81	6 Jan 78	+4:217
80	20 Nov 77	+5:03
79	27 Sep 77	+1:157
78	9 Sep 77	+4:297
77	28 Jul 77	+3:567
76	17 Jul 77	+0:16
75	11 Jul 77	+5:277
74	10 Jul 77	-6:017
73	23 Jun 77	-3:32
72	22 Jun 77	-2:167
71	23 May 77	-1:387
70	17 May 77	+2:23
69	29 Apr 77	+5:337
68	30 Apr 77	+5:077
67	11 Apr 77	-4:44

	Date	Narragansett Bay Overpass Time Narragansett, RI
66	25 Mar 77	-1:45
65	29 Jan 77	-5:58
64	24 Dec 76	-0:25
63	19 Nov 76	+4:22
62	14 Oct 76	-1:20
61	13 Oct 76	-1:09
60	4 Oct 76	+4:29
59	25 Sep 76	+1:11
58	8 Sep 76	+2:05
57	7 Sep 76	+3:07
56	20 Aug 76	-6:03
55	11 Aug 76	+0:47
54	6 Jul 76	-5:57
53	10 Jun 76	+4:13
52	23 May 76	-5:58
51	22 May 76	-5:19
50	13 May 76	+2:17
49	5 May 76	-2:34
48	4 May 76	-1:27
47	20 Mar 76	-1:46
46	12 Mar 76	+5:10
45	14 Feb 76	+3:24
44	13 Feb 76	+3:39
43	16 Nov 75	+3:36
42	6 Nov 75	+0:21
41	28 Oct 75	-4:28
40	1 Oct 75	+5:52
39	14 Sep 75	-5:18
38	13 Sep 75	-4:22
37	5 Sep 75	+2:46
36	9 Aug 75	+1:01
35	30 Jul 75	-3:04
34	22 Jul 75	+2:43
33	4 Jul 75	-5:26
32	24 Jun 75	+1:41
31	28 May 75	-0:03
30	20 May 75	-5:38
29	1 May 75	-2:21
28	23 Apr 75	+4:43
27	22 Apr 75	+5:23
26	14 Apr 75	+0:36
25	27 Mar 75	+2:27
24	9 Mar 75	+4:20
23	28 Feb 75	+0:38
22	27 Feb 75	+2:55

Narragansett Bay

	Date	Overpass Time Narragansett, RI
21	26 Jan 75	+3:02
20	9 Dec 74	+5:48
19	27 Sep 74	+5:13
18	10 Sep 74	-3:57
17	17 Jul 74	+4:23
16	1 Apr 74	-5:05
15	14 Mar 74	-2:28
14	24 Feb 74	+1:00
13	13 Dec 73	-0:07
12	2 Oct 73	-1:33
11	10 Aug 73	+4:55
10	23 Jul 73	-3:05
9	30 May 73	+4:31
8	29 May 73	+5:08
7	24 Apr 73	-2:29
6	6 Apr 73	+0:19
5	19 Mar 73	+2:18
4	28 Feb 73	+5:47
3	8 Oct 72	+1:55
2	1 Sep 72	-4:09
1	28 Jul 72	+1:00

Boston Harbor

	Date	Overpass Time Boston, MA
51	30 Apr 82	-0:44
50	14 May 81	+1:39
49	8 Apr 81	-4:08
48	8 Jan 81	-2:42
47	21 Dec 80	-0:29
46	10 Oct 80	-2:05
45	4 Sep 80	+2:37
44	9 Jul 79	-0:53
43	21 Oct 78	-4:51
42	28 Mar 78	-4:05
41	9 Mar 78	-1:29
40	11 Feb 78	-4:39
39	6 Jan 78	+1:07
38	28 Jul 77	+0:27
37	10 Jul 77	+2:52
36	22 Jun 77	+0:41
35	23 May 77	-5:02
34	17 May 77	-1:36
33	29 Apr 77	+2:13

Boston Harbor

	Date	Overpass Time Boston, MA
32	11 Apr 77	+4:43
31	29 Jan 77	+2:48
30	24 Dec 76	-3:53
29	13 Oct 76	-4:38
28	4 Oct 76	+0:55
27	25 Sep 76	-2:14
26	7 Sep 76	-0:37
25	20 Aug 76	+2:53
24	11 Aug 76	-2:55
23	6 Jul 76	+3:18
22	22 May 76	+3:50
21	13 May 76	-1:06
20	4 May 76	-4:52
19	20 Mar 76	-5:08
18	13 Feb 76	+0:24
17	6 Nov 75	-3:00
16	28 Oct 75	+4:49
15	1 Oct 75	+2:42
14	13 Sep 75	+4:37
13	30 Jul 75	-6:17
12	24 Jun 75	-2:10
11	28 May 75	-3:52
10	1 May 75	-5:54
9	22 Apr 75	+2:14
8	27 Feb 75	-1:25
7	27 Sep 74	+1:33
6	17 Jul 74	+0:47
5	13 Dec 73	-3:37
4	2 Oct 73	-5:06
3	29 May 73	+1:38
2	28 Feb 73	+2:26
1	1 Sep 72	+5:00

APPENDIX 2

TIDE DATA FOR HCMM PASSES

Overpass Times are Before (-) or After (+) Actual High Tide at the Nearest Tide Recording Station

Date	Overpass Times	
	Delaware Bay	New York Bight
5/11/78	+2:21/	+3:11/
5/20/78	-4:06/	
5/21/78	-6:07/	
5/31/78	-1:45/	-0:58/
5/31/78	-3:30	-2:37
6/05/78		-5:09
6/11/78	+1:04/	+2:00
6/11/78	+2:45/	
6/12/78	+0:32	
6/15/78		+0:02
6/16/78	-1:40/	+0:12
7/08/78	+3:03/	+3:50/
7/13/78		0:00/
7/18/78	-5:45/	-4:01
7/23/78		+2:49/
7/23/78	+3:45/	+4:27/
8/14/78		-2:52
8/18/78	-6:09	
8/19/78	+4:11/	
8/30/78	-5:27	
9/04/78	+5:07/	+5:56
9/09/78	+1:34/	
9/16/78	+5:41/	
9/20/78	+2:08/	+2:53
9/21/78	+1:36/	+2:26
9/26/78		-2:00/
10/11/78		-2:35
10/12/78		-3:18/
10/22/78	-4:04/	+1:13/
10/22/78	+0:10/	
10/23/78	-0:28	
11/02/78	+3:52	+4:35/
12/15/78	+4:07/	
12/21/78	+0:11/	
1/10/79	-4:41/	
2/02/79	+0:34	
2/28/79	+3:14/	+3:59
3/22/79	-2:12/	
4/07/79	-4:27/	
4/11/79		+5:40/
4/22/79		-3:47/
6/15/79	+0:25/	
8/01/79	-1:55	-0:59
9/18/79	+5:50	-5:27

Date	Overpass Times	
	Delaware Bay	New York Bight
10/15/79	-4:24	
11/17/79	+5:57	
11/21/79	+3:00	+3:45
11/22/79	+2:36	
11/27/79	-2:12	-1:29